ปฏิกิริยาการขจัดหมู่ออกซิเจนของกรดไขมันปาล์มมิติกโดยใช้เลปิโดโครไซต์เป็นตัวเร่งปฏิกิริยา

DEOXYGENATION OF PALMITIC ACID OVER LEPIDOCROCITE TITANATE CATALYSTS

นางสาว กนกพร ลิ้มสกุล

นาย ทรงลักษ์ จันทรพัฒโรจน์

นางสาว ทรายทอง ฝั่งสัน

โครงงานพิเศษนี้เป็นส่วนหนึ่งของการศึกษาตามหลักสูตรวิทยาศาสตรบัณฑิต

สาขาวิชา เคมีอุตสาหกรรม

คณะวิทยาศาสตร์

สถาบันเทคโนโลยีพระจอมเกล้าเจ้าคุณทหารลาดกระบัง

ปีการศึกษา 2556

ปฏิกิริยาการขจัดหมู่ออกซิเจนของกรดไขมันปาล์มมิติกโดยใช้เลปิโดโครไซต์เป็นตัวเร่งปฏิกิริยา

Deoxygenation of palmitic acid over lepidocrocite titanate catalysts

นางสาว กนกพร ลิ้มสกุล

นาย ทรงสิทธิ์ จันทรชัยโรจน์

นางสาว ทรายทอง สังสัน

โครงงานพิเศษนี้เป็นส่วนหนึ่งของการศึกษาตามหลักสูตรวิทยาศาสตรบัณฑิต

สาขาวิชา เคมีอุตสาหกรรม

คณะวิทยาศาสตร์

สถาบันเทคโนโลยีพระจอมเกล้าเจ้าคุณทหารลาดกระบัง

ปีการศึกษา 2556

DEOXYGENTION OF PLAMITIC ACID OVER LEPIDOCROCITE TITANATE CATALYSTS

MISS KANOKPORN LIMSAKUL

MR. SONGSIT JUNTARACHAIROT

MISS SAITHONG SANGSAN

A SPECIAL PROJECT SUBMITTED IN PARTIAL FULFILLMENT

OF THE REQUIREMENT FOR THE DEGREE OF BACHELOR OF SCIENCE

IN INDUSTRIAL CHEMISTRY

FACULTY OF SCIENCE

KING MONGKUT'S INSTITUTE OF TECHNOLOGY LADKRABANG

ACADEMIC YEAR 2013

Project Title	Deoxygenation of palmitic acid over lepidocrocite titanate catalysts		
Student	Ms. Kanokporn	Limsakul	ID.53050151
	Mr. Songsit	Juntarachairot	ID.53050230
	Ms. Saithong	Sangsan	ID.53050232
Degree	Bachelor of Science		
Program	Industrial Chemistry		
Year	2013		
Advisor	Assoc. Prof. Dr. Tawan Sooknoi		
Co – Advisor	Dr. Tosapol Maluangnont		

Faculty of Science, King Mongkut's Institute of Technology Ladkrabang, has approved this special project submitted in partial fulfillment of the requirement for the degree of Bachelor of Science in academic year 2013.

Committees	Signatures
Asst. Prof. Dr. Montree Thongkam	
Asst. Prof. Dr. Sutha Sutthiruangwong	
Assoc. Prof. Dr. Tawan Sooknoi	
Dr. Tosapol Maluangnont	

Special project Title	Deoxygenation of palmitic acid over lepidocrocite titanate catalysts		
Students	Miss Kanokporn	Limsakul	ID.53050151
	Mr. Songsit	Juntarachairot	ID.53050230
	Miss Saithong	Sangsan	ID.53050232
Degree	Bachelor of science		
Program	Industrial chemistry		
Year	2013		
Special project Advisor	Assoc. Prof. Dr. Tawan	Sooknoi	
Co-advisor	Dr. Tosapol	Maluangnont	

Abstract

Various types of lepidocrocite titanates ($K_{0.8}Zn_{0.4}Ti_{1.6}O_4$, $K_{0.8}Li_{0.27}Ti_{1.73}O_4$, $K_{0.9}Mg_{0.45}Ti_{1.55}O_4$) were prepared and modified by the conventional solid state synthesis. $K_{0.8}Zn_{0.4}Ti_{1.6}O_4$ was converted to the protonic form before exfoliation with TBAOH or TMAOH and restacking with KOH. The suspension of exfoliated nanosheets showed λ_{max} at 266 nm regardless of the type of tetraalkylammonium cations used. The re-assembled $K_{0.8}Zn_{0.4}Ti_{1.6}O_4$ co-existed with anatase phase, as confirmed by X-ray diffraction and Raman spectroscopy. Substitution of alkali and alkaline earth ion (Li^+, Mg^{2+}) into lepidocrocite titanate showed increasing basicity and surface area, especially for the re-assembled sample. The pristine and re-assembled titanates were used as catalysts in deoxygenation of palmitic acid at 375-400° C. The liquid products were analyzed by gas chromatography and mass spectrometry. The results showed that C-31 ketone was primarily formed by ketonization of palmitic acid. C-17 ketone and C-14 long chain hydrocarbon were obtained as main products from cracking of the C-31 ketone. The activity of deoxygenation over re-assembled titanate was higher than that over the pristine catalyst due to the presence of anatase phase. In contrast, the yield of C-14 long chain hydrocarbon over the pristine catalyst is greater than that over the re-assembled one. $K_{0.8}Li_{0.27}Ti_{1.73}O_4$ showed high activity in deoxygenation of palmitic acid, for which 21% yield of C-14 long chain hydrocarbon was obtained. Moreover, the activity of deoxygenation and yield of products increased with contact time and temperature. The presence of dense layer provided high selectivity to C-14 long chain hydrocarbons, while basicity of the catalyst was responsible for the activity in cracking.

ACKNOWLEDGEMENT

The author wishes to gratefully thank the project advisor and co-advisor, Assoc.Prof.Dr.Tawan Sooknoi for their supports, supervisions, inspiration, suggestion and encouragement throughout this thesis.

We also thank Asst.prof.Dr.Montree Thongkam and Asst.Prof.Dr.Sutha Sutthiruangwong for serving as the chairperson and the committee, and for valuable comments.

We also appreciate the supports from the Department of Chemistry, Faculty of science, King Mongkut's Institute of Technology Ladkrabang for the equipments, chemicals and facilities.

We would like to extend our thanks to Mr.Boonyawat Wuttitham, Mr.Thanasak Solos and Mr.Ayut Witsuthammakul for their help and advices in working the data analysis, support and encouragement.

We would like to extend our sincere appreciation to all teachers, my friends and my member of this research group for their constant guidance, advice, support and encouragement.

Finally, we deeply appreciate and thank our parents and family for their love and supports.

Miss Kanokporn Limsakul

Mr. Songsit Juntarachairot

Miss Saithong Sangsan

CONTENTS

CONTENTS (continues)

CONTENTS (continues)

page

List of table

List of figure

CHAPTER 1

INTRODUCTION

1.1 Motivation

In recent years, the demand for fuels and petrochemicals is increasing in sharp contrast to the declining availability of petroleum feedstock. The search for renewable feedstock for the production of fuels and petrochemicals is therefore currently being extensively conducted [1-3]. One of such potential feedstock is fatty acids, obtainable from the hydrolysis of animal fats and vegetable oils, both of which are cheap, abundant, and are considered renewable [4,5].

Fatty acids can be converted to fuels and petrochemicals through the reaction known as *decarboxylation*, where hydrocarbons are produced as a desired product, together with carbon dioxide gas (CO_2) as a byproduct. The hydrocarbon products are the terminal alkenes, or alpha-olefins following **(Eq. 1.1).** In this reaction, the carboxylic group of fatty acid is believed to be adsorbed on the surface of a catalyst; the adsorbed species consequently transforms into a metal carboxylate salt which can be decomposed at high temperature. Yet, another reaction known as *deacetylation* could take place, yielding carbon monoxide (CO) and H_2O in addition to alpha-olefins as shown in **(Eq. 1.2)** through the ketene intermediates. Compared to the starting fatty acid, the alkenes will have 2 carbon atoms less in deacetylation, but only one carbon atom less in decarboxylation. These two reactions where an oxygen atom is removed are known collectively as deoxygenation.

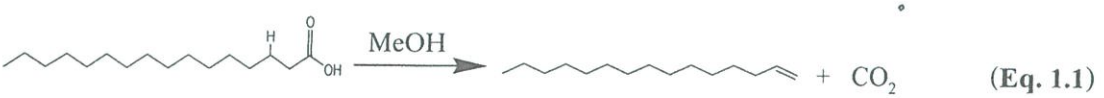

(Eq. 1.1)

(Eq. 1.2)

In those two reactions, it is known that materials with base functionality are active catalysts. Examples include common basic oxides such as MgO and CaO [2]. However, the low surface area of these common oxides limits the number of active sites available for the interaction with fatty acids. The search for a catalyst with basic functionality and high surface area is therefore required. In this regard, a family of layered titanate known as lepidocrocite

is a potential candidate owing to its basic functionality and its ability to undergo the post-synthesis modification into a form possessing high surface area [6,7].

In this research, the deoxygenation of palmitic acid $C_{15}H_{31}COOH$ (taken as a representative of the fatty acid) into long chain alpha-olefins will be studied. Alpha-olefins have found widespread use in a variety of products such as polymers, lubricants, surfactants, etc. It is expected that the alpha-olefins will be obtained as a result of the decomposition of the metal palmitate into carbon dioxide and C_{15} radical; the latter species subsequentlyeliminates hydrogen atom which gives rise to C_{15} unsaturated hydrocarbons, preferably an alpha olefin. We propose the use of a layered titanate having the lepidocrocite structure in such reaction as active catalysts through their basic functionality. Lepidocrocite studied includes the composition $K_{0.8}Zn_{0.4}Ti_{1.6}O_4$, $K_{0.8}Mg_{0.40}Ti_{1.60}O_4$ and $K_{0.8}Li_{0.27}Ti_{1.73}O_4$ where a different degree of basicity comes from the presence of the different cations (Zn^{2+}, Mg^{2+} and Li^{+}) in the structure, which in turn affects the basicity at the oxygen atoms and the resulting solids. For both of them, not only the pristine crystallites but also the materials undergoing the post-synthesis modification will be studied.

We will report in details a series of post-synthesis process including proton exchange, exfoliation, and restacking, which ultimately yields a high-surface-area lepidocrocite as active basic catalysts. By comparing the composition $K_{0.8}Zn_{0.4}Ti_{1.6}O_4$, $K_{0.8}Mg_{0.40}Ti_{1.60}O_4$ and $K_{0.8}Li_{0.27}Ti_{1.73}O_4$, we hope to gain better understanding on the role of the cations in the structure toward the catalytic activity in the deoxygenation of fatty acid. We will conduct an investigation on the optimization of the catalytic conditions as well, including the reaction temperature and the contact time.

1.2 Objective

1.2.1 To obtain LAOs from deoxygenation of palmitic acid.

1.2.2 To conduct the synthesis of lepidocrocite titanates that are base catalysts .

1.2.3 To obtain appropriate reaction condition for decarboxylation with lepidocrocite catalysts.

1.3 Scopes of project

1.3.1 Catalyst preparation by physical mixed, ion exchange and restacking of lepidocrocite titanates.

1.3.2 Characterization of lepidocrocite titanates by X-ray Diffraction (XRD) Thermogravimetric analysis (TGA). Raman spectroscopy. UV-VIS spectrophotoscopy, BET surface area, Scanning Electron Microscope (SEM).

1.3.3 Analysis of liquid products by Gas chromatography with flame ionization detector (GC-FID) and analysis of gas products by online Gas chromatography with a thermal conductivity detector (GC-TCD).

1.4 Expected result

It is expected that a new approach for production of long chain α-olefin from the natural feedstock will be obtained.

CHAPTER 2

THEORY AND LITERATURE REVIEWS

2.1 Fatty acids

Fatty acids are aliphatic monocarboxylic acids, present mainly as triglycerides from animal fats (e.g., butter, lard, beef), vegetable oils (e.g., jatropha oil, coconut oil, soybean oil, palm oil), or waxes. Natural fatty acids commonly have an unbranched chain with even number of carbon atoms, mostly 16-22, and the acids can be either saturated or unsaturated [8,9,10]. Fatty acids can be produced by a hydrolysis of triglycerides in fat or biological oils with the removal of glycerol. Table 2.1 shows the composition of common fatty acids in vegetable oils (taken from [8]).

Saturated fatty acids are long-chain carboxylic acids that usually have between 12 and 24 carbon atoms and have no double bonds. The term "saturated" comes from the fact that the C-C bonds are all saturated with hydrogen (3 hydrogen atoms for the terminal carbon atoms, and 2 hydrogen atoms for the rest). On the other hand, unsaturated fatty acids have one or more double bonds between carbon atoms, where hydrogen atoms can be added into [11].

The world production of fatty acids from the hydrolysis of natural fats and oils is about a total of 4 million metric tons per year [12]. Fatty acids not only make up the largest proportion of the current consumption of raw materials in the chemical industry. They are also ultimately consumed in a wide variety of end-use industries. The extent of the chemical reaction which are used to transform these renewable materials, taken palmitic acid as a representative for fatty acids, into fuels are summarized below.

Table 2.1: Fatty acid compositions (wt%) of common vegetable oils

Fatty acid	Notation*	Palm	Olive	Peanut	Soybean	Rape	Sunflower	Grape	H.O.sunflower	Almond	Corn
Lauric	C12:0	0.1	0.0	0.0	0.0	0.0	0.0	0.0	0.0	0.0	0.0
Myristic	C14:0	0.7	0.0	0.1	0.0	0.0	0.0	0.1	0.0	0.0	0.0
Palmitic	C16:0	36.7	11.6	8.0	11.3	4.9	6.2	6.9	4.6	10.4	6.5
Palmitoleic	C16:1	0.1	1.0	0.0	0.1	0.0	0.1	0.1	0.1	0.5	0.6
Stearic	C18:0	6.6	3.1	1.8	3.6	1.6	3.7	4.0	3.4	2.9	1.4
Oleic	C18:1	46.1	75.0	53.3	24.9	33.0	25.2	19.0	62.8	77.1	65.6
Linoleic	C18:2	8.6	7.8	28.4	53.0	20.4	63.1	69.1	27.5	7.6	25.2
Linolenic	C18:3	0.3	0.6	0.3	0.1	7.9	0.2	0.3	0.1	0.8	0.1
Arachidic	C20:0	0.4	0.3	0.9	0.3	0.0	0.3	0.3	0.3	0.3	0.1
Godoleic	C20:1	0.2	0.0	2.4	0.3	9.3	0.2	0.0	0.0	0.0	0.1
Behenic	C22:0	0.1	0.1	3.0	0.0	0.0	0.7	0.0	0.7	0.1	0.0
Erucic	C22:1	0.0	0.0	0.0	0.3	23.0	0.1	0.0	0.0	0.0	0.1
Lignoceric	C24:0	0.1	0.5	1.8	0.1	0.0	0.2	0.0	0.3	0.2	0.1
Nervenic	C24:1	0.0	0.0	0.0	0.0	0.0	0.0	0.0	0.0	0.4	0.0

*This notation indicates the number of carbon atoms and the number of double bond. For example, C12:0 indicates a fatty acid with a total number of 12 carbon atoms, without any double bond.

2.1.1 Palmitic acid

Palmitic acid $CH_3(CH_2)_{14}CO_2H$, or hexadecanoic acid in IUPAC nomenclature with the structure shown in Figure 2.1, is the most common fatty acid (saturated) found in animals, plants and microorganisms [13]. As the name indicates, palmitic acid is a major component of the oils from palm trees (palm oil, palm kernel, and palm kernel oil), although it can also be found in meats, cheeses, butter, and dairy products. Palmitate is a term for the salts and esters of palmitic acid. The palmitate anion is formed when palmitic acid is put into a condition with basic pH values [13,14].

Figure 2.1 The molecular structure of palmitic acid.

2.2 Reactions of fatty acids

2.2.1 Esterification

The chemistry of fatty acids is similar to other carboxylic acids, including esterification and acid-base reactions. Esterification is a reaction between a carboxylic acid and an alcohol, forming an ester as the reaction product as shown in **Equation 2.1**. Esters are common in biological materials, and can serve as an alternative fuel [15,16].The initial step is the protonation of the acid to give an oxonium ion (1), which undergoes an exchange reaction with an alcohol to give the intermediate (2); this intermediate can lose a proton to become an ester (3). Although each step in the process is reversible, the presence of a large excess of the alcohol displaces the equilibrium to the right such that esterification proceeds virtually to completion.

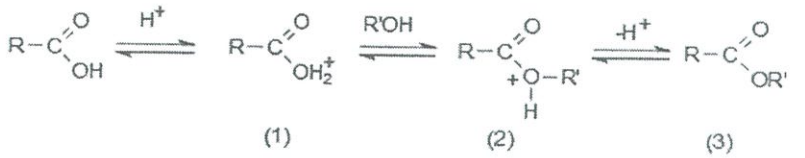

(Eq. 2.1)

2.2.2 Deoxygenation

Deoxygenation is a chemical reaction involving the removal of oxygen atoms from a starting molecule. In this context, a carboxyl group (-COOH) is split off as carbon dioxide (CO_2). It is a novel method for the production of diesel-like fuels from renewable resources such as vegetable oils and animal fats, and is being investigated in several laboratories [17]. Chemical decarboxylation often requires extensive heating in high-boiling solvents. For example, catalytic decarboxylation of lauric acid (**Eq. 2.2**) has been studied over Pd/C catalyst in a continuous process at 255-300°C. Very high selectivity (>95 %) to the desired products, namely C_{11} hydrocarbons can be achieved [18].

$$CH_3\text{-}(CH_2)_{10}\text{-}CO_2H \longrightarrow CH_3\text{-}(CH_2)_9\text{-}CH_3 + CO_2 \quad \textbf{(Eq. 2.2)}$$

The conversion of lauric acid declined substantially to a steady state level within 10-20 minutes of the time-on-stream. The initial concentration of lauric acid was decisive for the catalyst deactivation; the higher the initial concentration of fatty acids, the more extensive catalyst deactivation.

2.3 Base catalysts

The use of a solid base catalyst instead of a basic solution offers several process advantages. These include the elimination of a quenching step (with the associated reduction in the aqueous waste), and the opportunity to operate in a continuous process. Several types of heterogeneous catalysts with base functionality are known as shown in **Table 2.2** [19]. A major group of basic catalysts is that of the supported or unsupported metal oxides. The basicity originates from O^{2-} anions on the surface which can have different coordination numbers depending on the crystalline planes where those oxygen atoms belong to. The catalytic activity for some of them (BaO, SrO, CaO, MgO) in the transesterification of vegetable oils into biodiesel has been reported [20]. The drawbacks of these common oxides are that they have low surface areas which limit the number of active sites available for the reaction. Also, some of them are slightly soluble in methanol which is used as a solvent, thereby reducing the lifetime of a catalyst [21]. Considering that K_2O, MgO, ZnO and TiO_2 are known as basic catalysts (Table 2.2), it is interesting to see what would be the catalytic activity of oxides having these active cations altogether in a crystal. Lepidocrocite titanate falls into this category as will be described in Section 2.3.2.

Table 2.2: Different categories of basic oxides [19]

Single component metal oxides

- Alkaline earth oxides
- Alkali metal oxides
- Rare earth oxides
- The O_2, ZrO_2, ZnO, TiO_2

Zeolites

- Alkali ion-exchanged zeolites
- Alkali ion-added zeolites

Supported alkali metal ions

- Alkali metal ions on alumina
- Alkali metal ions on silica
- Alkali metal on alkaline earth oxide
- Alkali metals and alkali metal hydroxides on alumina

Clay minerals

- Hydrotalcite
- Chrysotile
- Sepiolite

Non-oxide

- KF supported on alumina
- Lanthanide imide and nitride on zeolite

The amount and strength of basic sites on the surface of basic oxides can be determined by several techniques, including the color change of the acid–base indicators, or the adsorption of acidic molecules followed by their detection with a variety of techniques (UV, IR, XPS, ESR, etc.). Usually, the catalytic activities correlate well with the amount (or strength) of basic sites [19]; the latter can be poisoned by acidic molecules such as HCl, H_2O, and CO_2.

2.3.1 Hydrotalcite

Hydrotalcites of general formulae $[M^{2+}_{1-x}M^{3+}_{x}(OH)_2]^{x+}(A_{x/n})n^{\cdot}yH_2O$ are another class of solid base whose the basic properties can be controlled by the variation in composition. The structure of hydrotalcites (**Figure 2.2**) is based upon layered double hydroxides with brucite-like hydroxide ($Mg(OH)_2$) layers, containing octedrally coordinated M^{2+} and M^{3+} cations. Due to residual positive charges of the hydroxide layers resulting from isomorphous substitution of M^{2+} by M^{3+}, there are anions residing in the interlayer space to preserve charge neutrality.

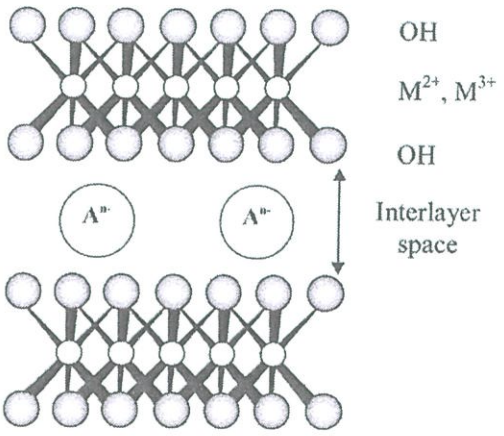

Figure 2.2 Representation of the structure of hydrotalcite [21]

The variation in the relative amount of M^{2+}/M^{3+} is known to modify the basic properties of the material. The stable hydrotalcite structures are reported to form for compositions over the range $0.25 < x < 0.44$ where M^{3+} is Al and M^{2+} is Mg^{2+} [22]. Outside of these limits, the high density of Al^{3+} (or Mg^{2+}) will lead to the formation of $Al(OH)_3$ (or $Mg(OH)_2$). The basic sites in hydrotalcites originate from O^{2-} (strong basicity), O^- (located near hydroxyl groups, and having medium basicity), and OH groups (weak basicity). The addition of Al^{3+} alters the distribution of acid-base sites through the introduction of Al^{3+}–O^{2-} sites which are of moderate Lewis acidity and are of only medium basicity. The effect of Mg-to-Al ratio over a range of compositions where the hydrotalcite phase is stable, on the resulting catalytic activity in liquid phase transesterificiation of vegetable oil has been investigated [22].

2.3.2 Lepidocrocite titanate

Lepidocrocite-type structure refers to the structure of γ-FeOOH. We will describe here the structure of the lepidocroite titanate $H_xTi_{2-x/4}\square_{x/4}O_4$ ($x \sim 0.7$; $\square$ is the vacancy) as an example. The structure can be constructed from the edge sharing of $(Ti,M)O_6$ octahedra, which extend into the sheets (or layers) along the *a*- and *c*-direction of the orthorhombic unit cell [22] as shown in **Figure 2.3.** These sheets stack together along the *b*-direction like a pile of paper, resulting in 2-dimensional crystallites with the preferred orientation along the *b*-axis. The sheet as an elementary unit is roughly 1.3-nm thick, having only 3 layers of atoms [23]. The general composition of lepidocrocite titanates has the formula $A_xM_yTi_zO_4$, where A is usually an alkali metal, M is usually a transition metal having the valence not equal to +4 such as Zn or Mg [24], or the cation vacancy. The subscripts x, y and z indicates appropriate stoichiometry. Because of the substitution of M^{n+} ($n < 4$) or the formation of the cation vacancy, the $(Ti,M)O_6$ layers become negatively charged. In order to preserve charge neutrality, alkali metal cations A^+ are usually incorporated between the layers.

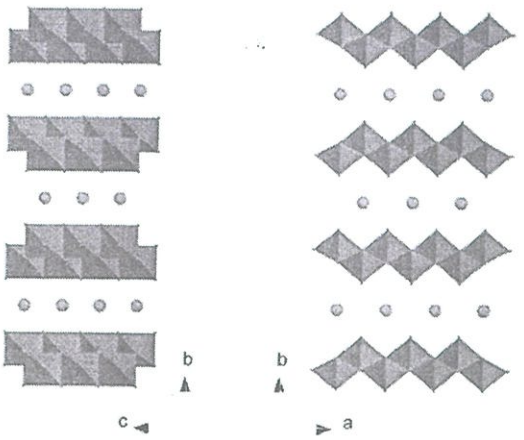

Figure 2.3 The crystal structure of lepidocrocite titanate viewed on the *bc* plane (left) and on the *ab* plane (right). The green polyhdedra represent the $(Ti,M)O_6$ units, whereas the blue dots represent the alkali metal cations located between the layer. Taken from [6].

Lepidocrocite titanates have excellent ion-exchange/intercalation reactivities. The A^+ cations originally located between the layers can be replaced by a wide variety of guest species such as inorganic and/or organic cations, protons, and surfactants. For example, the ion exchange of K^+ in $K_{0.8}Li_{0.27}Ti_{1.73}O_4$ with H^+ results in $H_{1.07}Ti_{1.73}O_4{\cdot}H_2O$ where $H^+{\cdot}H_2O$ residing between the layer. For the mentioned composition, the repeating distance along the *b*-direction increased from 1.55 nm to 1.84 nm as a result of the ion exchange [25]. The ion exchange of

guest species into the layers with a consequence of the change in the distance between the layers is specifically called *intercalation*. In extreme cases, the intercalation of bulky molecules will pry apart the layers so that they become infinitely separated. The known exfoliation reagent is the aqueous solution of tetrabutylammonium cations, $(C_4H_9)_4N^+$ or TBA^+, although a smaller cations such as tetramethylammonium cations, $(CH_3)_4N^+$ or TMA^+, can also be used [23]. The reaction is facilitated by the increased interlayer separation in the H-form (in relative to the K-form), and also by the acid-base chemistry between the interlayer H^+ cations and the OH^- from TBAOH. The resulting product is the aqueous suspension of the atomically-thin sheets, called *nanosheets*. The nanosheets can be re-assembled back to a solid having less-ordered crystal structure and higher surface area by the process called *restacking*, where alkali metal cations smaller than TBA^+ are added to the aqueous suspension.

Lepidocrocite titanates have shown to be interesting materials in a variety of applications [26]. They serve as building blocks for the fabrications of several nanostructures such as thin films, porous aggregates, hollow shells, nanotubes. However, the basicity of lepidocrocite titanates has not been reported so far, despite the fact that they have layered structure similar to layered double hydroxides (LDHs) and hydrotalcites, both of which are well known to exhibit basicity [27]. This research will study the basicity of two compositions of the lepidocrocite titanates, $K_{0.8}M_{0.4}Ti_{1.6}O_4$ (M = Zn, Mg), and study their use as a catalyst in the decarboxylation of fatty acids into fuel oils. The characteristic of fuel oils will be discussed in Section 2.4.

2.4 Fuel oils

Fuel oils can be traditionally divided into two main types: distillate fuel oils and residual fuel oils [28]. Distillate fuel oils are vaporized and condensed during a distillation process, resulting in the fuel having a definite boiling range and do not contain high boiling oils or asphaltic components. On the other hand, a residual fuel oil can contain any amount of the residue from crude distillation. The terms "distillate" and "residual" fuel oil are losing their significance, since fuel oils are now made for specific uses and may be distillates, residuals or mixtures of the two.

The terms "domestic" fuel oils, "diesel" fuel oils, and "heavy" fuel oils are more indicative of their uses. Domestic fuel oils are distillate fuel oils which are primarily for a home-use (e.g., kerosene, stove oil, and furnace fuel oil). Diesel fuel oils are also distillate fuel

oils, although residual oils (or their mixture with distillate oils) have been successfully used. Heavy fuel oils include a variety of oils ranging from distillates to residual oils that must be heated to 260C (500°F) or higher before they can be used. Generally, they consist of residual oils blended with distillates to suit specific needs. Included among heavy fuel oils are various industrial oils.

Similar to kerosene, stove oil is always a straight-run fraction from suitable crude oils, whereas other fuel oils are usually blends of two or more fractions, one of which is usually the cracked gas oil. The straight-run fractions available for blending into fuel oils are heavy naphtha, light and heavy gas oils, reduced crude, and pitch. Cracked fractions such as light and heavy gas oils from catalytic cracking, cracking coil tar, and fractionator bottoms from catalytic cracking, may also be used as blends to meet the specifications of the different fuel oils.

Since the boiling ranges, sulfur contents, and other properties of even the same fraction vary from crude oil to crude oil and with the way the crude oil is processed, it is difficult to specify fuel oils, and to specify which fractions will be blended for producing specific fuel oils. In general, however, furnace fuel oils is a blend of straight-run gas oil and cracked gas oil to produce a product boiling in the 175 - 345 °C (350 - 650°F) range.

Diesel fuel oil is essentially similar to furnace fuel oil, but the proportion of cracked gas oil is usually less since the high aromatic content of the cracked gas oil reduces the cetane value of the diesel fuel. Cetane number is a measure of the tendency of a diesel fuel to knock in a diesel engine. The scale is based upon the ignition characteristics of two hydrocarbons, namely *n*-hexadecane (cetane) and heptamethylnonane whose the structure are shown in **Figure 2.4.**

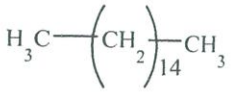

n-hexadecane (cetane)

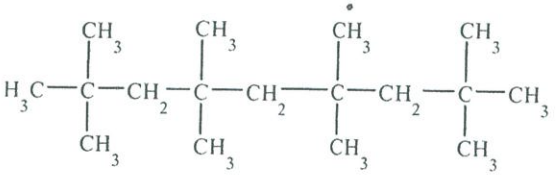

heptametylnonane

Figure 2.4 The chemical structure of *n*-hexadecane (cetane) (left) and heptamethylnonane (right).

Cetane has a short delay period during ignition and is assigned a cetane number of 100; heptametylnonane has a long delay period and has been assigned a cetane number of 15. While the octane number is meaningful for automobile fuels, the cetane number relates to the ignition quality of diesel fuels, and is equivalent to the percentage by volume of cetane in the blend with heptametylnonane, which matches the ignition quality of the test fuels (ASTM D-613).

Heavy fuel oils usually contain pitch, reduced crude, or cracking oil tar, which is mixed (cut mixed) to a specified viscosity with cracked gas oil and fractionator bottoms. For some industrial purpose in which flames or fuel gases contact the products (ceramics, glass, heat treating, and open hearth furnaces), fuel oils must be blended to contain minimum sulfur contents; therefore, low-sulfur residues are preferable for these fuels.

The manufacture of fuel oils at one time largely involved using what was left after removing desired products from crude petroleum. Presently, fuel oil manufacture is a complex matter of selecting and blending various petroleums to meet definite specifications, and the production of a homogeneous, stable fuel oil requires the presence of both experience and a quality control in a laboratory [29].

2.5 Linear α-olefins

The term 'olefin' refers to compounds of carbon and hydrogen which has at least one double bond in the structure. Olefins are also known as alkenes. Short-chain olefins, like ethylene, are cracked form naphtha or natural gas. Ethylene is then oligomerized into longer chain linear α-olefins (LAOs), ranging from 6 to 30 carbons in length. α-olefins are characterized by their high purity, high degree of linearity, and a double bond uniformly positioned between the first and second carbon. For drilling fluid applications, α-olefins in the C_{14} to C_{18} range are used because they have the appropriate physical properties (viscosity, pour point, flash point, etc). *Internal* olefins are then produced from LAOs by catalytically moving the double bond to different locations in the molecule. As a result, the pour point of the fluid decreases significantly, thus enabling these materials to be used successfully in deep-water applications. Internal olefins used as base fluids for drilling muds typically have carbon chain lengths in the C_{15} to C_{18} range [28].

The structure of LAOs (or normal α-olefins, NAOs) is distinguishable from other mono-olefins with a similar molecular formula by (i) the linearity of the hydrocarbon chain, and (ii) the position of the double bond at the 1-(or alpha) position, (**Figure 2.5**). LAOs cover a range of hydrocarbons having different carbon atoms which are industrially important, including 1-butene, 1-hexene, 1-octene, 1-decene, 1-dodecene, 1-tetradecene, 1-hexadecene, 1-octadecene, and higher blends of C_{20}-C_{24}, C_{24}-C_{30}, and C_{20}-C_{30} ranges.

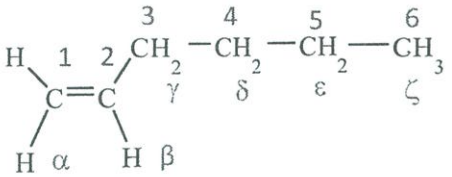

Figure 2.5. The molecular structure of 1-hexene, a typical LAOs

2.5.1 Synthesis

2.5.1.1 Oligomerization

Ethylene-oligomerization process has been developed by Shell and is called the Shell Higher Olefin Process (SHOP) [30-32]. In this process, ethylene oligomerization is catalyzed by nickel complexes which give rise to ethylene oligomers having a Shultz-Flory distribution. The composition of the oligomers can be adjusted to the required composition through a series of reactions combining the isomerization of the olefins with the disproportionation between the light and heavy olefins.

Alternatively, Idemitsu Kosan Co., Ltd., developed a new ethylene oligomerization process based on the catalyst consisting of $ZrCl_4$, an alkylaluminum compound, and a Lewis base; the distribution of products in this process can be adjusted by changing the ligand structure of the alkylaluminum complex [33].

2.5.2 Applications of LAOs

There is a wide range of applications for LAOs[34,35]; selected examples are shown in **Table 2.3.** LAOs with small carbon numbers such as 1-butene, 1-hexene and 1-octene, are used as co-monomers in the production of polyethylene. High density polyethylene (HDPE) and linear low density polyethylene (LLDPE) use approximately 2-4% and 8-10% of these co-monomers, respectively.

Another significant use of C_4-C_8 LAOs is for a production of linear aldehydes via oxo synthesis (hydroformylation). The linear aldehydes are subsequently used in a production of short-chain fatty acid (by the oxidation of an intermediate aldehyde), or of linear alcohols for plasticizer application (by the hydrogenation of an aldehyde). The predominant application of 1-decene is in making poly-alphaolefin synthetic lubricant basestock (PAO), and to makesurfactants in a blend with higher LAOs.

Table2.3: Application of LAOs

LAOs	Application*
1-Decene ($C_{10}H_{20}$)	Detergent alcohols, poly-alphaolefins, alkyl aromatics, plasticizer alcohols, epoxides, di-/poly-halides, personal care, flavors and fragrances
1-Dodecene ($C_{12}H_{24}$)	Detergents, plasticizer alcohols, poly-alphaolefins, alkyl aromatics, ADMA, ASA, epoxides, mercaptans, di-/poly-halides, alkyl silanes, personal care products, flavors and fragrances
1-Tetradecene ($C_{14}H_{28}$)	Maleic anhydride copolymers, AOS, alkyl aromatics, ADMA, ASA, epoxides, mercaptans, di-/poly-halides, alkyl silanes, personal care products, flavors and fragrances
1-Hexadecene ($C_{16}H_{32}$)	Maleic anhydride copolymers, AOS, alkyl aromatics, ADMA, ASA, lube oil additives, epoxides, metal working fluids, di-/poly-halides, alkylsilanes, personal care products, flavors and fragrances
1-Octadecene ($C_{18}H_{36}$)	Maleic anhydride copolymers, AOS, alkyl aromatics, ADMA, ASA, lube oil additives, epoxides, metal working fluids, di-/poly-halides, alkyl silanes, personal care products, flavors and fragrances
Alpha olefin C_{20-24}	Lube oil additives, personal care products, epoxides, alkyl aromatics, drilling fluids, maleic anhydride copolymers, pour point depressants
Alpha olefin C_{24-28}	Epoxides, di-/poly-halides, candles, pour point depressants, personal care products

*Abbreviation: ADMA - alkyldimethylamine; ASA – acetylsalicylic acid; AOS – sodium alpha-olefin sulfonate.

C_{10}-C_{14} LAOs are used to make surfactants for aqueous detergent formulations. They may be reacted with benzene to make linear alkyl benzene (LAB); LAB is further sulfonated to give linear alkyl benzene sulfonate (LABS), a popular and relatively low-cost surfactant for household and industrial detergent applications. Additionally, C_{14} has found other

applications, including the reactants for the synthesis of chloroparaffins, which are used as an on-land drilling fluid basestock replacing the use of diesel or kerosene. Although C_{14} is more expensive than middle distillates, it is more biodegradable, is less irritating to the skin, less toxic, and is therefore easier to handle.

C_{16}-C_{18} linear olefins find their primary application as the hydrophobes in oil-soluble surfactants and as lubricating fluids themselves. They are also being used as a synthetic drilling fluid base for high value, primarily off-shore synthetic drilling fluids. The preferred materials for the synthetic drilling fluid application are linear *internal* olefins, which can be made by isomerizing LAOs to olefins with a double bond at the internal position. The higher internal olefins form a more lubricious layer at the metal surface and are recognized as better lubricants. Another significant application for C_{16}-C_{18} olefins is in paper sizing. LAOs are, once again, isomerized into linear internal olefins which are subsequently reacted with maleic anhydride to make an alkyl succinic anhydride (ASA), a popular paper sizing chemical.

C_{20}-C_{30} LAOs production capacity is only 5-10% of the total production of a linear alpha olefin plant. They are used in a number of reactive and non-reactive applications, including as a feedstock to make heavy linear alkyl benzene (LAB), and to make low molecular weight polymers which are used to enhance properties of waxes

2.6 Literature and Reviews

Catalytic decarboxylation is a well-established chemical reaction in organic process. It has been widely applied in organic synthesis, and has been studied in broad reaction conditions and over various types of catalysts [36]. Yet, reports on the decarboxylation of fatty acid over metal oxide catalysts are rather limited.

Recently, Taweesin [12] studied deoxygenation of palmitic acid over common basic oxides such as MgO, CaO, SrO and BaO in a semi-batch reactor. The investigation was done employing a 1/1 or 0.5/1 (mol/mol) of catalysts/palmitic acid at the optimized temperature of 460°C. These alkaline earth metal oxides showed high activity (>70% yield) in the deoxygenation of palmitic acid. These oxides, however, have quite a low surface area. We expect that catalysts with large surface area might exhibit high catalytic activity at ever lower temperature. In this regard, a porous aggregate of lepidocrocite titanate as obtained from the restacking of the colloidal nanosheets, is a potential candidate as high surface area catalysts.

Ko et al [37] has reported that hydrotalcites are active in the decarboxylation of oleic acids into fuels in the absence of hydrogen gas. The reaction was performed at 300, 350, and 400°C in an autoclave reactor. It was proposed that oleic acid and MgO reacted via saponification at low temperature. At 400°C, a 100 % conversion was achieved. Hydrotalcites are a class of layered metal hydroxides, where metal cations are coordinated to hydroxide anions, forming layer crystals. It is interesting to broaden the use of layer metal oxides to include lepidocrocite titanates in the catalytic conversion of fatty acids into fuels, and to compare results with those from layered hydroxides such as hydrotalcites

Hoelderich et al. [38] has employed Pd/C as a catalyst in the conversion of oleic acid into hydrocarbons with a continuous gas flow reactor. The catalysts were analyzed by various techniques, including surface area determination, X-ray diffraction, thermogravimetric analysis, and temperature programmed desorption. The maximum selectivity of 28.5 mol% (averaged over 4 h time on stream) to heptadecane and heptadecenes was obtained at the temperature as low as 380°C, but with a large amount of the catalyst (5 g). The use of expensive metal such as palladium stimulates the search for cheaper chemicals. We note that oxides of titanium are relatively cheap.

Ng et al. [39] has compared the decarboxylation of oleic acid (dissolved in dodecane) in both batch and flow reactor at 300°C. The total pressure was kept at 1.5 MPa under Ar gas. In a batch reactor, the agitation speed was kept at 1000 rpm. In a fixed bed tubular flow reactor, oleic acid (0.2 M in dodecane) was continuously fed through the catalyst bed. In this study we use a flow reactor to test the activity of decarboxylation; we expect that the use of a flow reactor might enhance the activity of a catalyst in this reaction.

CHAPTER 3

EXPERIMENTAL DETAILS

3.1 Reagents

1. Titanium dioxide powder (APS Ajax Finechem). 99.5%
2. Potassium hydrogen phthalate (Carlo Erba), ≥99.8 %
3. Magnesium oxide powder (Fluka), ≥98 %
4. Lithium carbornate (Acros), ≥99 %
5. Palmitic acid (Fluka), ≥97 %
6. Tetrabutylammonium hydroxide [$(C_4H_9)_4NOH$] in water, 1 M (Fluka)
7. Tetramethylammonium hydroxide [$(CH_3)_4NOH$] in water, 20wt% (Fluka)
8. Potassium chloride (Fisher scientific), ≥ 99.8 %
9. Potassium carbonate (Carlo Erba), ≥99 %
10. Hydrochloric acid, concentrated (Carlo Erba), ≥37 %
11. n-Dodecane (Merck), ≥99 %
12. Zinc oxide powder (Nano Materials Technology Co., Ltd.)
13. Nitrogen gas, high purity(99.99%), PRAXAIR
14. Hydrogen gas, high purity(99.99%), PRAXAIR
15. Helium gas, high purity(99.99%), PRAXAIR
16. Air, high purity(99.99%), PRAXAIR

3.2 Apparatus

1. Catalytic testing rig
2. Clamp
3. Furnace
4. Dewar
5. Gas chromatograph (Hewlett Packard, HP 6890 series GC system, Scientific Instrumental Service Centre, KMITL)
6. Heating tape
7. Magnetic stirrer
8. Mechanical shake

9. Oven

10. Reactor

11. Trap condenser

12. Vials

13. X-ray powder diffractometer (Rigaku, DMAX 2200/Ultima+, Faculty of Science, Chulalongkorn University)

14. Thermogravimetric analyzer (Perkin-Elmer, Scientific Instrument Service Centre, KMITL)

15. Raman spectrometer (Thermoscientific, DXR Smart Raman, College of Nanotechnology, KMITL)

16. UV-visible spectrophotometer (T60, Bangkok High LAB Co., Ltd., Scientific Instrumental Service Centre, KMITL)

17. SEM (ZEISS, EVO/MA10, College of data storage innovation, KMITL)

3.3 Experimental procedure

3.3.1 Preparation of catalyst

3.3.1.1 Solid state synthesis

Potassium carbonate was dried in and oven at 200°C for at least overnight before use. Other chemicals can be used as received. The procedure reported herein was slightly modified from that in the literature [23]. In a typical synthesis, a mixture of K_2CO_3 (5.5816 g), ZnO (3.2876 g) and TiO_2 (12.9079 g) which corresponds to the required stoichiometry for $K_{0.8}Zn_{0.4}Ti_{1.6}O_4$, was prepared and intimately mixed in a mortar for 20 minutes before being placed in an alumina crucible. The mixture was then heated at 800°C for an hour followed by the grinding. Then the mixture was re-heated at 900°C 20 hours. All the heat treatment was performed in a muffle furnace. This material will be tested as a catalyst, and will be hereafter called "pristine KZn".

The magnesium-containing lepidocrocite can be made with some modifications using the mixture of K_2CO_3 (18.2658 g), MgO (2.6639 g) and TiO_2 (21.1096 g). The mixture was heated in a tube furnace where the temperature was programmed at 800°C 1 hour (once), and 800°C 20 hours (twice), with grinding between each step. This material will be called "pristine KMg" hereafter.

The lithium-containing lepidocrocite can be made with some modifications using the mixture of K_2CO_3 (18.3332 g), Li_2CO_3 (3.3120 g) and TiO_2 (22.9234 g). The mixture was heated in a tube furnace where the temperature was programmed at 800°C 1 hour (once), and 800°C 20 hours (twice), with grinding between each step. This material will be called "pristine KLi" hereafter.

3.3.1.2 Proton exchange

Potassium ions in pristine KZn were replaced with protons by ion exchange. The solid was magnetically stirred with 1 M HCl for 3 days (solid-to-solution ratio of 1 g to 100 mL). This is the known method in the literature and was frequently utilized to prepare a variety of lepidocrocite containing proton [6]. During the ion exchange, the acid was renewed every day. After that, the solid was filtered, washed with deionized water until the solid was free from acid, and then air-dried at room temperature. The material obtained from pristine KZn is called "HZn".

3.3.1.3 Exfoliation

An amount of 0.40 g of HZn was reacted with the diluted solution of TBAOH, where the molar ratio of the TBA^+ cations in the solution to the proton in the solid equals 1 [6]. This ratio corresponds to the dilution of 1.85 mL of the commercially available 1 M TBAOH to a total volume of 100 mL with deionized water. The solid-to-solution ratio was kept at 0.4 g/100 mL. The mixture was mechanically shaken at 180 rpm for 7 days. The mixture initially comprising of solids and the clear, colorless liquid gradually transformed into a milky suspension within 7 days, indicating the exfoliation of lepidocrocite crystals into individual layers [25,40]. An exfoliation with TMAOH can be performed similarly with the adjustment to the volume taken from commercial TMAOH.

3.3.1.4 Restacking of the nanosheets

An amount of 100 mL of 2 M KOH was added dropwise into the suspension of the nanosheets, where the amount of added K^+ is in excess (e.g., 120-fold in this example) relative to that of TBA^+ (or TMA^+) in the suspension. The mixture was left standing overnight. Precipitates were filtered, washed until free from excess TBAOH (or TMAOH), as checked by

the pH measurement. The final solid was dried at room temperature overnight, giving "re-assembled KZn".

3.3.2 Characterization of lepidocrocite titanate

3.3.2.1 Structural analysis using X-ray diffraction

The crystalline phase of the materials prepared can be identified, and the corresponding unit cell parameters can be determined, using XRD measurement. The sample was ground before it was packed on the sample holder. Analysis was done employing Bruker diffractometer (Cu K α radiation, 40 kV, 30 mA), covering the range 2θ = 5-65°, at the rate of 0.02°/step and a scanning rate of 0.6 s/step.

3.3.2.2 Determination of specific surface area by nitrogen adsorption

Surface area of the catalysts can be determined by a Gas Adsorption Analyzer (Autosorb-1C, Quantachrome). Approximately, 0.01-0.05 g of the sample was loaded into the cell, which was attached to the outgassing station equipped with a heating mantle. The temperature is raised to 350°C during which the outgassing was conducted. After that, nitrogen gas was introduced to the sample cell where the adsorption can be measured at the range of the partial pressure (P/P_0) from 10^{-6} to 1.0. The adsorption isotherm and the corresponding surface area was analyzed using *BET equation* as shown in **Equation 3.1.**

$$\frac{1}{\upsilon\left[(p_0/p)-1\right]} = \frac{c-1}{\upsilon_m c}\left(\frac{p}{p_0}\right) + \frac{1}{\upsilon_m c} \qquad \text{Equation 3.1}$$

where p and p_0 are the equilibrium and the saturation pressure of adsorbates at the temperature of adsorption, υ is the adsorbed gas quantity (for example, in volume units), υ_m is the monolayer adsorbed gas quantity, and C is the *BET constant*. The concept of the theory is an extension of the Langmuir theory, which is a theory for monolayer molecular adsorption to multilayer adsorption with the following hypotheses: (a) gas molecules physically adsorb on a solid in layers infinitely; (b) there is no interaction between each adsorption layer; and (c) the Langmuir theory can be applied to each layer.

3.3.2.3 Determination of basicity by back titration

Prior to analysis, a 0.1 M primary standard solution of potassium hydrogen phthalate was prepared and employed to determine the exact concentration of the 0.1 M NaOH solution. The known concentration of this NaOH solution allows the calculation of the exact concentration of 0.1 M acetic acid used in back titration.

In back titration experiment, an amount of 25 mL of 0.1 M acetic acid was pipetted into an Erlenmeyer flask containing a known amount of lepidocrocite sample (roughly 0.05 g). The content was left unstirred for 30 minutes, after which it was carefully filtered. An aliquot of 10 mL of this filtrate was pipetted into another Erlenmeyer flask, where 2-3 drops of phenolphthalein indicator was added. This aliquot was titrated with 0.1 M NaOH solution, and the end point was reached when the solution turned from clear, colorless into faint pink. The titration was repeated by taking an aliquot of another 10 mL of the filtrate. The reported values are the average of two replicates, where the standard deviation between the two is within 5%. The basicity is expressed as the mole of acid consumed over the mass of the catalyst (mol/g).

The basicity of the blank is obtained by similar procedures except that no catalyst was added to the mixture. The blank sample would account for the change in the amount of acetic acid by the environment, such as the loss (or gain) during equilibration, filtration, etc.

3.3.2.4 Thermal stability of lepidocrocite titanate and of palmitic acid

The thermal stability of lepidocrocite samples was determined from the mass loss after being heated to high temperature, as measured by a Perkin-Elmer thermogravimetric analyzer (Pyris 1). Approximately 10 mg of lepidocrocite was loaded to the platinum plan, after which the exact mass was recorded by the instrument. The sample was then heated from room temperature to 900°C at the heating rate of 10°C/min under the flow of nitrogen gas (20 mL/min).

The thermal stability of palmitic acid can be performed similarly, with the exception that nitrogen gas was replaced with oxygen gas (50 mL/min).

3.3.2.5 Raman Spectroscopy

The powder of the sample to be investigated was manually pressed into the sample holder. Raman spectra were collected using DXR Smart Raman (Thermoscientific) at College of Nanotechnology, KMITL, from 50-4000 cm^{-1}. The laser employed has the wavelength of 532

nm, and the laser power was 5 mW. A total of 15 spectra were collected per one sample, with the exposure time of 2 s each.

3.3.3 Catalytic activity testing

The lepidocrocite catalyst was pressed, crushed, and sieved into 600-850 μm. The sieved material was subsequently packed into the glass reactor and covered by glass wool and glass bead. The schematic diagram of the reactor is shown in Figure 3.1. The reactor is positioned at the center of a vertical tube furnace. Nitrogen is used as a carrier gas, where its flow rate was controlled by a mass flow controller and was checked by a bubble flow meter. Before activity testing, the catalyst was activated by heating from room temperature to 800°C (2°C/min) and held at 800°C for an hour under the stream of air zero (20 mL/min). Then, 5% wt/wt palmitic in p-xylene was fed into the reactor by an HPLC pump at a flow rate of 0.0250 ml/min. The catalytic testing was conducted for a total time on stream (TOS) of 6 hours. The product effluents were trapped at 0°C by an ice bath and collected hourly.

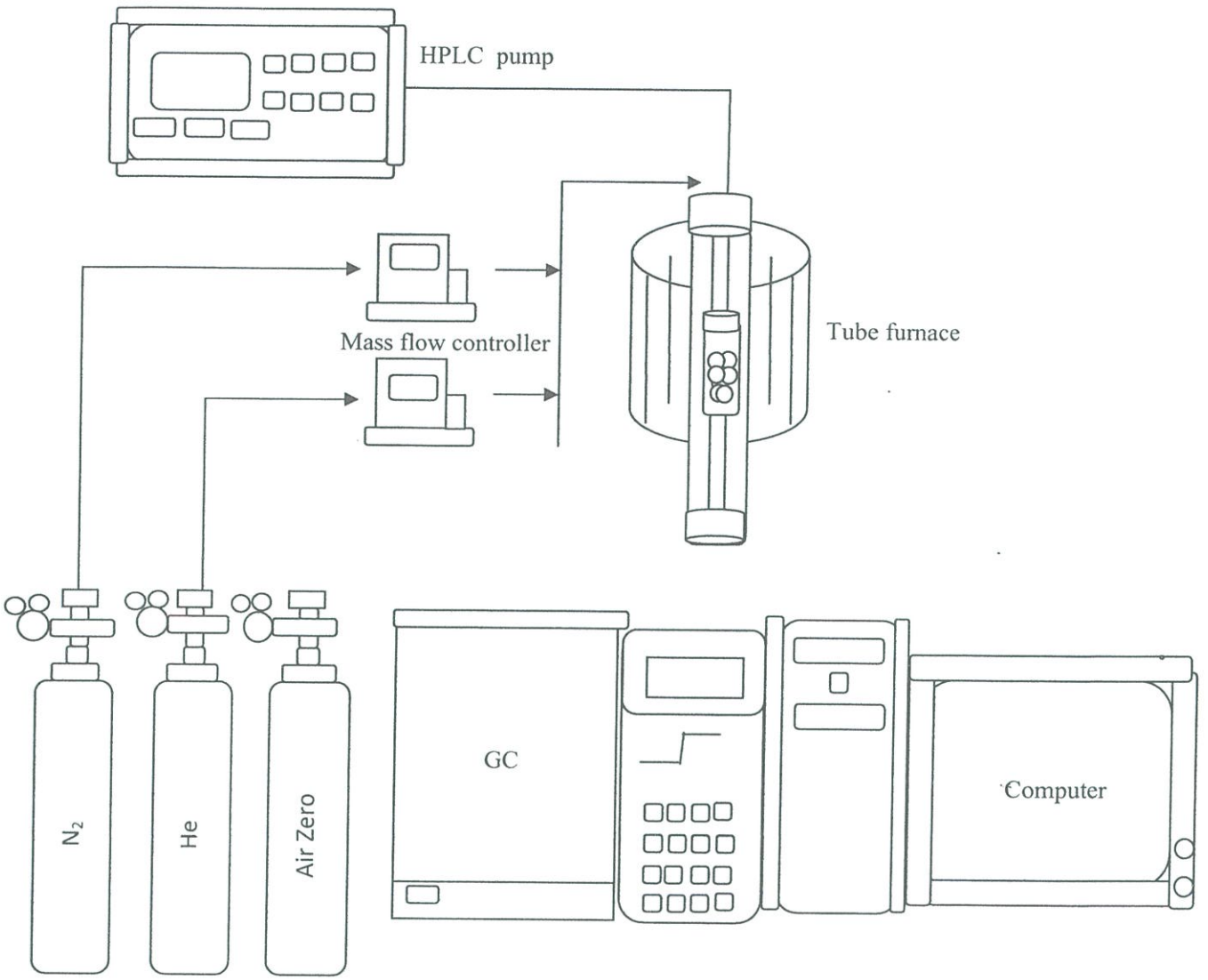

Figure 3.1 Scheme of the catalytic activity testing rig.

3.3.4 **Analysis of products**

The liquid products were analyzed by an HP6890 gas chromatograph (Hewlett-Packard) equipped with the flame ionization detector (FID) and a capillary column DB-5 (length 30 m; internal diameter 0.25 mm; film thickness 0.25 μm). The maximum temperature is 350°C, with nitrogen gas as a carrier gas. The initial temperature was set at 40°C and was held there for 10 minutes. After that, the temperature was raised to 280°C at the ramp rate of 15°C/min. The temperature was held constant at 280°C for another 60 minutes.

Gaseous products were analyzed with an online HP5890 gas chromatograph equipped with a thermal conductivity detector and a packed column. The temperature of the injection port was set at 200°C, that of the column oven at 40°C, and that of the TCD detector at 180°C. An HP 5890 gas chromatograph coupled with a mass spectrometer as a detector (GC-MS) was employed to identify the structure of the reaction products.

CHAPTER 4

RESULTS AND DISCUSSION

4.1 Characterization of catalysts

4.1.1 Solid state synthesis

A white powder $K_{0.8}Zn_{0.4}Ti_{1.6}O_4$ "pristine KZn" can be prepared by the conventional solid state synthesis as described in Chapter 3. The material possessed high crystallinity (**Figure 4.1a**) where several reflections with high intensity can be seen. The *hkl* indexes are shown atop of each peak following the previous structure determination reported in ref [41]. We obtained the unit cell parameter (based on an orthorhombic unit cell) a = 0.3812(4), b = 1.570(9), and c = 0.2987(3) nm (the standard deviation at the last digit is shown in parenthesis), in reasonable agreement with those reported in [41]. Details can be found in **AppendixA1.**

The XRD pattern shows the presence of preferred orientation, where *0k0* peaks have a higher intensity than other *hkl* peaks. This finding is typical for layered materials as the crystals tend to stack face-to-face. The absence of any other peaks indicates that there are no crystalline phases existing as an impurity in the sample. Table 4.1 compares the unit cell parameter of KZn obtained in this work vs the reported value.

The catalyst $K_{0.9}Mg_{0.45}Ti_{1.55}O_4$ "KMg" and $K_{0.8}Li_{0.27}Ti_{1.73}O_4$ "KLi" can be synthesized similarly. The respective XRD pattern is shown in Figure 4.1c and d, respectively. The general patterns are similar to the reported patterns (Groult et al. for KMg [41] and Sasaki et al. for KLi [23]. However, due to poor crystallinity of these two materials, we did not attempt the calculation of the lattice parameter. "KZn" with high crystallinity was selected for further structural modification.

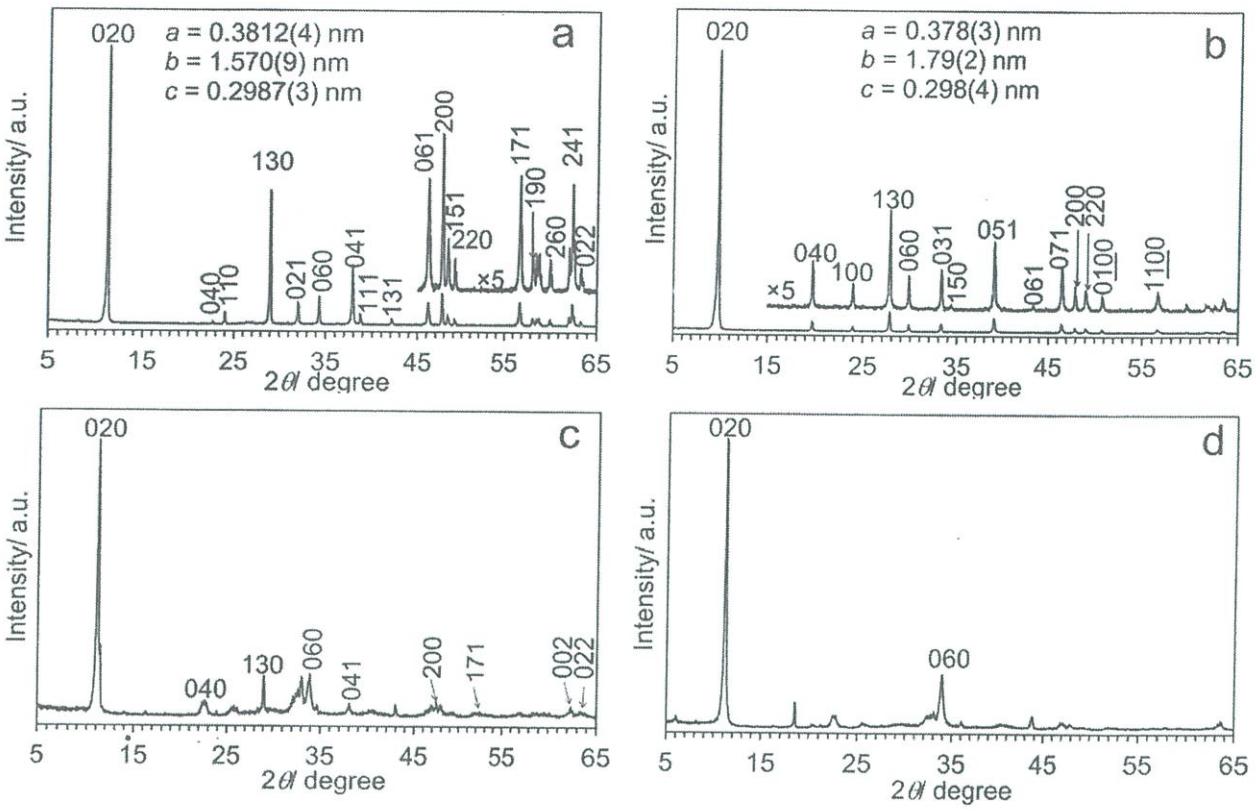

Figure 4.1 XRD pattern of (a) "pristine KZn", (b) HZn, (c) KMg, and (d) KLi.

Table 4.1: Unit cell parameters for the orthorhombic cell of KZn and HZn.

Compound	*a*/ nm	*b*/ nm	*c*/ nm
KZn pristine [41]	0.38064(5)	1.5692(5)	0.29850(5)
KZn pristine (this work)	0.3812(4)	1.570(9)	0.2987(3)
HZn (this work)	0.378(3)	1.79(2)	0.298(1)

4.1.2 Ion exchange

After ion exchange of KZn, the proton form "HZn" remained as white powder. **Figure 4.1b** shows that HZn had high crystallinity and had preferred orientation along the *b*-direction. The positions of *hkl* reflections in the XRD pattern are different from those of the pristine KZn, suggesting at least the change in the unit cell parameter. Although the proton exchange of lepidocrocite titanates of various compositions has been reported, we are not aware of the ion exchange of KZn. The product HZn can be indexed base on an orthorhombic unit cell, with a = 0.378(3), b = 1.79(2), and c = 0.298(4) nm. (Details can be found in Appendix A2.) The unit cell parameter a and c remained relatively constant from KZn to HZn, while the parameter b showed an increase of 1.79-1.57 = 0.22 nm. This means that the in-plane (*ac*) structure of lepidocrocite titanate is practically the same, and the change occurred along the *b*-direction only; that is, the ion exchange is topotactic. It has been reported that upon proton exchange of $K_{0.8}Ti_{1.73}Li_{0.27}O_4$ to $H_{1.07}Ti_{1.73}O_4 \cdot H_2O$, an increase in the b value of 0.287 nm was observed [23] and ascribed to the ion exchange of K^+ with $H^+ \cdot H_2O$. An increase in *b*-value from KZn to HZn agrees with the incorporation of $H^+ \cdot H_2O$ at the interlayer region. The presence of these species is supported by thermal analysis (below) and Raman spectroscopy (**Figure 4.7d**).

Subjecting "HZn" to high temperature resulted in two regions of the mass loss as shown in **Figure 4.2a.** The first one is from 50-100°C (9.5%) while the second one is from 120-500°C (9.0%). For lepidocrocite titanate, the first mass loss [6], is usually ascribed to water molecules intercalated between the layers, while the second one to the decomposition of layered structure into a 3D oxide (e.g., anatase). Gao *et al.* [6] reported that the acid exchange of $Cs_xZn_{x/2}Ti_{2-x/2}O_4$ (x = 0.7) resulted in protonated material with the composition $H_{2x}\square_{x/2}Ti_{2-x/2}O_4 \cdot H_2O$ (x = 0.7) where Zn^{2+} cations were leached out from the layer. In such process, two protons will be incorporated for every zinc cation removed. The starting composition in our work is $K_{0.8}Zn_{0.4}Ti_{1.6}O_4$ (or $K_xZn_{x/2}Ti_{2-x/2}O_4$ with x = 0.8), which as will be shown below, exhibited a similar behavior to $Cs_xZn_{x/2}Ti_{2-x/2}O_4$ (x = 0.7). We first propose that the proton exchange of $K_{0.8}Zn_{0.4}Ti_{1.6}O_4$ results in "HZn" with the composition $H_{1.6}\square_{0.4}Ti_{1.6}O_4 \cdot 0.8H_2O$. Then, the latter underwent following thermal transformations:

$H_{1.6}\square_{0.4}Ti_{1.6}O_4 \cdot 0.8H_2O(s) \rightarrow H_{1.6}\square_{0.4}Ti_{1.6}O_4(s) + 0.8H_2O(g)$ **(Eq. 4.1)**

$H_{1.6}\square_{0.4}Ti_{1.6}O_4(s) + 0.4O_2(g) \rightarrow 2Ti_{0.8}\square_{0.2}O_2 + 0.8H_2O(g)$ **(Eq. 4.2)**

By employing the formula weight of 156.592 g/mol for $H_{1.6}\square_{0.4}Ti_{1.6}O_4 \cdot 0.8H_2O$ and that of water for 18. the mass loss in **(Eq. 4.1)** and **(Eq. 4.2)** equals (0.8×18/156.592)×100% = 9.20% each, in agreement with the observed mass loss in the first (9.5%) and second (9.0%) step shown in **Figure 4.2a.**

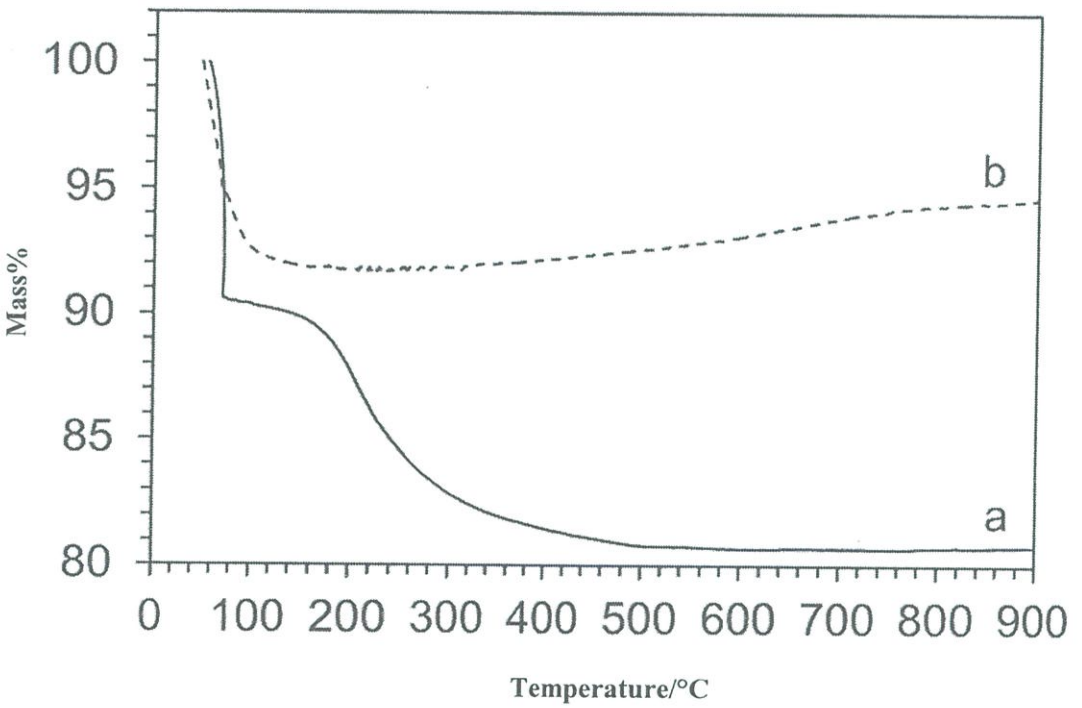

Figure 4.2 Mass loss curve of (a) "HZn", and (b) re-assembled/non-calcined KZn (exfoliated with TBAOH).

Alternatively, if we assume that the proton exchange of $K_{0.8}Zn_{0.4}Ti_{1.6}O_4$ resulted in $H_{0.8}Zn_{0.4}Ti_{1.6}O_4 \cdot H_2O$ where protons exchanged only with potassium cations, and that zinc cations remained in the layer, relevant transformations could be:

$H_{0.8}Zn_{0.4}Ti_{1.6}O_4 \cdot H_2O(s) \rightarrow H_{0.8}Zn_{0.4}Ti_{1.6}O_4(s) + H_2O(g)$ **(Eq. 4.3)**

$H_{0.8}Zn_{0.4}Ti_{1.6}O_4(s) \rightarrow Zn_{0.4}Ti_{0.8}O_2 + 0.8TiO_2(s) + 0.4H_2O(g)$ **(Eq. 4.4a)**

$H_{0.8}Zn_{0.4}Ti_{1.6}O_4(s) \rightarrow 1.6TiO_2(s) + 0.4ZnO(s) + 0.4H_2O(g)$ **(Eq. 4.4b)**

Equation 4.3 would result in a mass loss of (18/185.556)×100% = 9.7% in fair agreement with the observed value for the first mass loss, considering that the number of water molecule in **(Eq. 4.3)** was roughly set to 1. However, reactions **(Eq. 4.4a)** or **(Eq. 4.4b)** would give a mass loss of only (0.4×18/185.556)×100% = 3.9%, far from the observed value of 9.0%. Therefore, the presence of zinc in "HZn" is unlikely. Elemental analysis confirming the absence of Zn in "HZn" will be beneficial in confirming this assignment.

4.1.3 Exfoliation

Exfoliation of stacks of HZn into individual elementary layers was accomplished by the mechanical shaking of HZn with either TBAOH (180 rpm) or TMAOH (80 rpm) for 7 days. In all cases, the starting mixture containing white powder and clear, colorless TBAOH (or TMAOH) liquid gradually changed into a white suspension. The Tyndall effect was observed for all suspensions after the shaking for 7 days as shown in the inset of Figure 4.3. The suspension scattered the light (from the laser pointer) throughout its content. Such a colloidal suspension indicates the separation of stacks of titanate layers into individual, elementary layers known as nanosheets [23]. Therefore, it can be inferred that pristine KZn was exfoliated into individual layers upon the reaction of the proton-exchanged form HZn with TBAOH (or TMAOH).

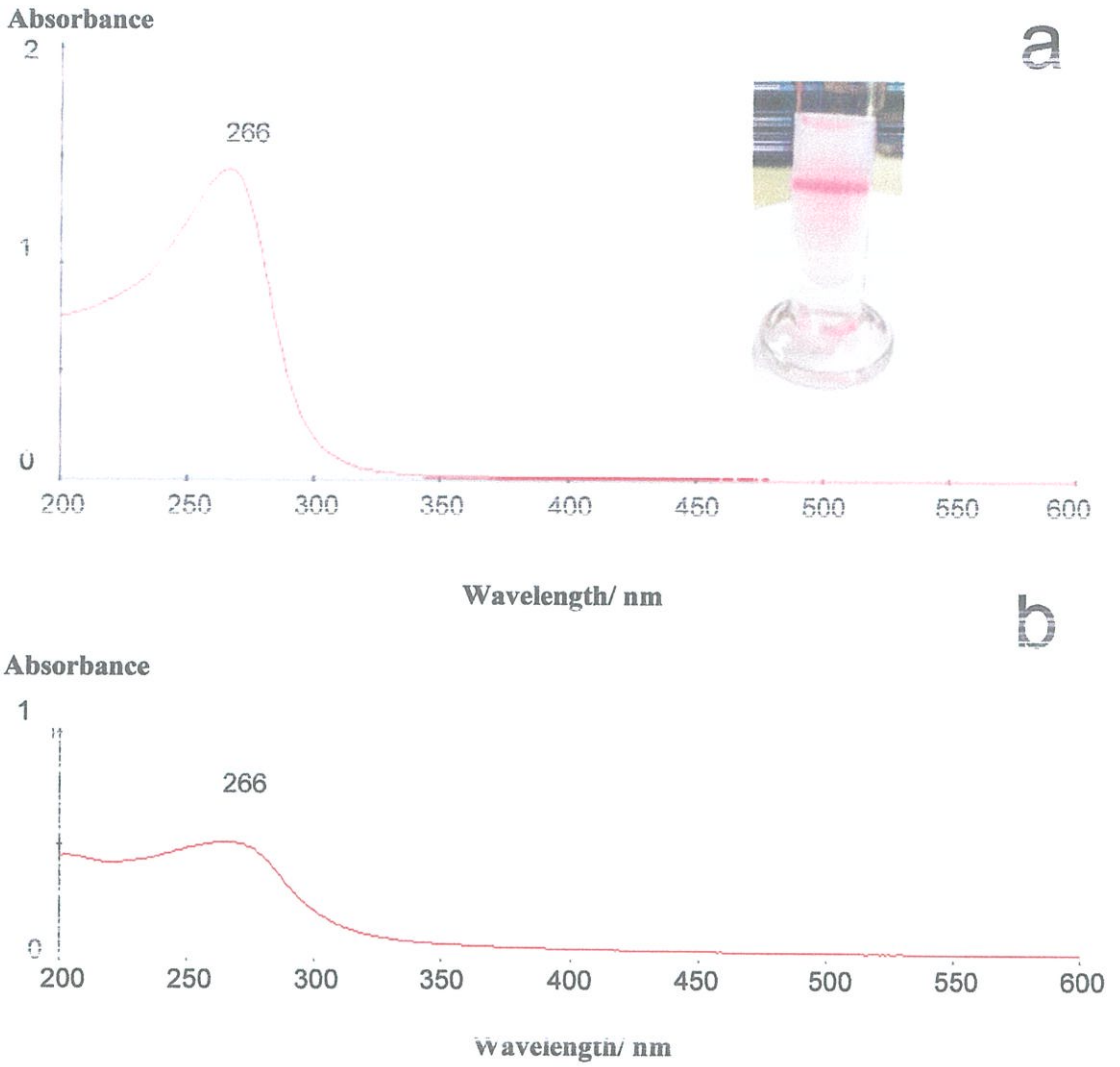

Figure 4.3 UV-visible spectrum of titanate suspension at a nominal concentration of 0.008 g/L, prepared from the mechanical shaking of HZn with (a) TBAOH, and (b) TMAOH.Inset in (a) is a representative photograph showing the Tyndall effect of titanate nanosheets (nominal concentration 4 g/L) prepared via the mechanical shaking of HZn with TBAOH at 180 rpm for 7 days.

The obtained suspension at the nominal concentration of 4 g/L was diluted to a concentration of 0.008 g/L before subjecting to an analysis by UV-vis spectroscopy. As shown in **Figure 4.3a** and **b**, the suspension showed λ_{max} at 266 nm regardless of the type of tetraalkylammonium cations used. This value is similar to that reported for nanosheets prepared from $Cs_{0.7}Ti_{1.825}\square_{0.175}O_4$ and exfoliated with TBAOH [42], indicating the similarity in the electronic structure of titanate nanosheets.

The particle size of nanosheets in the suspensions was analyzed by dynamic light scattering (DLS). This technique assumes rigid, spherical colloidal particles which do not represent the thin, flexible nanosheets. However, it is a quick and easy method of characterizing the "size" of colloidal particles. Each suspension was analyzed six times and the values were averaged **(Figure 4.4)**. We found the particle size of the nanosheets prepared by TMA^+ to be in the range 2-7 μm, while that by TBA^+ is relatively homogeneous at ~400 nm. The larger size of nanosheets made with TMA^+ relative to that with TBA^+ is in agreement with previous report with $K_{0.8}Ti_{1.73}Li_{0.27}O_4$. The lower mechanical stress (due to the intercalation of smaller TMA^+cations) results in relative larger nanosheets. On the other hand, larger cations such as TBA^+ create a larger mechanical stress to the crystals, leading to their fracture and consequently smaller nanosheets [25].

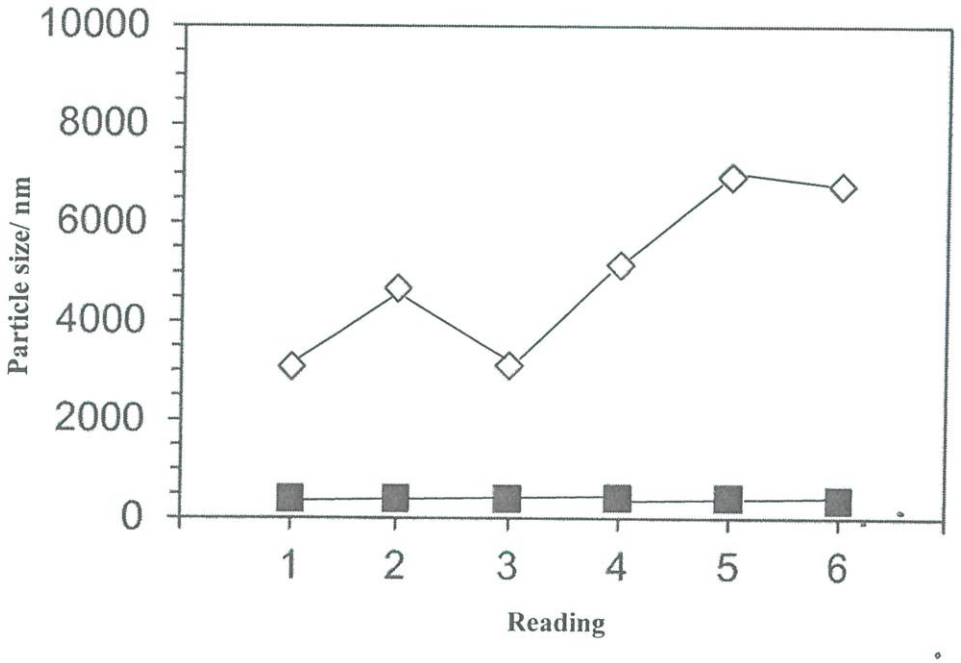

Figure 4.4 Particle sizes of nanosheets from the reaction with TMAOH or TBAOH as determined from DLS. Each suspension was analyzed 6 times.(◊ TMAOH, ■ TBAOH)

4.1.4 Restacking

Restacking was accomplished by the dropwise addition of 2 M KOH into the titanate suspension containing exfoliated nanosheets. Upon addition of KOH, The large amount of K^+ cations (in this work the molar ratio of K^+/(tetraalkylammonium cation) = 116) compete with tetraalkylammonium cation in adsorption onto the surface of the negatively charged nanosheets. The electrostatic attraction between K^+ cations and nanosheets is stronger than that between

TBA^+ (or TMA^+) and nanosheets, resulting in "re-assembled KZn". The recovered sample was approximately 90% of the theoretical amount.

Thermogravimetric analysis (**Figure 4.2b**) on the re-assembled KZn (exfoliated with TBAOH) showed ~7% mass loss, which we ascribed to intercalated water molecules. This assignment will be discussed further below based on XRD results. As the testing for catalytic activity will be performed at high temperature (375-400°C), all catalysts were calcined at 450°C for 2 h before further characterization. The re-assembled materials (**Figure 4.5c, d**) are white powder similar to pristine KZn (**Figure 4.5a**) and HZn (**Figure 4.5b**). These photographs show that different materials at the same weight occupy different volumes. KZn appears to be the one with the highest density. HZn greatly swelled, likely due to the incorporation of water molecules. The restacked/calcined KZn also occupied a larger volume, reflecting the porous nature compared to pristine KZn.

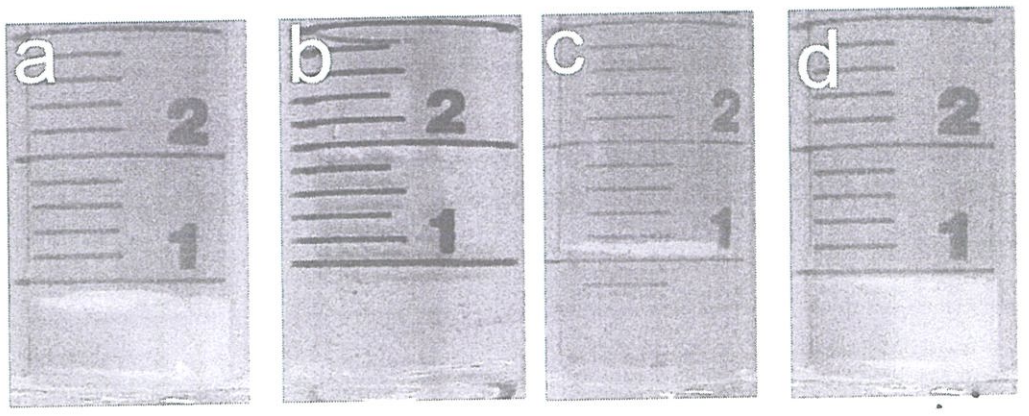

Figure 4.5 Photographs showing the appearance of (a) pristine KZn, (b) HZn, (c) re-assembled/ calcined KZn (exfoliated from TMAOH), and (d) re-assembled/calcined KZn (exfoliated from TBAOH). Each sample weighted 1 g.

Figure 4.6a showed the XRD pattern of the as-made, re-assembled KZn (exfoliated with TBAOH), with the strongest peak at 9.8° 2θ, corresponding to d = 0.90 nm. Compared to the pristine KZn with d = 0.78 nm, this finding indicates the expansion of 0.12 nm likely due to the inclusion of water as $K(H_2O)_n^+$ between the layers. Although this pattern is similar to that of HZn which shows the strongest peak at d = 0.90 nm too, the restacking with H^+ in the presence of excess KOH is unlikely due to the basic pH of the reaction mixture. The other peaks are at 2θ = 19.3°, 28.9°, 48.3° and 62.8° correspond to d = 0.459, 0.309, 0.188 and 0.148 nm

respectively. The ratio of peak positions relative to d = 0.90 nm of the first peak is roughly 1/2, 1/3, 1/5 and 1/6. Therefore, all the peaks in **Figure 4.6a** can be indexed (from left to right) as 010, 020, 030, 050 and 060, suggesting the preferred orientation along the *b*-direction. Other *hkl* peaks are not observed, likely reflecting the disorder in other directions as a result of restacking.

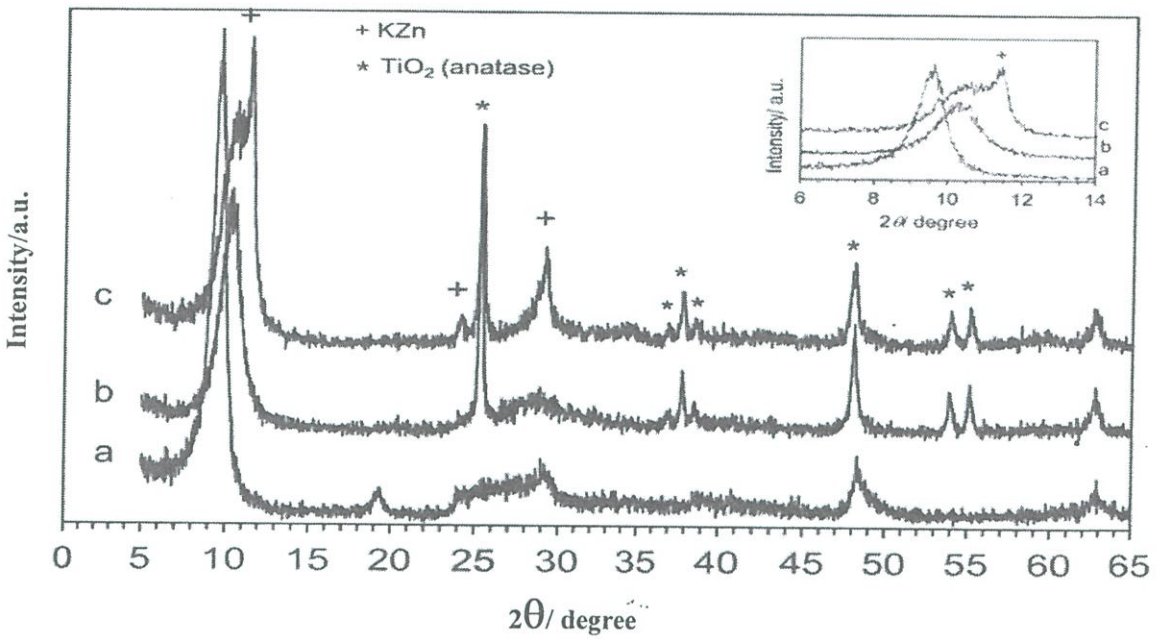

Figure 4.6 XRD pattern of restacked KZn from the exfoliation with TBAOH without (a) or with calcination (b); and from the exfoliation with TMAOH with calcination (c). Inset shows the zoom in from 2θ= 6-14°.

Upon heat treatment to make the re-assembled/calcined KZn (exfoliated with TBAOH), a series of sharp peaks emerged as shown in **Figure 4.6b**, characteristics of TiO_2 anatase. Therefore, part of Ti of the as-made, restacked KZn left the TiO_6 octahedra in the layer and transformed into anatase upon calcination at 450°C for 2 h. As shown in the inset of **Figure 4.6,** the first peak after calcination is at 2θ = 10.34° (or d = 0.85 nm) contracted from the value in the as-made material, but still slightly larger than d = 0.78 nm in pristine KZn. This suggests that TiO_2 form might be between the layer and acts as a pillar.

Figure 4.6c shows the XRD pattern for re-assembled KZn (exfoliated with TMAOH) after calcination. This material comprises of 3 phases, namely the one with d = 0.85 nm, TiO_2 anatase, and pristine KZn (labeled in the Figure by the symbol +). It is interesting to see how different materials, which might contain more than one crystalline phase, would act as a catalyst toward palmitic acid deoxygenation.

The crystallite size along the stacking direction can be calculated from Scherrer's equation, employing the FWHM of the strongest *0k0* peak. Results are shown in **Table 4.2.** The crystallite size greatly decreased from 40-50 nm in the pristine KZn (and HZn) to only 5 nm in restacked material (exfoliated with TBAOH) after calcination. The reduction in the crystallite is as expected [6]. As the XRD pattern for re-assembled material (exfoliated with TMAOH) after calcination (**Figure 4.6c**) greatly overlapped with the peak of KZn, we did not calculate the crystallite size for this sample. Additionally, employing FWHM at 2θ around 25.3°, the crystallite size of anatase was calculated to be 26.3 nm and 30.3 nm for re-assembled/calcined KZn exfoliated from TBAOH and TMAOH respectively.

Table 4.2: Crystalline size of catalysts prepared.

Composition	.FWHM/ degree	Crystalline size/ nm
$K_{0.8}Zn_{0.4}Ti_{1.6}O_4$ "Pristine KZn"	0.160	49.9
HZn	0.188	42.4
Re-assembled/as-made KZn (exfoliated with TBAOH)	1.045	12.9
Re-assembled/calcined KZn (exfoliated with TBAOH)	1.453	5.4

The Raman spectrum of $Cs_{0.7}Ti_{1.65}Ni_{0.35}O_4$ has been reported by Gao *et al.* [43] to show peaks at 192, 279, 375, 435, 552 (very weak), 645, 732 and 835 cm^{-1}. Pristine KZn (**Figure 4.7a**) showed the peak at 115, 141, 190, 280, 373, 433, 654, 750 and 819 cm^{-1}, all match well with the reported position except the first two peaks (115 and 141 cm^{-1}) which were more or less present in that work with different intensity from us, but the position was not reported. Similarly, $H_{0.7}Ti_{1.825}\square_{0.175}O_4 \cdot H_2O$ showed the peak at 183, 270, 387, 449, 558, 658, 704, 803 (very weak) and 908 (very weak) cm^{-1} [44]. The Raman spectrum for HZn (**Figure 4.7d**) shows peaks at the 115 (weak), 181, 270, 381, 446, 560, 722 and 914 cm^{-1}, matched well those reported. The peak at 115 cm^{-1} present in HZn might be too low in intensity to be detected in $H_{0.7}Ti_{1.825}\square_{0.175}O_4 \cdot H_2O$, while the peaks at 803 and 908 cm^{-1} present in $H_{0.7}Ti_{1.825}\square_{0.175}O_4 \cdot H_2O$ might be too low in intensity to be detected in HZn. In short, the Raman spectra collected for pristine KZn and HZn confirms the assignment of lepidocrocite-type structure as observed by XRD results.

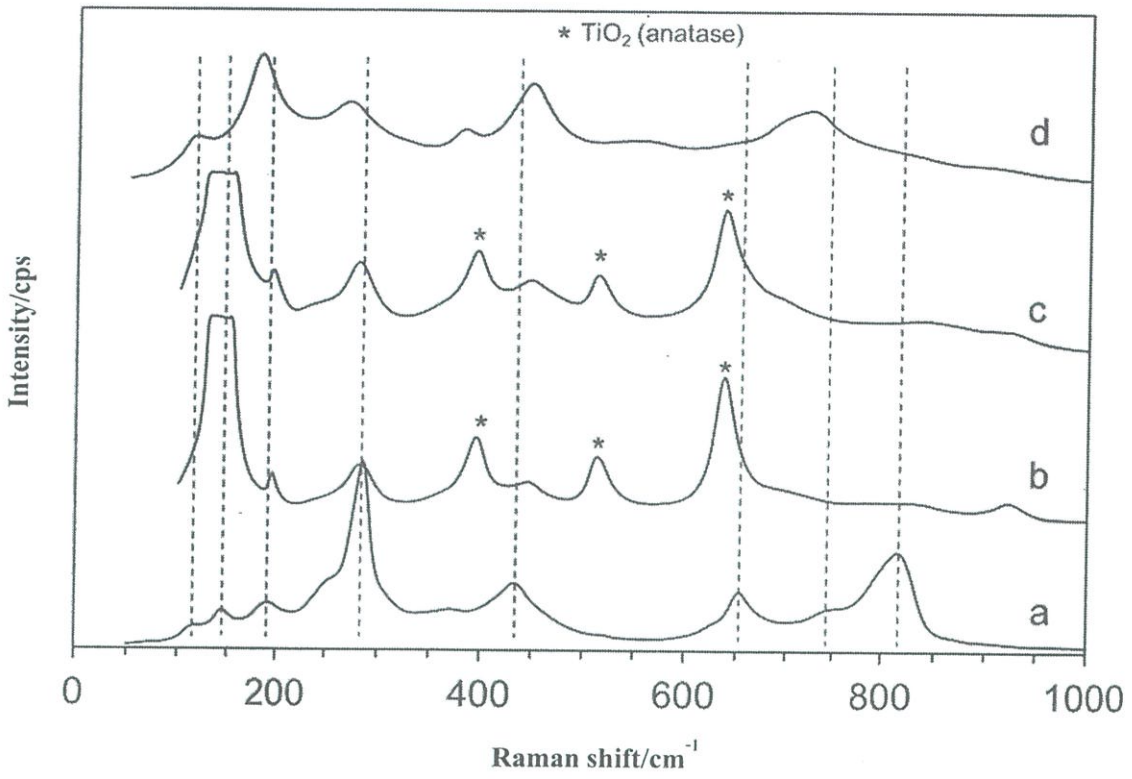

Figure 4.7 Raman spectra of (a) pristine KZn, (b) re-assembled/calcined KZn (exfoliated with TBAOH), (c) re-assembled/calcined KZn (exfoliated with TMAOH), and (d) HZn.

Raman spectrum of re-assembled/calcined KZn (obtained from the exfoliation by TBAOH) is shown in **Figure 4.7b**. The presence of anatase as found in XRD is confirmed by Raman bands marked with the asterisk (*). The band at 100-600 cm^{-1} in this sample is more or less similar to that in pristine KZn with some modifications to the relative intensity, thereby confirming the short-range order where TiO_6 octahedra are linked forming 2D lepidocrocite-layer. The peak at 819 cm^{-1} in pristine KZn was ascribed to Ti-O vibration sticking out into the interlayer regions [45]. The absence of this peak in the calcined/re-assembled sample could be due to the fact that K^+ cations reside in the environment different from that in pristine KZn as a result of a restacking process. A detailed assignment of Raman spectra of re-assembled KZn awaits further investigation. The Raman spectrum of re-assembled/calcined KZn (obtained from the exfoliation by TMAOH) in **Figure 4.7c** shows similar features to that in **Figure 4.7b** just mentioned.

4.1.5 Textural properties

Table 4.3 shows surface area and pore volume of catalysts prepared. Upon exfoliation and restacking, the surface area of KZn has increased by 7-9 times, and the pore volume has increased by 7-10 times, in agreement with larger volume of the solid for the same mass (**Figure 4.5**). For pristine lepidocrocite with different compositions, the surface area is in the order: $K_{0.8}Ti_{1.73}Li_{0.27}O_4$ > $K_{0.7}Mg_{0.35}Ti_{1.65}O_4$ > $K_{0.8}Zn_{0.4}Ti_{1.6}O_4$. This different might reflect the intrinsic textural property of each crystal.

Table 4.3: Surface area, pore volume and pore size of catalysts prepared.

Catalyst	Surface area (m^2/g)	Pore volume (cm^3/g)
$K_{0.8}Zn_{0.4}Ti_{1.6}O_4$ "Pristine KZn"	3.1	0.012
Re-assembled/calcined KZn (exfoliated with TBAOH)	27.7	0.114
Re-assembled/calcined KZn (exfoliated with TMAOH)	21.7	0.085
$K_{0.7}Mg_{0.35}Ti_{1.65}O_4$	12.9	0.039
$K_{0.8}Ti_{1.73}Li_{0.27}O_4$	28.2	0.041

Figure 4.8a shows the SEM image of pristine KZn. The layered-nature of crystallites with tightly-stacked layers is visible (see the circle in **Figure 4.8a**.) The size of the crystallites can be up to 4 μm. In the exfoliation of HZn with TMAOH, the "size" of nanosheets was found to be 2-7 μm (**Figure 4.4**). As TMA^+ cations have a small ionic size, the exfoliation by TMA^+ is thought to preserve the lateral size of the crystals. Therefore, the "size" of crystallites (seen by SEM) vs that of nanosheets (determined by DLS) is in the same order of magnitude. Upon proton exchange to HZn, the two dimensional nature is preserved together with the expansion of the layers (**Figure 4.8b**). This result is as expected considering the change in the interlayer spacing from d = 1.57 nm in KZn to 1.79 nm in HZn. **Figure 4.8c** shows the irregular nature of re-assembled/calcined KZn. The loosely-stacked nature of this material is in agreement with the expectation. The rough surface could be due to the presence of TiO_2 (anatase) as found from XRD, although its presence cannot be confirmed confidently by SEM.

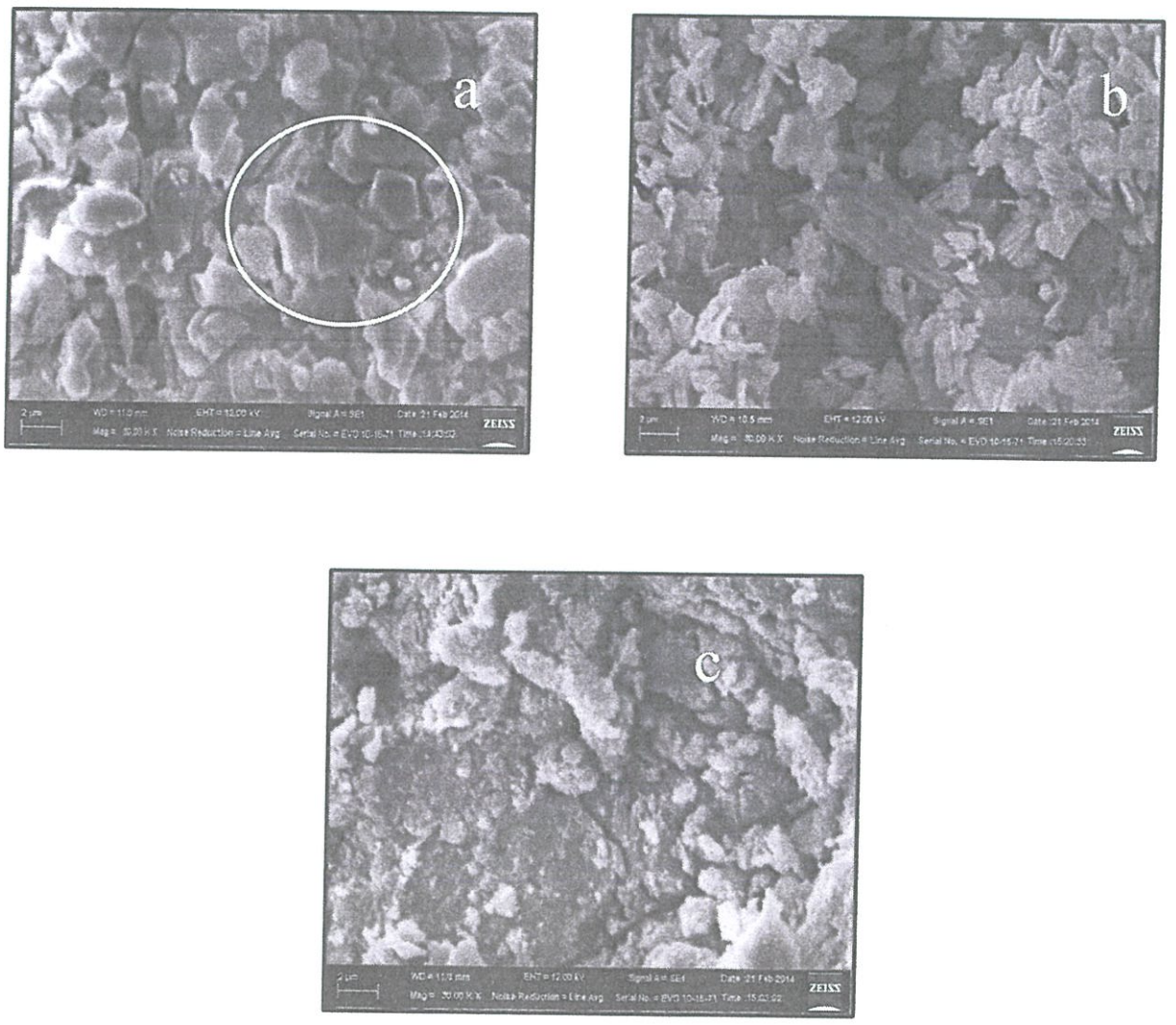

Figure 4.8 SEM images of (a) pristine KZn, (b) HZn and (c) re-assembled/calcined KZn (exfoliated with TBAOH). All scale bars are 2 μm.

4.1.6 Basicity

Table 4.4 shows the basicity of prepared materials after the solids were soaked into acetic acid. The amount of acetic acid neutralizing basic sites on the surfaces was determined by back-titration with sodium hydroxide, in the unit of mmol/g. It can be seen that the basicity of restacked KZn increases by ~3-6 fold from the pristine KZn. For pristine lepidocrocite of different compositions, the basicity is in the order: $K_{0.8}Li_{0.27}Ti_{1.73}O_4$ > $K_{0.9}Mg_{0.45}Ti_{1.55}O_4$ > $K_{0.8}Zn_{0.4}Ti_{1.6}O_4$. This order is as expected as cations of group I (e.g., Li) and group II (e.g., Mg) are considered more basic than transition metals (such as Zn).

Table 4.4: Basicity of various catalysts prepared

Catalyst	Basicity (mmol/g)
$K_{0.8}Zn_{0.4}Ti_{1.6}O_4$ "pristine KZn"	1.15
Re-assembled, calcined KZn (exfoliated with TMAOH)	4.07
Re-assembled, calcined KZn (exfoliated with TBAOH)	6.78
$K_{0.9}Mg_{0.45}Ti_{1.55}O_4$	2.57
$K_{0.8}Li_{0.27}Ti_{1.73}O_4$	3.59
Hydrotalcite	8.40

4.2 Deoxygenation of palmitic acid over lepidocrocite titanates.

The deoxygenation of palmitic acid via ketonization over pristine KZn lepidocrocite titanate catalyst was studied in a fixed bed flow reactor. The liquid products were analyzed by GC-FID and identified by GC-MS. The product distribution obtained from the reaction over the pristine KZn at various contact time (W/F) are shown in **Figure 4.9.**

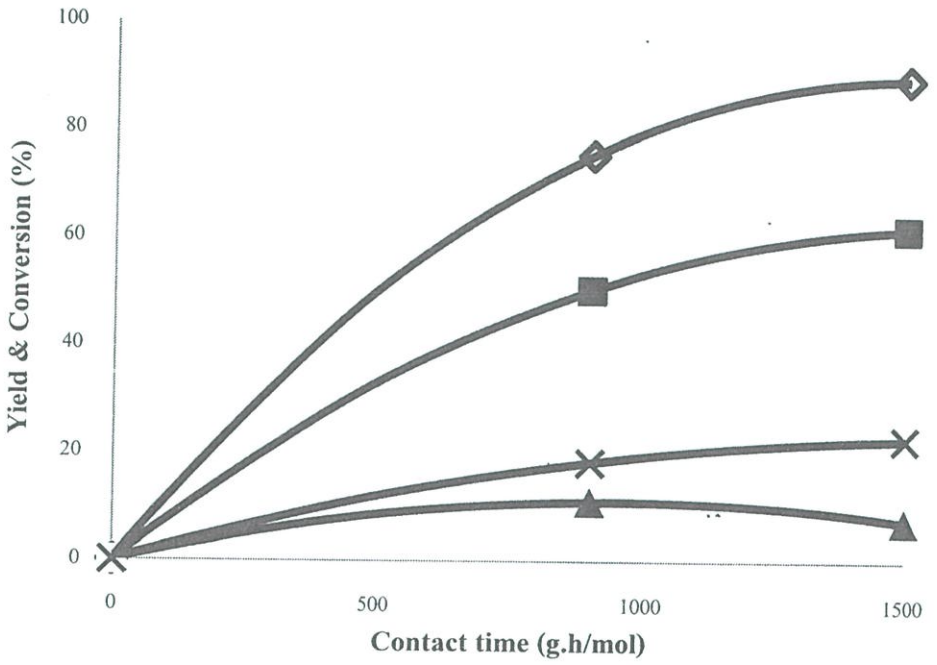

Figure 4.9 Conversion and yield of products from the reaction of palmitic acid over pristine $K_{0.8}Zn_{0.4}Ti_{1.6}O_4$, as a function of contact time time (W/F). Conversion (◊), C-31 ketone (■), Cracking ketone (▲), Hydrocarbon (✕).

Reaction conditions : 375°C, 15 ml/min of N_2, 5% palmitic acid in p-xylene, contact time 900 and 1500 g.hr/mol.

It can be seen from **Figure 4.9**, that the conversion was increased with contact time (W/F), since the activity is in proportion with the number of active sites. As number of active site is increased, yields of product are also increased as shown in **Table 4.5.**

Table 4.5: Product distribution from reaction of palmitic acid over pristine KZn at various contact time.

	W/F(g·h/mol)	
	900	1500
Conversion	72.43	85.6
product distribution		
C-31 Ketone	47.3	58.6
C-17 Ketone	4.9	4.2
Heavy ketone & Alcohol	5.0	2.9
Total hydrocarbon (Unsat./Sat.)	15.0 (1.9)	17.7 (2.6)
C-14	8.9 (2.2)	11.8 (3.4)
C-13	1.9 (4.0)	2.2 (4.9)
C-12	1.0 (0.6)	1.2 (0.6)
C-11	0.6 (1.1)	0.8 (14.0)
C-10	1.7 (2.6)	0.7 (3.1)
< C-10	0.9	1.0
gas product yield (%)	0.2	2.2

Reaction conditions : 375°C, 15 ml/min of N_2, 5% palmitic acid in p-xylene, contact time 900 and 1500 g.h/mol.

It can be seen that C-31 ketone is the main product for the reactions. It is suggested that C-31 ketone is formed by ketonization of palmitic acid on the Ti-O-Ti surface. This reaction is resulted from the coupling of surface palmitates. One of the adsorbed palmitic acid could be enolized and readily undergo nuecleophilic attack to another adjacent palmitate to yield the β-ketoacid [44]. Such intermediate can then decarboxylate to from C-31 ketone and CO_2, as demonstrated in **Figure 4.**

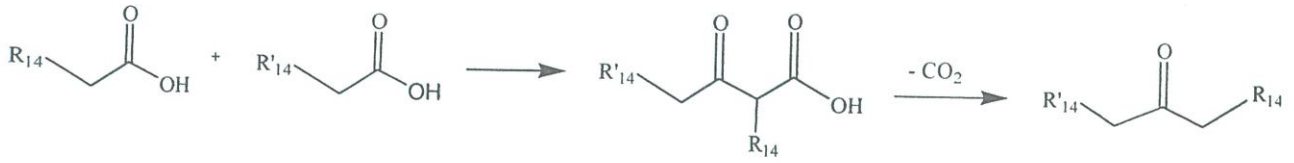

Figure 4.10 Ketonization of palmitic acid.

The decomposition of β- ketoacid is evidenced by the observed CO_2 in the gas products. as shown in **Figure 4.11.** In addition hydrocarbon gas is obtained from the reaction.

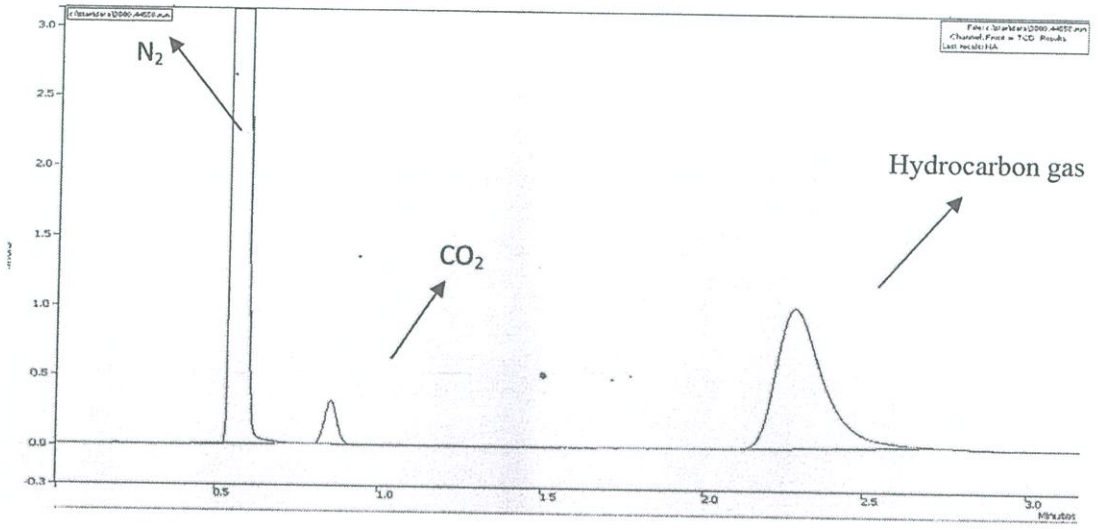

Figure 4.11 Chromatogram of gas product from deoxygenation of palmitic acid over the re-assembled/calcined KZn (exfoliated with TBAOH).

It is interesting that high conversion is obtained despite the pristine KZn has extremely low surface area (~$3m^2/g$). If the reaction occurred only at the surface, a low conversion should be expected. Hence, it is suggested that the reaction does not take place only at the external surface of the catalyst. The palmitic acid may diffuse into the crystal interlayer and undergo ketonization. This is supported by an observed increase in crystallite size of pristine KZn after the reaction (**Figure 4.12**).

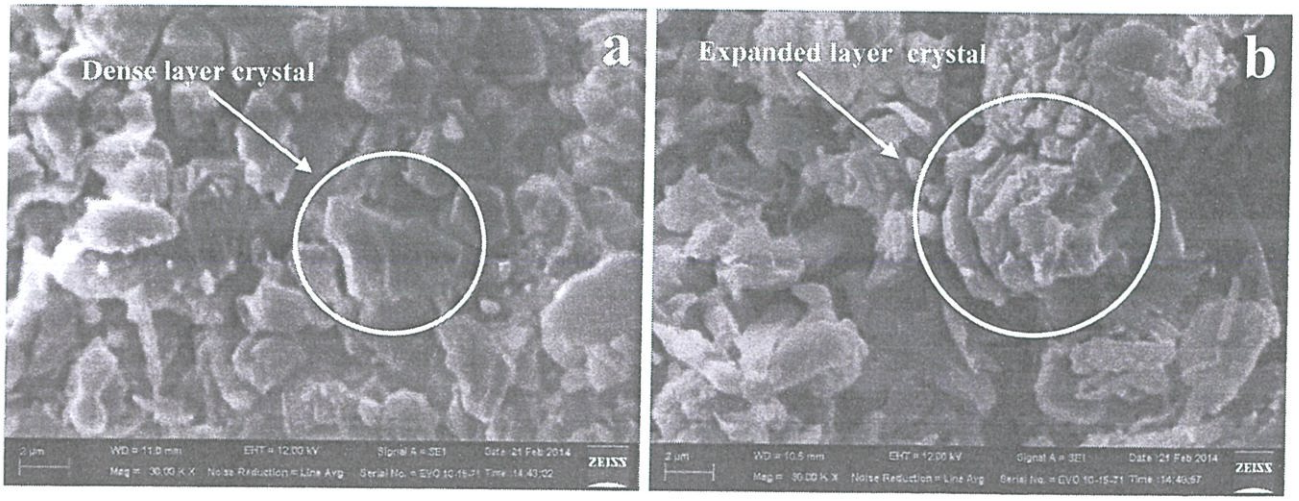

Figure 4.12 SEM of pristine KZn a) before run reaction, b) after run reaction.

It can be seen from **Figure 4.12** that the dense layer is expanded and pristine KZn crystal appeared to be larger. This implies that the palmitic acid may diffuse into the interlayer of pristine KZn and interacts with the internal exchangeable alkaline cations, that posseses strong basicity. Accordingly ketonization of palmitic acid can be largely promoted in the interlayer, as seen by such a high conversion.

In addition to C-31 ketone, C-17 ketone and hydrocarbons especially C-14 long chain hydrocarbons are also obtained (**Table 4.5**). It is not possible that C-17 ketone is directly produced form the palmitic acid (C16 carboxylic acid). The most likely argument is that C-17 ketone is cracked from C-31 ketone. This is because cracking at C17-C18 position of C-31 ketone can be easily promoted by intramolecular H-transfer to the carbonyl group, as demonstrated in **Figure 4.13.**

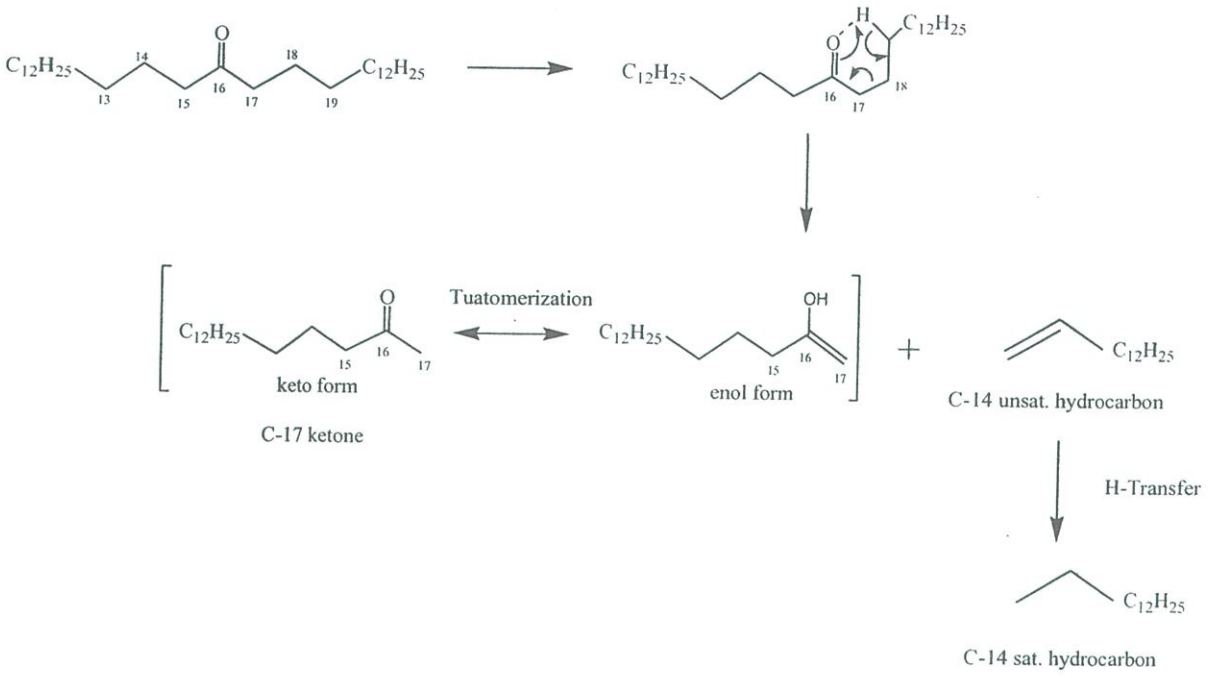

Figure 4.13 Cracking of C-31 ketone to form C-17 ketone and C-14 long chain hydrocarbons.

In a support manner, C-14 long chain hydrocarbons are especially obtained. Moreover, these C-14 long chain hydrocarbons were mainly unsaturated, as shown in **Table 4.5**. The observed saturated hydrocarbon is produced by H-transfer from the coke formation, that can be evidenced by the deactivation of the catalyst, as shown in **Figure 4.14.**

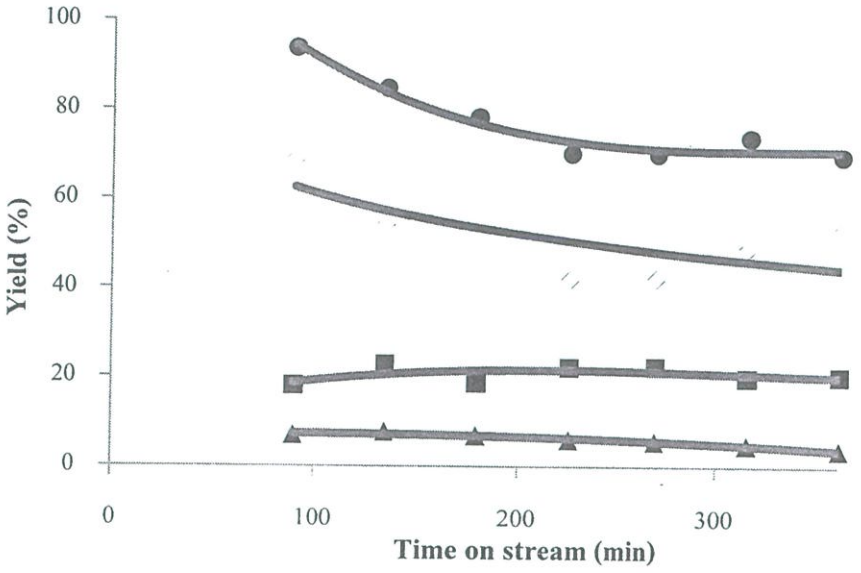

Figure 4.14 Conversion and yield of products from the reaction of palmitic acid over pristine KZn as a function of cont tactime (W/F). Conversion (●), C-31 ketone (◊), Cracking ketone (▲), Hydrocarbon (■).

Reaction conditions : 375°C, 15 ml/min of N_2, 5% palmitic acid in p-xylene, contact time 1500 g.h/mol.

It is worth mentioned that heavy ketone and hydrocarbons smaller than C-14 were also produced (**Table 4.5**). This indicates that C-31 ketone can be cracked at other positions. As the primary product (C-31 ketone) was initially formed and trapped in the interlayer that possess strong basic sites, cracking of such intermediate can be particularly promoted at high temperature.

As discussed above, C-14 long chain hydrocarbons and C-17 ketones were obtained in parallel from the cracking of C-31 ketone. Hence yield of C-14 long chain hydrocarbons should be the same as that C-17 ketones. However, higher yield of C-14 long chain hydrocarbons was observed, as compared to that of C-17 ketone. This indicates that C-14 long chain hydrocarbon is not produced only by cracking of C-31 ketones, but also from the deacetylation of palmitic acid, as shown in **Figure 4.15**.

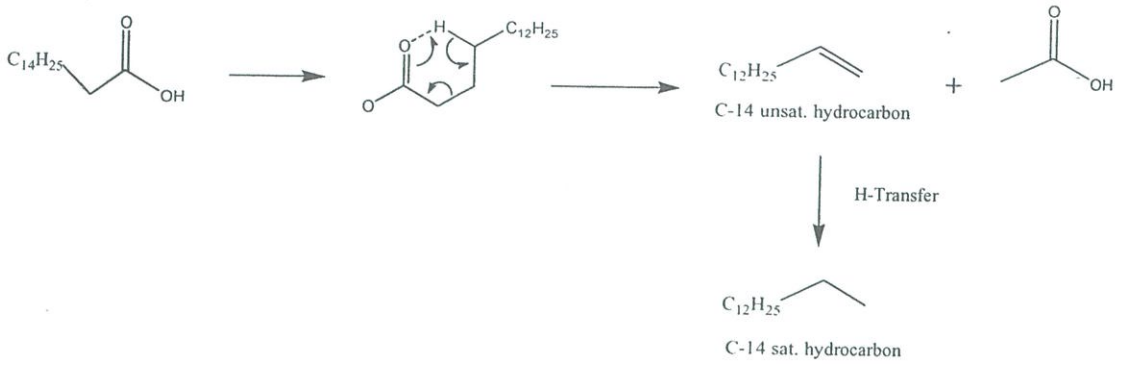

Figure 4.15 Deacetylation of palmitic acid to form C-14 unsatuated hydrocarbon.

The palmitate species can undergoes deacetylation by β carbon-carbon bond cleavage to form C-14 unsaturated hydrocarbons and acetic acid, that could be decomposed to coke, CO_2, CO and water. As discussed earlier, C-14 unsaturated hydrocarbons can be saturated by H-transfer from the coke and even cracked to lower molecular weight hydrocarbons.

From the above observation and discussion, the overall reaction pathway for deoxygenation of palmitic acid over lepidocrocite titanates can be proposed, as depicted in **Figure 4.16.**

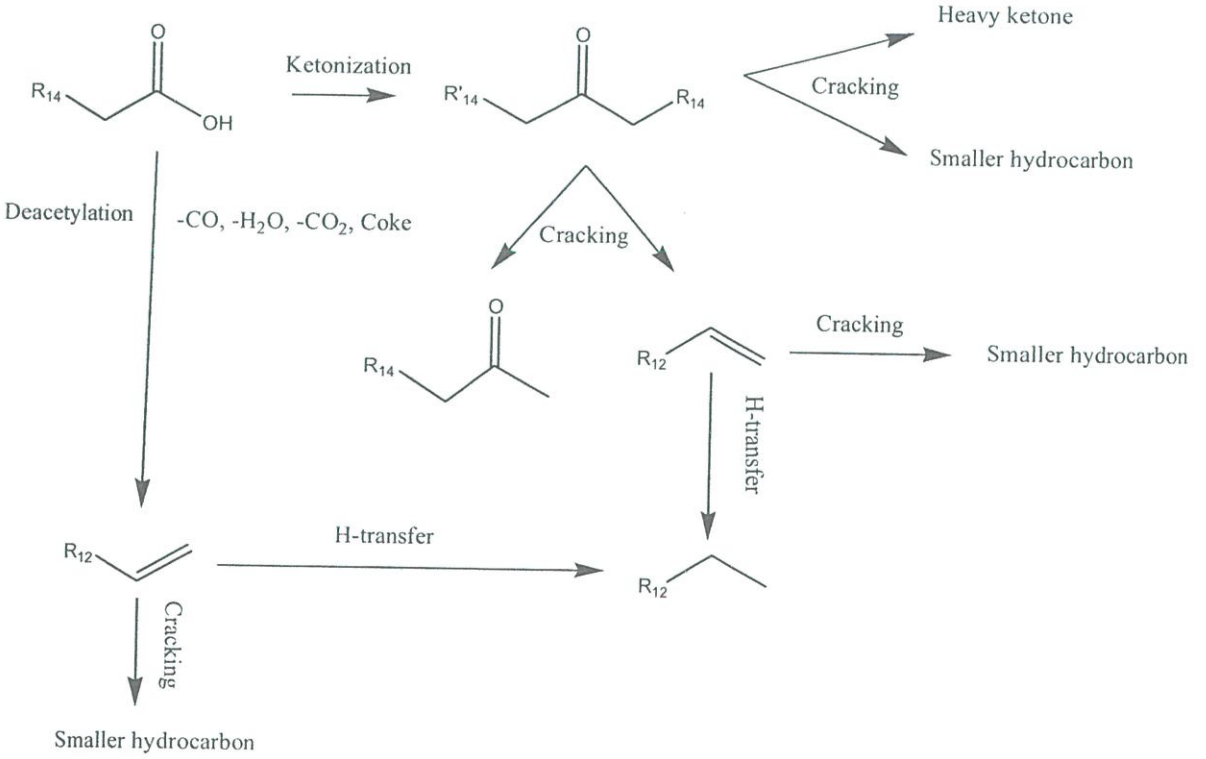

Figure 4.16 Proposed overall reaction of palmitic acid over lepidocrocite titanate.

Although the coke formation is continuously formed over the catalyst, deactivation is observed only for ketonization as shown in (**Figure4.17a**). The cracking activity is retained as seen by stable yields of hydrocarbons (**Figure 4.18b**).

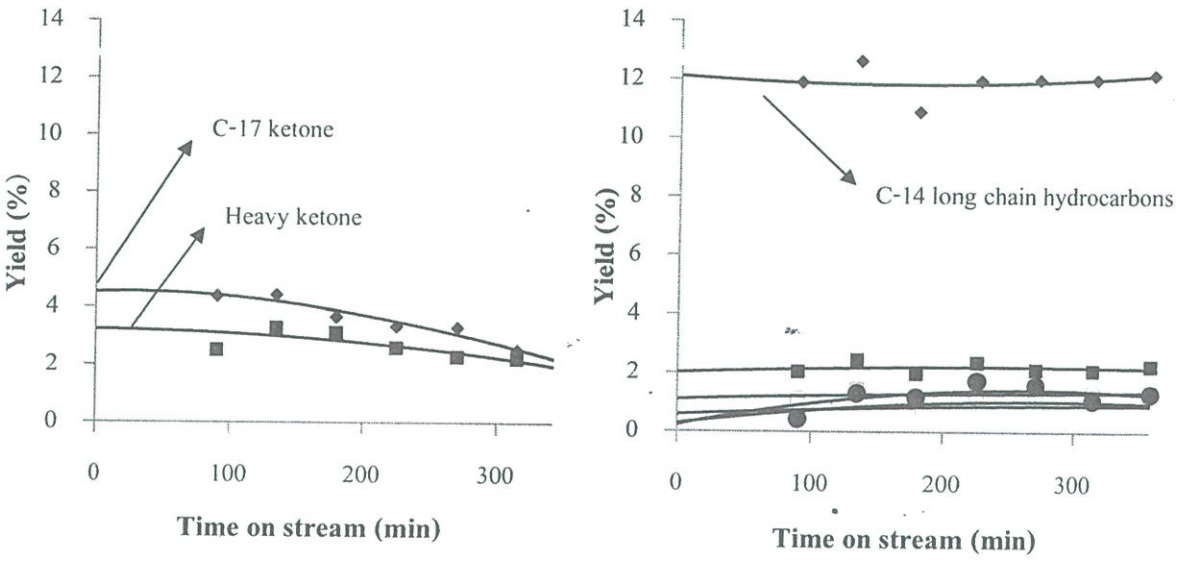

Figure 4.17 Yield of products from the reaction of 5 % wt palmitic acid over lepidocrocite titanate ($K_{0.8}Zn_{0.4}Ti_{1.6}O_4$). (◆) C-17 ketone, (■) heavy ketone (a), (◆) C-14, (■) C-13, (□) C-12, (✱) C-11, (△) C-10, (●) light hydrocarbon (b).

Reaction conditions: 375 °C, 1 atm, 15 ml/min of nitrogen, 5 % palmitic acid in p-xylene, contact time 1500 g.h/mol.

It is clear that lepidocrocite possesses oxygen vacancy that promotes ketonization to form larger molecular weight product (i.e. C-31 ketone). Such high molecular weight species can be decomposed and deposited on the oxygen vacancy sites leading to catalyst deactivation. While the basic sites of the catalyst promote cracking of C-31 ketone or long chain hydrocarbons to produce smaller molecular weight product such as C-17 ketone and C-14 long chain hydrocarbons and light hydrocarbons. These species can be easily diffuse out of the interlayer leaving the active basic site for further cracking.

As the palmitic acid was diffused and reacted with catalyst in the interlayer. The re-assembled $K_{0.8}Zn_{0.4}Ti_{1.6}O_4$ catalyst were tested to understand the effect of layer structure on the reaction, as shown in **Table4.6.**

Table4.6: The product distribution of deoxygenation over pristine $K_{0.8}Zn_{0.4}Ti_{1.6}O_4$, re-assembled $K_{0.8}Zn_{0.4}Ti_{1.6}O_4$(TMA) and re-assembled $K_{0.8}Zn_{0.4}Ti_{1.6}O_4$ (TBA)

	W/F(g.h/mol)		
	1500	1500	1500
Catalyst	KZn	KZn(TMA)	KZn(TBA)
Conversion	85.6	96.6	96.1
Product distribution			
C-31 ketone	58.6	58.3	66.7
C-17 ketone	4.2	15.1	13.6
Heavy ketone & alcohol	2.9	2.05	0.8
Total hydrocarbon	17.7	15.3	11.5
C-14	11.8	8.4	4.8
C-13	2.2	2.6	1.9
C-12	1.2	1.8	1.5
C-11	0.8	1.2	0.9
C-10	0.7	1.3	1.7
< C-10	1.0		0.7
gas product	2.2	2.9	3.5

Reaction conditions: 375°C, 1 atm, 15 ml/min of N_2, 5% palmitic acid in p- xylene, contact time 1500 g.h/mol

It can be seen that the re-assembled catalyst ($K_{0.8}Zn_{0.4}Ti_{1.6}O_4$ (TMA) and $K_{0.8}Zn_{0.4}Ti_{1.6}O_4$ (TBA)) that contain incomplete layer shows a conversion higher than that over pristine $K_{0.8}Zn_{0.4}Ti_{1.6}O_4$ catalyst that possesses dense layers. This is because the re-assembled catalyst has surface area higher than that of pristine $K_{0.8}Zn_{0.4}Ti_{1.6}O_4$ catalyst. Moreover, XRD pattern of the re-assembled catalyst shows additional TiO_2 anatase phase (section : characterization). The presence of anatase phase can promote ketonization as evidenced by high yield of C-31 ketone. However, yield of cracking product is relatively low for the re-assembled catalyst. This is because the primary product (C-31 ketone) is mainly formed on the external surface (i.e. TiO_2 antase) of the catalyst. Accordingly, C-31 ketone can be easily desorbed from the catalyst

surface without further cracking. It is cleared that the layer structure play significant role on selectivity to long chain hydrocarbon.

As the basicity is responsible for cracking of C-31 ketone to hydrocarbons, alkaline and alkaline earth cations are doped into lepidocrocite and the product distribution of the deoxygenation of palmitic acid over these catalysts ($K_{0.8}Li_{0.27}Ti_{1.73}O_4$ and $K_{0.9}Mg_{0.45}Ti_{1.55}O_4$) are shown in **Table4.7.** For a comparison, reaction over hydrotalcite (Mg, Al) is also investigated.

Table 4.7: The product distribution of basicity effect

	W/F(g.h/mol)			
	1500	1500	1500	1500
Catalyst	KZn	KLi	KMg	HT2.5
Conversion	85.6	97.9	96.5	96.9
Product distribution				
C-31 ketone	58.6	39.2	41.5	35.5
C-17 ketone	4.2	20.5	18.1	20.8
Heavy ketone & alcohol	2.9	2.9	10	16.2
Total hydrocarbon	17.7	34.5	26.5	22.6
C-14	11.8	20.7	16.5	2.4
C-13	2.2	3.5	2.8	7
C-12	1.2	2.6	1.8	3.7
C-11	0.8	1.7	1.5	2.4
C-10	0.7	3.1	2.9	2.1
< C-10	1	2.9	1	5
gas product	2.2	0.7	0.4	1.8

Reaction conditions: 375°C, 1 atm, 15 ml/min of N_2, 5% palmitic acid in p- xylene, contact time 1500 g.h/mol.

It can be seen that lepidocrocite containing Li and Mg in the layer ($K_{0.8}Li_{0.27}Ti_{1.73}O_4$ and $K_{0.9}Mg_{0.45}Ti_{1.55}O_4$) shows a relatively higher conversion, as compared to that over pristine $K_{0.8}Zn_{0.4}Ti_{1.6}O_4$ catalyst. This is because incorporation of alkaline and alkaline earth cations in the lepidocrocite would result in higher basicity of the catalyst. This is evidenced by basicity

measurement as shown in **Table 4.4**. Hence, palmitic acid can readily adsorb and activated on the $K_{0.8}Li_{0.27}Ti_{1.73}O_4$ and $K_{0.9}Mg_{0.45}Ti_{1.55}O_4$catalyst.

Accordingly, yield of C-31 ketone is relatively low while higher yield of hydrocarbon is obtained, as compared with those over pristine $K_{0.8}Zn_{0.4}Ti_{1.6}O_4$ catalyst. This suggests that C-31 ketone can be cracked over the additional basic sites of the $K_{0.8}Li_{0.27}Ti_{1.73}O_4$ and $K_{0.9}Mg_{0.45}Ti_{1.55}O_4$ catalysts. It is worth noting that, over these basic lepidocrocite, yield of C-17 ketone is similar to that of C-14 long chain hydrocarbons. This indicates that these species are directly obtained from cracking of C-31 ketone. Hence, the observed yield of smaller hydrocarbons shall not be obtained only from C-31 ketone cracking. This is inconsistent with the observed low yield of heavy ketone over $K_{0.8}Li_{0.27}Ti_{1.73}O_4$ and $K_{0.9}Mg_{0.45}Ti_{1.55}O_4$ catalysts. It is likely that C-14 long chain hydrocarbons can be additionally produced from deacetylation of palmitic acid and undergo cracking to short chain hydrocarbon as observed. Moreover, the reaction over $K_{0.8}Li_{0.27}Ti_{1.73}O_4$ give a relative higher activity to short chain hydrocarbons, as compared to $K_{0.9}Mg_{0.45}Ti_{1.55}O_4$. This is because the basicity of $K_{0.8}Li_{0.27}Ti_{1.73}O_4$ is higher than that of $K_{0.9}Mg_{0.45}Ti_{1.55}O_4$ **(Table 4.4).**

It is noteworthy that, $K_{0.8}Li_{0.27}Ti_{1.73}O_4$ and $K_{0.9}Mg_{0.45}Ti_{1.55}O_4$ show higher activity and activity and selectivity to hydrocarbon products, as compared to the typical basic catalyst, such as hydrotalcite. This is due to the presence of the dense layer that control cracking of C-31 ketone to C-17 ketone and C-14 long chain hydrocarbons. While hydrotalcite that contain no layer structure after calcination (XRD pattern) gives a hydrocarbon product selectivity, similar to the re-assembled catalyst ($K_{0.8}Zn_{0.4}Ti_{1.6}O_4$ (TMA) and $K_{0.8}Zn_{0.4}Ti_{1.6}O_4$ (TBA)).

Despite the alkaline and alkaline earth cations doped into the titanate layer of lepidocrocite plays important role for cracking C-31 ketone to hydrocarbon, there is certain amount of C-31 ketone remained in the product mixture from the reaction at 375°C. Accordingly, the reaction at high temperature (400°C) may well enhance cracking of such ketone, as shown in **Table 4.8.**

Table 4.8: Conversion and yield of product from deoxygenation at different temperature.

	Reaction temperature (°C)	
	375	400
W/F (g·h/mol)	1500	1500
Conversion	98.1	100.0
Product distribution		
C-31 Ketone	39.3	28.5
C-17 Ketone	20.5	24.2
Heavy ketone	2.9	3.1
Total hydrocarbon (Unsat. / Sat.)	34.5 (4.4)	45.6 (4.7)
C-14	20.7 (11.0)	27.2 (7.4)
C-13	3.5 (8.0)	4.5 (9.8)
C-12	2.6 (0.5)	3.7 (0.5)
C-11	1.7 (1.7)	1.9 (2.3)
C-10	3.1 (1.8)	3.7 (0.7)
Light hydrocarbon	3.1	4.6
Gas product yield (%)	0.9	2.5

Reaction conditions: 1 atm, 15 ml/min of nitrogen, 5%wt palmitic acid in p-xylene, contact time 1500 g.h/mol

It can be seen that the reaction, at higher temperature promotes higher cracking activity. This is supported by an observed higher yield of all hydrocarbon products while C-31 ketone is decreased at high temperature. It is also interesting that C-14 long chain hydrocarbons yield is higher than the C-17 ketone. This suggests that deacetylation of palmitic acid is additionally promoted at high temperature. It is noted that yield of unsaturated hydrocarbon is relatively higher than that of the saturated hydrocarbon. This is because at high temperature H-transfer is limited as the coke formation are decreased. The relatively low deactivation can be explained by a better desorption of the products from the interlayer at high temperature. This can be supported by a better stability of the reaction at 400°C, as shown in **Figure 4.18.**

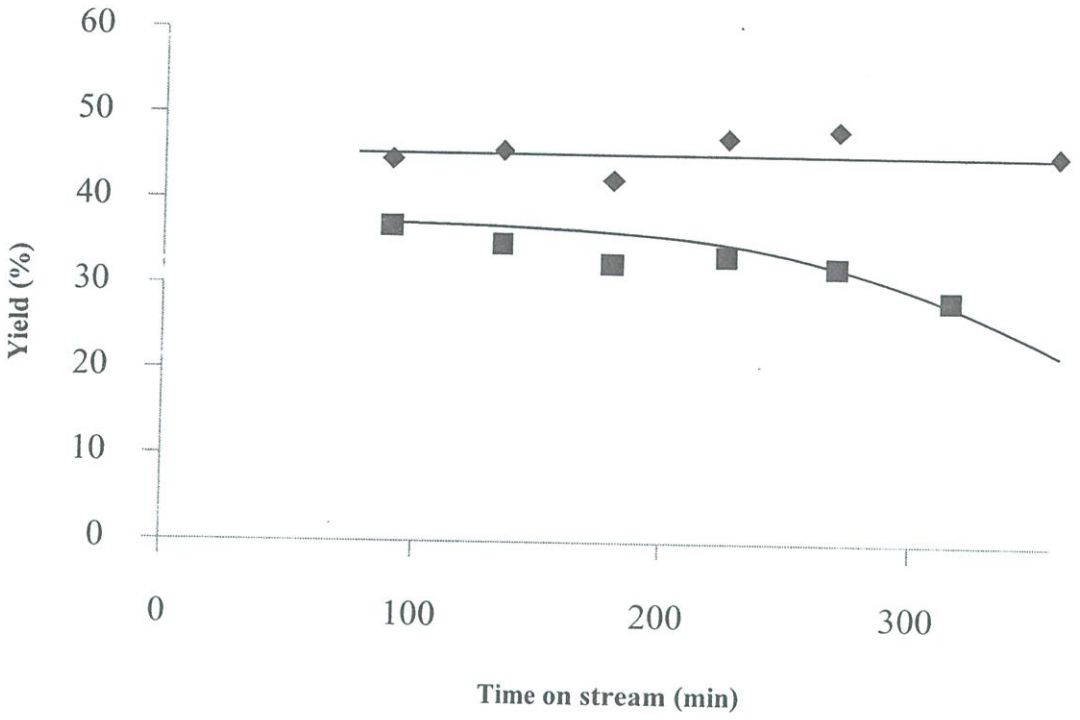

Figure 4.18 Yield of hydrocarbon products at temperature (■) 375°C, (◆) 400°C.

CHAPTER 5

CONCLUSION AND SUGGESTION

5.1 Conclusion

The lepidocrocite ($K_{0.8}Zn_{0.4}Ti_{1.6}O_4$, $K_{0.8}Li_{0.27}Ti_{1.73}O_4$, $K_{0.9}Mg_{0.45}Ti_{1.55}O_4$) were prepared by the conventional solid state synthesis. The pristine $K_{0.8}Zn_{0.4}Ti_{1.6}O_4$ possessed high crystallinity while $K_{0.8}Li_{0.27}Ti_{1.73}O_4$ and $K_{0.9}Mg_{0.45}Ti_{1.55}O_4$ showed lower crystallinity. When Li and Mg cations were incorporated into lepidocrocite titanates, The basicity and surface area increased. $K_{0.8}Zn_{0.4}Ti_{1.6}O_4$ was converted into the protonic form $H_{0.8}\square_{0.4}Ti_{1.6}O_4 \cdot H_2O$ before subjecting to the exfoliation with either TBAOH or TMAOH. The particle size of the nanosheets prepared by TMA^+ is in the range of 2-7 μm while that by TBA^+ is approximately 400 nm. As the exfoliated sample were restacked, the re-assembled lepidocrocite contained anatase TiO_2 phase after calcination. The basicity and surface area of the re-assembled titanates were higher than that of the pristine $K_{0.8}Zn_{0.4}Ti_{1.6}O_4$.

The deoxygenation of palmitic acid to produce long chain hydrocarbons was carried out in the fixed bed reactor. Palmitic acid was primarily ketonized to C-31 ketone, which was then cracked to C-17 ketone and C-14 long chain hydrocarbons. Deacetylation of palmitic acid to C-14 long chain hydrocarbons and cracking to smaller hydrocarbon were also observed. Study of contact time showed that the conversion and yields of hydrocarbon products increased with the number of active sites. Deoxygenation can take place at both interlayer and external surface of the catalyst. Deactivation of the catalyst was observed only for ketonization since high molecular weight species were deposited mainly on the oxygen vacancy sites. The re-assembled $K_{0.8}Zn_{0.4}Ti_{1.6}O_4$ showed a relatively higher activity for deoxygenation, as compared to the pristine $K_{0.8}Zn_{0.4}Ti_{1.6}O_4$. The anatase phase present in the re-assembled titanates played an important role in the conversion of palmitic acid to C-31 ketone. On the other hand, the re-assembled titanates gave lower yield of C-14 long chain hydrocarbons, as compared to the

pristine $K_{0.8}Zn_{0.4}Ti_{1.6}O_4$. This was due to the lack of ordered interlayer structure that was responsible for cracking activity and selectivity to hydrocarbons. High basicity and high surface area of the $K_{0.8}Li_{0.27}Ti_{1.73}O_4$ and $K_{0.9}Mg_{0.45}Ti_{1.55}O_4$ resulted in high activity and yield of C-14 long chain hydrocarbons. Moreover, the presence of dense layers controlling cracking of C-31 ketone, leads to an improved selectivity to hydrocarbon, when compared to calcined hydrotalcite 2.5 without a layer structure. The reaction at higher temperature (400°C) dose not only gives high activity in deoxygenation to hydrocarbon, but also decrease the deactivation rate. In addition, deacetylation of palmitic acid can be enhanced at high temperature.

5.2 Suggestion

5.2.1 The reduction of lepidocrocite titanates catalyst could be performed to generate a higher concentration of oxygen vacancy. Which might promote the ketonization of palmitic acid.

5.2.2 The catalyst with different alkali and alkaline earth loading should be investigated, in order to verify the role of basicity on the yield of long chain hydrocarbon.

REFERENCES

[1] A. Kawashima, K. Matsubara, K. Honda. "Development of heterogeous base catalysts for biodiesel production." Bioresource Technology., vol.99, 2008. pp. 3439-3443.

[2] A. Zhang, Q. Ma, K. Wang, X. Liu, P. Shuler, Y. Tang. "Naphthenic acid removal from crude oil through catalytic decarboxylation on magnesium oxide." Applied Catalysis A., vol. 3039, 2006. pp. 103-109.

[3] B.Q. Xu, H.P. Wang, S.H. Chai, Y. liang. "Sustainable production of acrolein: Gas-phase dehydration of glycerol over Nb_2O_5 catalyst." Journal of Catalysis., vol. 250. pp. 342-349.

[4] J.V. Gerpen. "Biodiesel processing and production" Fuel Processing Technology., vol. 86, 2005. pp. 1097-1107.

[5] F. Ma, M.A. Hanna. "Biodiesel production: a review." Bioresource Technology., vol. 70, 1999. pp. 1-15.

[6] T. Gao, H. Fjellvag, P. Norby. "Defect chemistry of a Zinc-Doped Lepidocrocite Titanate $Cs_xTi_{2-x/2}Zn_{x/2}O_4$ (x=0.7) and its protonic Form." Chemistry of materials., vol. 21, 2009. pp. 3503-3513.

[7] T. Sasaki, M. Watanabe, Y. Michive, Y. Komatsu, F. Izumi, S. Takenovchi. "Preparation and Acid Base Properties of a Protonated Titanate with the Lepidocrocite-like Layer Structore." Chemistry of materials., vol. 7, 1995. pp. 1001-1007.

[8] R.J. Maria, F.M. Carmen, C. Abraham, R. Lourdes and P. Angel. "Influence of fatty acid omposition of raw materials on biodiesel properties" Bioresource Technology, vol.100, 2009. pp.261-268

[9] Elmhurst college. "Fatty Acids"

[Online]: http://www.elmhurst.edu/_chm/vchembook/551fatty acida.html.

[10] A. baca. "Animal fat as fuel alternative" [Online] : http://www.polimerieuropa.com/ 200page.lasso.html.2001

[11] "Fatty acid" [Online] : http://en.wikipedia.org/wiki/Fatty_acid

[12] S. Taweesin. "linear long chain hydrocarbon s from deoxygenation of palmitic acid over metal oxides." Master Thesis, KMITL. 2010. pp. 4.

[13] J. Beare-Rogers, A. Dieffenbacher and J.V. Holm. "Lexicon of lipid nutrition (IUPAC Technical Report)." Pure applied chemistry., vol.73, 2001. pp. 685-744.

[14] E. Freìmy. "Memoire sur les produits de la saponification de l'huile de palme." Journal de Pharmacie et de Chimie XII., 1842. pp. 757.

[15] E. Fischer. "esterification" [Online] : http://en.wikipedia.org/wiki/Esterification

[16] S. Chongkhong, C. Tongurai, P. Chetpattananondh and C. Bunyakan. "Biodiesel production by esterification of palm fatty acid distillat" Biomass and Bioenergy, vol.31. 2007. pp. 563-568.

[17] "deoxygenation"[Online] : http://en.wikipedia.org/wiki/Deoxygenation

[18] P. Mki-Arvela, M. Snre, K. Ernen, J. Myllyoja and D.Y. Murzin. "Continuous decarboxylation of lauric acid over Pd/C catalyst" Fuel, vol.87,2008. pp. 3543-3549.

[19] H. Hattori, Catalysts in Petroleum Refining & Petrochemicals, Dhahran, Saudi Arabia. "Solid Base Catalysts: Fundamentals and Applications" 2010.

[20] U. Schuchardta, R. Serchelia and R.M. Vargas, Instituto de Química, Universidade Estadual de Campinas, C.P. 6154,13083-970 Campinas - SP, BrazilbInstituto de Química, Universidade Federal da Bahia, Campus de Ondina. "Transesterification of Vegetable Oils : a Review" 1997. pp. 40170-290.

[21] D.G. Cantrell, L.J. Gillie, A. F. Lee and K. Wilson. "Structure-reactivity correlations in MgAl hydrotalcite catalysts for biodiesel synthesis" Applied Catalysis A: General, vol. 287, 2005. pp. 183–190.

[22] Y.B. Wang, J.M. Jehng. "Hydrotalcite-like compounds containing transition metals as solid base catalystsfor transesterification" Chemical Engineering Journal, vol. 175, 2011. pp. 548 554.

[23] T. Sasaki, F. Kooli, M. Iida, Y. Michiue, S. Takenouchi, Y. Yajima, F. Izumi, B.C. Chakoumakos and M. Watanabe. "A Mixed Alkali Metal Titanate with the Lepidocrocite-like Layered Structure. Preparation, Crystal Structure, Protonic Form, and Acid-Base Intercalation Properties" Chemistry of Materials, 1998, 10, 4123-4128.

[24] H. Song, A.O. Sjastad, Ø.B. Vistad, T. gao and P. Norby. "Preparation of Nb-substituted titanates by a novel sol-gel assisted solid state reaction" Inorganic Chemistry, vol. 48, 2009. pp. 6952-6959.

[25] T. Maluangnont, K. Matsuba, F. Geng, R. Ma, Y. Yamauchi and T. Sasaki. "Osmotic Swelling of Layered Compounds as a Route to Producing High-Quality Two-Dimensional Materials. A Comparative Study of Tetramethylammonium versus Tetrabutylammonium Cation in a Lepidocrocite-type Titanate" Chemistry of Materials, 25, 2013, 3137.

[26] G. Navarro, R. Acevedo, A. Soto, M. Herane. "Synthesis and characterization of Lepidocrocite and its potential applications in the adsorption of pollutant species" Journal of Physics, vol. 134, 2008. pp. 12 -23.

[27] M. Leo´n, E. Dı´az, S. Bennici, A. Vega, S. Ordo´n˜ez and A. Auroux Ind. "Adsorption of CO_2 on Hydrotalcite-Derived Mixed Oxides: Sorption Mechanismsand Consequences for Adsorption Irreversibility" Engineering Chemistry Research, vol. 49, 2010. pp. 3663–3671.

[28] R. Altõn , S. Cß etinkaya , H.S. Yucesu. "The potential of using vegetable oil fuels as fuel for dieselengines" Energy Conversion and Management, vol. 42 , 2001. pp. 529-538.

[29] J.G. Speight. "The chemistry and Technology of Petroleum Fourth edition" CRC Press Taylor & Francis Group, the united states of America, 2007.

[30] G.R. Lappin, L.H. Nemec, J.D. Sauer, J.D. Wagner. "Higher Olefins" Kirk-Othmer Encyclopedia of Chemical Technology, 2000, Vol. 17, pp. 709–728.

[31] P.W.N.M. Leeuwen, N.D. Clément, M.J.L. Tschan. "New processes for the selective productionof 1-octene" Coordination Chemistry Reviews, vol. 255, 2011. pp. 1499–1517.

[32] J. Skupinska. "Oligomerization of α-olefins to higher oligomers" Chemical Review, vol. 91, 1991.pp. 613–648.

[33] Y. Shiraki, Y. Nakamoto, Y. Souma "ZrC_{l4}-TEA-EASC three-component catalyst for the oligomerization of ethylene: the role of organoaluminum co-catalysts and additives" Journal of Molecular Catalysis A: Chemical., vol. 187, 2002. pp. 283–294.

[34] Chevron Phillips Chemical Company. "Normal Alpha Olefins" [Online]. Available : http://www.cpchem.com/enu/nao_a_applications.asp

[35] Sadrameli S.M. and Alex E.S. Green. "Systematics of renewable olefins from thermal cracing of canola oil" Journal of Analytical and Applied Pyrolysis, vol. 78, 2007. pp. 445-451.

[36] S.J. Eduardo and M. Crocker. "Catalytic deoxygenation of fatty acids and their derivatives to hydrocarbon fuels via decarboxylation/decarbonylation" Chemical Technology and Biotechnology, vol. 87, 2012. pp. 1041-1050.

[37] J.G. Na, B.E. Yi, J.N. Kim, K.B. Yi, S.Y. Park, J.H. Park, J.N. Kim, C.H. Ko. "Hydrocarbon production from decarboxylation of fatty acid without hydrogen" Catalysis Today, vol. 156, 2010. pp. 44–48.

[38] M. Arend, T. Nonnen, W. F. Hoelderich, J. Fischer, J. Groos. "Catalytic deoxygenation of oleic acid in continuous gas flow for the production of diesel-like hydrocarbons" Applied Catalysis A: General, vol. 399. 2011. pp.198-204.

[39] E. Sari, M. Kim, S.O. Salley, K.Y. Simon Ng. "A highly active nanocomposite silica-carbon supported palladium catalyst for decarboxylation of free fatty acids for green diesel production: Correlation of activity and catalyst properties" Applied Catalysis A: General, vol. 467. 2013. pp. 261–269.

[40] R. Besselink, T. M. Stawski, H. L. Castricum, D.H.A. Blank and J.E. Elshof. "Exfoliation and Restacking of Lepidocrocite-type Layered Titanates Studied by Small-Angle X-ray Scattering" J. Phys. Chem. C, vol. 114, 2010. pp. 21281–21286.

[41] D. Groult, C. Mercey, B. Raveau. "Nouveaux oxydes à structure en feuillets: Les titanates de potassium non-stoechiométriques $K_x(M_yTi_{2-y})O_4$", Journal of Solid State Chemistry,Volume 32, Issue 3, May 1980, Pages 289–296

[42] T. Sasaki and M. Watanabe. "Semiconductor Nanosheet Crystallites of Quasi-TiO_2 and Their Optical properties", Journal of physical Chemistry, vol.101, 1997, Pages 10159-10161.

[43] T. Gao, P. Norby, H. Okamoto and Helmer Fjellvag. "Synthesis, Structure, and Magnetic properties of Nickle-Doped Lepidocrocite Titanates", Inorganic Chemistry, vol.48, 2009, Pages 9409-9418.

[44] T. Gao, Helmer Fjellvag, and Poul Norby. "Crystal Structure of Titanate Nanotube: A Raman Scattering Study", Inorganic Chemistry, vol.48, 2009, Pages 1423-1432.

[45] H. Song, A.O. Sjastad, O.B. Vistad, T.Gao, and P.Norby. "Preparation of Nb-Substituted Titanates by a Novel Sol-Gel Assisted Solid State Reaction", Inorganic Chemistry, vol.48, 2009, Pages 6952-6959.

APPENDIX A

CHARACTERIZATION OF CATALYSTS

Table A1:List of peak positions (in 2θ), the corresponding values of d spacing, and hkl index for pristine KZn.

2θ	h	k	l	d (Å)
11.3	0	2	0	7.824
21.68	0	4	0	3.928
23.96	1	1	0	3.705
28.98	1	3	0	3.079
32.02	0	2	1	2.793
34.03	0	6	0	2.611
37.86	0	4	1	2.374
38	1	1	1	2.326
42.04	1	3	1	2.146
42.1	0	6	1	1.965
47.7	0	2	0	1.904
47.86	1	5	1	1.881
49.14	2	2	0	1.852
56.74	1	7	1	1.621
58.14	1	9	0	1.584
58.16	2	2	1	1.584
60.04	2	6	0	1.574
62.4	0	0	2	1.539

Table A2: List of peak positions (in 2θ), the corresponding values of d spacing, and hkl index for HZn.

2θ	h	k	l	d (Å)
9.818	0	2	0	9.002
19.721	0	4	0	4.498
24	1	0	0	3.705
27.818	1	3	0	3.205
29.98	0	6	0	2.978
34	0	3	1	2.635
34.7	1	5	0	2.583
39.019	0	5	1	2.307
43.8	0	6	1	2.065
46.478	0	7	1	1.952
48	2	0	0	1.894
49.5	2	2	0	1.84
51.5	0	10	0	1.773
57.1	1	10	0	1.612

LANGMUIR ADSORPTION ISOTHERM

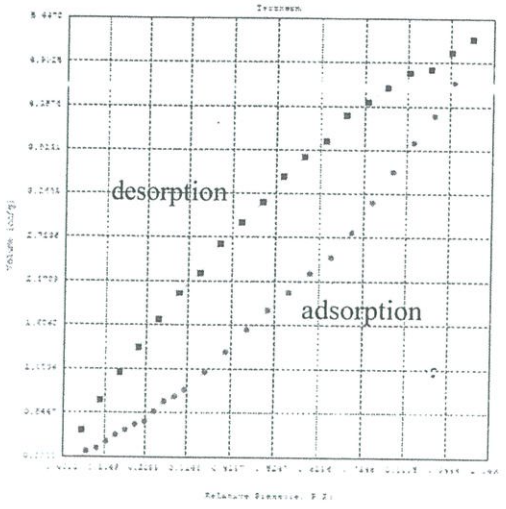

(a)

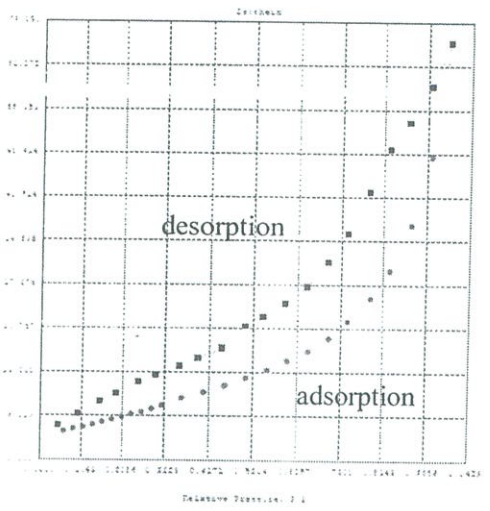

(b)

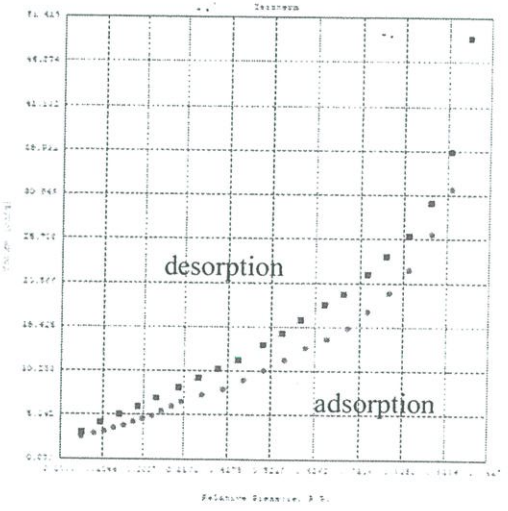

(c)

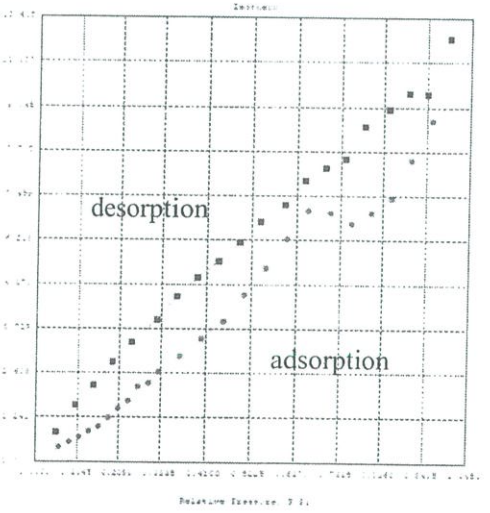

(d)

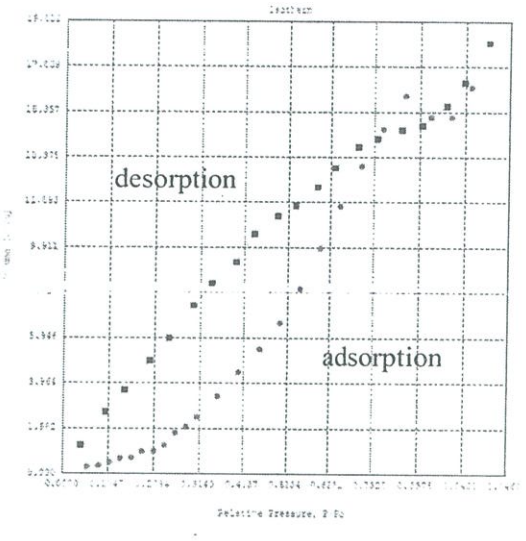

(e)

Figure A1 Adsorption-Desorption isotherm of (a) KZn Pristine, (b) calcined KZn (exfoliated with TBAOH), (c) calcined KZn (exfoliated with TMAOH), (d) KMg, (e) KLi.

Quantachrome Corporation
Quantachrome Autosorb Automated Gas Sorption System Report
Autosorb for Windows® Version 1.19

Sample ID	LPC K Zn Ti				
Description	Ads 32 Pts Des 20 Pts BET 11 pts				
Comments					
Sample Weight	0.1412 g				
Adsorbate	NITROGEN	Outgas Temp	300.0 °C	Operator	BcmB
Cross-Sec Area	16.2 Å²/molecule	Outgas Time	8.9 hrs	Analysis Time	320.8 min
NonIdeality	6.500E-05	P/Po Toler	2	End of Run	09/06 21:3
Molecular Wt	28.0134 g/mol	Equil Time	3	File Name	060906_1.RAW
Station #	1	Bath Temp.	77.35		

Isotherm

P/Po	Volume (cc/g) STP
5.8204e-02	0.0684
8.4133e-02	0.1044
1.0384e-01	0.1381
1.3385e-01	0.2707
1.6909e-01	0.3218
1.8385e-01	0.4086
2.0933e-01	0.4857
2.3369e-01	0.5653
2.5844e-01	0.6336
2.8415e-01	0.7487
3.0890e-01	0.8350
3.6813e-01	1.0494
4.0742e-01	1.1122
4.5774e-01	1.5753
5.0769e-01	1.8180
5.5804e-01	2.0360
6.0875e-01	2.2736
6.5818e-01	2.4763
7.0731e-01	2.7342
7.5609e-01	3.1590
8.0665e-01	3.5400
8.5675e-01	3.9049
9.0683e-01	4.2393
9.5584e-01	4.6478
9.8940e-01	5.1379
9.4808e-01	5.0226
8.9672e-01	4.9191
8.4430e-01	4.7742
7.9206e-01	4.6310
7.4196e-01	4.4122
6.9179e-01	4.2469
6.4268e-01	3.9210
5.9212e-01	3.7214
5.4236e-01	3.4763
4.9266e-01	3.1659
4.4266e-01	2.9537
3.9229e-01	2.6954
3.4309e-01	2.3741
2.9135e-01	2.0241
2.4234e-01	1.6878
1.9244e-01	1.3546
1.4244e-01	1.0416
9.2556e-02	0.7017

Figure A2 Langmuir plot data of KZn pristine.

Quantachrome Corporation
Quantachrome Autosorb Automated Gas Sorption System Report
Autosorb for Windows® Version 1.19

Sample ID	LPC(Zn) Restack				
Description	Ads 22 Pts Des 22 Pts BET 11 pts				
Comments					
Sample Weight	0.1113 g				
Adsorbate	NITROGEN	Outgas Temp	300.0 °C	Operator	Best
Cross-Sec Area	16.2 Å²/molecule	Outgas Time	15.6 hrs	Analysis Time	346.2 min
NonIdeality	6.580E-05	P/Po Toler	0	End of Run	12/28/2010 1
Molecular Wt	28.0134 g/mol	Equil Time	0	File Name	061225_1.RAW
Station #	1	Bath Temp.	77.35		

Isotherm

P/Po	Volume (cc/g) STP
5.7656e-02	4.4616
8.2421e-02	4.8693
1.0786e-01	5.1496
1.3264e-01	5.5604
1.5746e-01	5.9627
1.8253e-01	6.3665
2.0761e-01	6.7674
2.3234e-01	7.1913
2.5795e-01	7.6227
2.8282e-01	8.0459
3.0695e-01	8.5373
3.6344e-01	9.7754
4.0514e-01	10.7044
4.5503e-01	11.7422
5.0430e-01	12.9767
5.5399e-01	14.2851
6.0210e-01	15.7119
6.5250e-01	17.2224
7.0150e-01	19.1308
7.4735e-01	21.3819
8.0466e-01	25.4848
8.5190e-01	29.9768
9.0235e-01	37.0856
9.5060e-01	47.9187
9.9821e-01	65.0961
9.4850e-01	59.0664
8.9495e-01	53.8994
8.5036e-01	49.0679
7.9844e-01	42.3390
7.4737e-01	35.8224
6.9945e-01	31.3758
6.4837e-01	27.2156
5.9594e-01	24.5991
5.4323e-01	22.6158
5.0141e-01	21.1911
4.4637e-01	17.5844
3.9178e-01	16.1759
3.4360e-01	14.9336
2.9195e-01	13.4276
2.4871e-01	12.2830
1.9266e-01	11.5116
1.4577e-01	9.1998
9.3012e-02	7.1968

Figure A3 Langmuir plot data of calcined KZn (exfoliated with TBAOH).

Quantachrome Corporation
Quantachrome Autosorb Automated Gas Sorption System Report
Autosorb for Windows® Version 1.19

Sample ID	LP1 (Zn) TMA restacked						
Description	Ads 22 Pts Des 22 Pts BET 11 pts						
Comments							
Sample Weight	[illegible] g						
Adsorbate	NITROGEN	Outgas Temp	300.0 °C	Operator	Best		
Cross-Sec Area	16.2 Å²/molecule	Outgas Time	6.5 hrs	Analysis Time	[illegible] min		
NonIdeality	6.580E-05	P/Po Toler	2	End of Run	01/14/2014 2		
Molecular Wt	28.0134 g/mol	Equil Time	2	File Name	[illegible]_2.RAW		
Station #	1	Bath Temp.	77.35				

Isotherm

P/Po	Volume [cc/g] STP
5.1162e-02	2.5938
8.0982e-02	2.9611
1.0325e-01	3.2212
1.3261e-01	3.5730
1.5817e-01	3.9722
1.8266e-01	4.3193
2.0768e-01	4.6738
2.3297e-01	5.0120
2.5666e-01	5.5973
2.8191e-01	6.1381
3.0692e-01	6.6716
3.5665e-01	7.4544
4.0724e-01	8.1306
4.5614e-01	9.1932
5.0476e-01	10.3141
5.5405e-01	11.5910
6.0398e-01	12.9342
6.5470e-01	14.0065
7.0420e-01	15.2332
7.5104e-01	17.2624
8.0203e-01	19.3359
8.4899e-01	22.1068
9.0421e-01	26.2336
9.5033e-01	31.5297
9.9403e-01	43.9670
9.4871e-01	35.3680
9.0169e-01	29.8719
8.4820e-01	26.0950
7.9351e-01	23.6014
7.5164e-01	21.5633
6.9333e-01	19.3078
6.4398e-01	18.0073
5.9215e-01	16.2621
5.4672e-01	14.6333
5.0103e-01	13.3661
4.4175e-01	11.5780
3.9496e-01	10.4891
3.4761e-01	9.4750
3.0064e-01	8.3535
2.4217e-01	7.1093
1.9399e-01	6.1426
1.4662e-01	5.1664
9.0733e-02	4.2210

Figure A4 Langmuir plot data of calcined KZn (exfoliated with TMAOH).

Quantachrome Autosorb Automated Gas Sorption System Report
Version 1.5

Sample ID
Description
Comments
Sample Weight
Adsorbate NITROGEN
Cross-Sec Area
Nonideality
Molecular Wt

Outgas Temp 300.0 °C
Outgas Time 6.2 hrs

Operator
Analysis Time
End of Run
File Name

Isotherm

P/Po	Volume [cc/g] STP
5.7226e-02	0.4052
7.3536e-02	0.5611
1.0550e-01	0.6819
1.2535e-01	0.8536
1.5386e-01	0.9898
1.8311e-01	1.2351
2.1756e-01	1.4856
2.3341e-01	1.7069
2.5747e-01	2.1046
3.1361e-01	2.2098
3.0758e-01	2.5312
3.6708e-01	2.9600
4.0707e-01	3.4458
4.5781e-01	3.9368
5.0617e-01	4.6767
5.5516e-01	5.4306
6.0531e-01	6.2502
6.5535e-01	7.0482
7.0335e-01	6.9790
7.5554e-01	6.6337
8.0334e-01	6.9362
8.5521e-01	7.3979
9.0505e-01	8.4623
9.5420e-01	9.5669
9.9525e-01	11.9396
9.4127e-01	10.3178
8.9702e-01	10.3352
8.4944e-01	9.8766
7.9093e-01	9.3978
7.4467e-01	8.4939
6.9603e-01	8.2490
6.4752e-01	7.8899
5.9870e-01	7.2179
5.4106e-01	6.7291
4.9402e-01	6.1492
4.4665e-01	5.6197
3.9906e-01	5.1707
3.4984e-01	4.6472
3.0183e-01	3.9333
2.4167e-01	3.3437
1.9921e-01	2.7336
1.4582e-01	2.1353
9.7577e-02	1.5764

Figure A5 Langmuir plot data of KMg.

Quantachrome Autosorb Automated Gas Sorption System Report

Sample ID	[illegible]				
Description	[illegible]				
Comments					
Sample Weight	[illegible] g				
Adsorbate	NITROGEN	Outgas Temp	[illegible]	Operator	[illegible]
Cross-Sec Area	16.2 Å²/molecule	Outgas Time	[illegible]	Analysis Time	[illegible] min
NonIdeality	[illegible]	P/Po Toler	[illegible]	End of Run	[illegible]
Molecular Wt	[illegible] g/mol	Equil Time	[illegible]	File Name	[illegible]
Station #	[illegible]	Bath Temp.	[illegible]		

Isotherm

P/Po	Volume [cc/g] STP
5.7145e-02	0.2852
8.4001e-02	0.3557
1.0367e-01	0.4826
1.3361e-01	0.6623
1.5511e-01	0.6336
1.8822e-01	0.9639
2.0911e-01	0.9787
2.3357e-01	1.2435
2.5786e-01	1.7301
2.8307e-01	2.0459
3.0319e-01	2.4774
3.5666e-01	3.3824
4.0600e-01	4.4377
4.5637e-01	5.4415
5.0569e-01	6.6000
5.5428e-01	8.0851
6.0351e-01	9.8631
6.5249e-01	11.7176
7.0351e-01	13.4373
7.5455e-01	15.0927
8.0473e-01	16.5637
8.6213e-01	15.6246
9.1009e-01	15.6191
9.5641e-01	16.9348
9.9658e-01	18.3777
9.3954e-01	17.1570
8.9327e-01	16.1133
8.4217e-01	15.2464
7.9656e-01	15.0682
7.3976e-01	14.6847
6.9535e-01	14.3336
6.3911e-01	13.4174
5.9561e-01	12.5442
5.4159e-01	11.7374
4.9334e-01	11.2698
4.4047e-01	10.4832
3.9778e-01	9.2619
3.4200e-01	8.3238
2.9309e-01	7.3735
2.4232e-01	5.9375
1.9522e-01	4.9430
1.4170e-01	3.8543
9.7755e-02	2.7150

Figure A6 Langmuir plot data of KLi.

THERMOGRAVIMATIC ANALYSIS OF CATALYST

*Test condition; in nitrogen from 50 to 900°C (10°C/min)

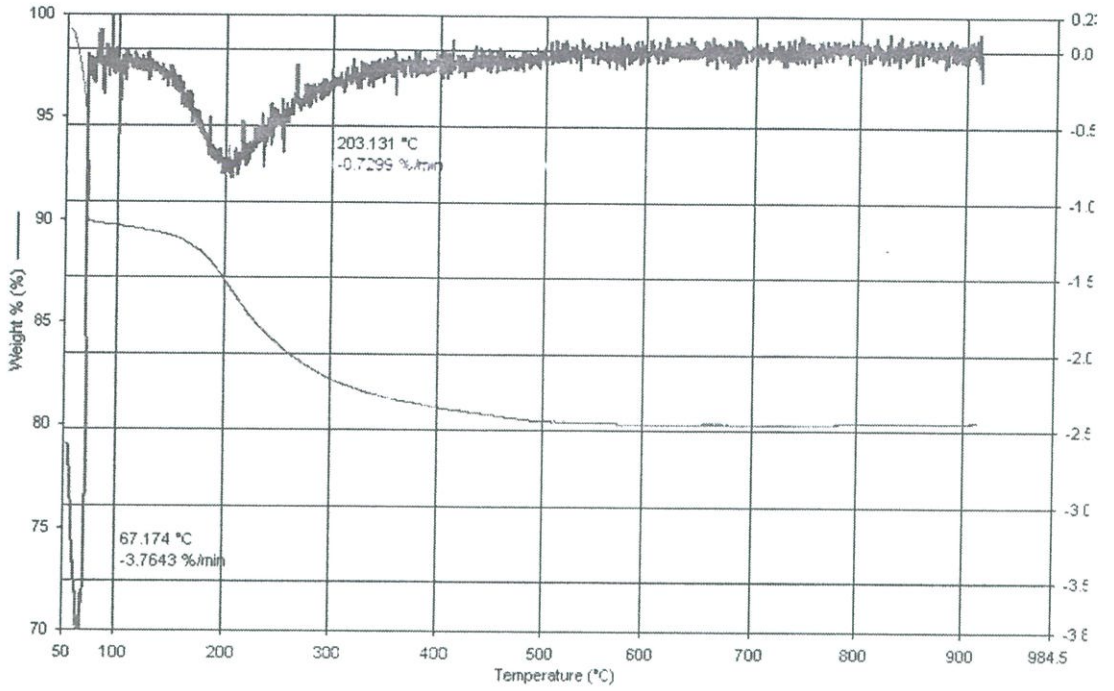

Figure A7 TGA event mask of HZn.

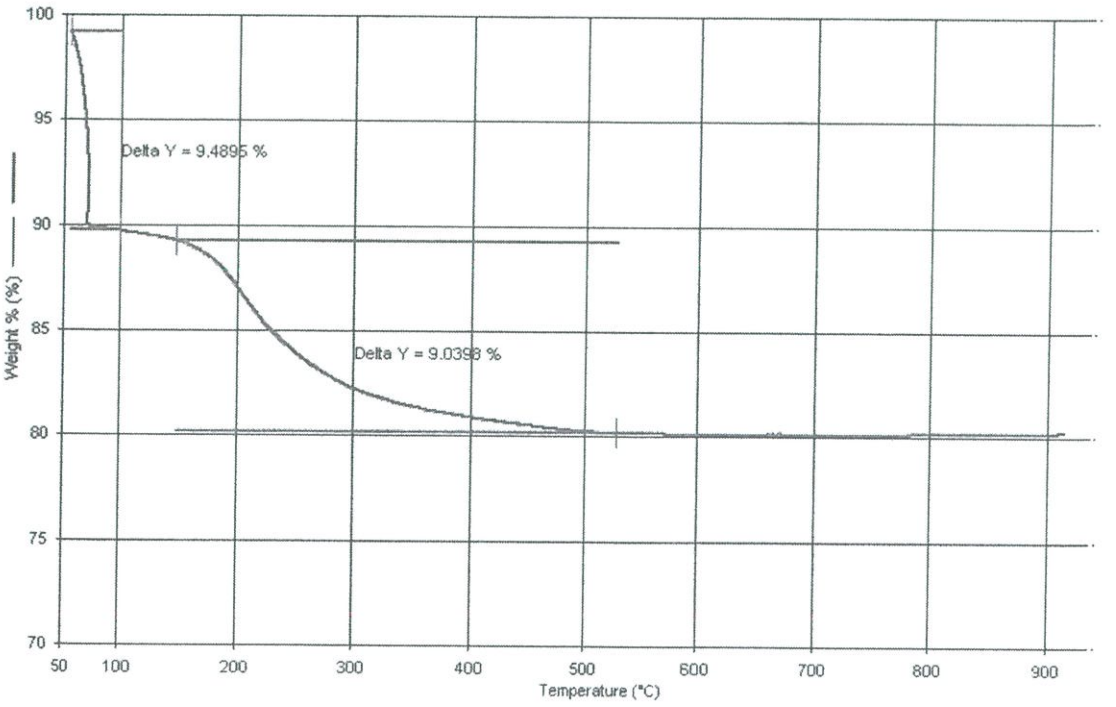

Figure A8 TGA delta y of HZn.

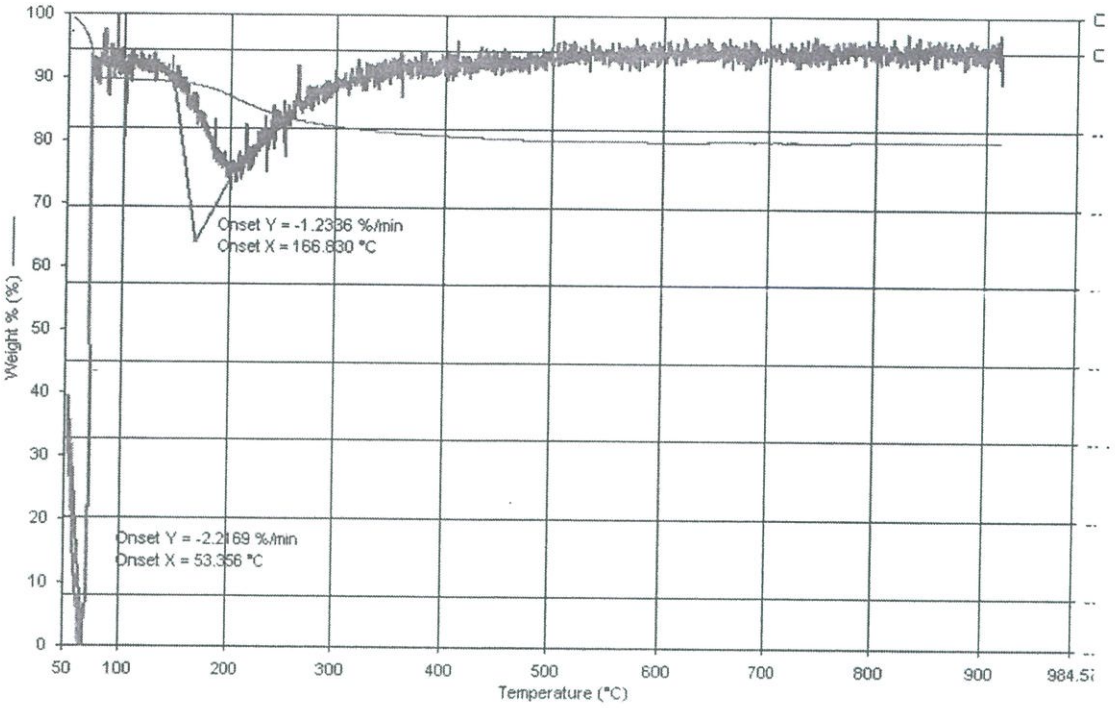

Figure A9 TGA on set of HZn.

APPENDIX B

CALCULATION

Calculation of catalytic parameter

W/F

$$W/F = \frac{\text{Weight of catalyst (g)}}{\text{Mole of reactant feed (mol/h)}}$$

In the reaction using mol/h of palmitic acid in feed and using 0.3726 grams of catalyst, the W/F is calculated as follow:

$$W/F = [0.3726\ (g)/\ 2.48 \times 10^{-4}\ (mol/h)]$$

$$= 1500\ g \cdot h/mol$$

In similar manner; W/F of catalysts with different catalyst weight and different feed rate are calculated.

Calculation of % yield from gas chromatography

From the chromatogram, the peaks of products distribution were identified using of reference standard for comparison. The summation of peak area obtained from chromatogram of a mixture product is shown in **Table B1**.

Table B1: The peak area for products.

Product	Peak area
C-14 Unsaturated hydrocarbon	150.13
C-14 Saturated hydrocarbon	0.00

*in formation of KLi in p-xylene, Contact time = 1500 g•h/mol, time on stream = 300 min.

In normalization method, the areas of all eluted peak were compute areas for differences in the detector response to different compound types. The concentration of the analyzed was found from the ratio of its area to the total area of all peaks.

Calculate the percent yield of each component in sample as follows:

$$\%\text{Yield in each product} = \frac{\text{Peak area of A} \times 100}{\text{Total area}}$$

Where A is the each product.

For example;

$$\%\text{Yield of C-14 Unsat.} = \frac{150.13 \times 100}{645.41}$$

$$= 0.60\%$$

The percent product yield of each sample which is obtained from above calculation is shown in **Table B2**.

Table B2: % Yield of product derived by normalization method.

Products	%Yield
C-14 Unsaturated hydrocarbon	23.26
C-14 Saturated hydrocarbon	0.00

*in formation of KLi in p-xylene, Contact time = 1500 g•h/mol, time on stream = 300 min.

Conversion

%Conversion can be calculated from the following equation.

$$\%\text{Conversion} = \frac{\text{Area total - Area feed}}{\text{Area total}}$$

For example;

$$\%\text{Conversion} = \frac{(645.41 - 236.70) \times 100}{645.41}$$

$$= 63.33\%$$

Selectivity

%Selectivity can be obtained from the following equation.

$$\%\text{Selectivity in each product} = \frac{\%\text{Yield in each product} \times 100}{\%\text{ Conversion}}$$

For example;

$$\%\text{Selectivity of C-14 Unsat.} = \frac{150.13 \times 100}{408.71}$$

$$= 36.73\%$$

APPENDIX C

GAS CHROMATOGRAM

Analysis gas product from gas chromatography

Prior analysis, the structure of products in sample is identified by GC-MS (gas chromatography with mass spectrometer detector). Then, the quantitative analysis of product was carried by GC-FID (gas chromatography with flam ionization detector) with the condition expressed in **Table C1.**

Table C1: The GC condition for quantitative analysis

Column	HP5 , 30 m x 0.32 mm x0.25
Temperature program	40°C (10 min hold) to 280°C (60 min hold) at 15°/min
Carrier gas	Nitrogen gas
Injector temperature	265 °C
Detector temperature	FID at 280 °C

Table C2: Chromatogram data of standard product distribution and feed.

Products or feed	Retention time of standard (min)	Products or feed	Retention of standard (min)
C9 unsat	14.081	C13 unsat	18.835
C9 sat	14.237	C13 sat	18.900
C10 unsat	15.668	C14 unsat	19.687
C10 sat	15.780	C14 sat	19.745
C11 unsat	16.885	C17 ketone	22.723
C11 sat	16.973	Palmitic acid	23.150
C12 unsat	17.913	C-31 ketone	31.326

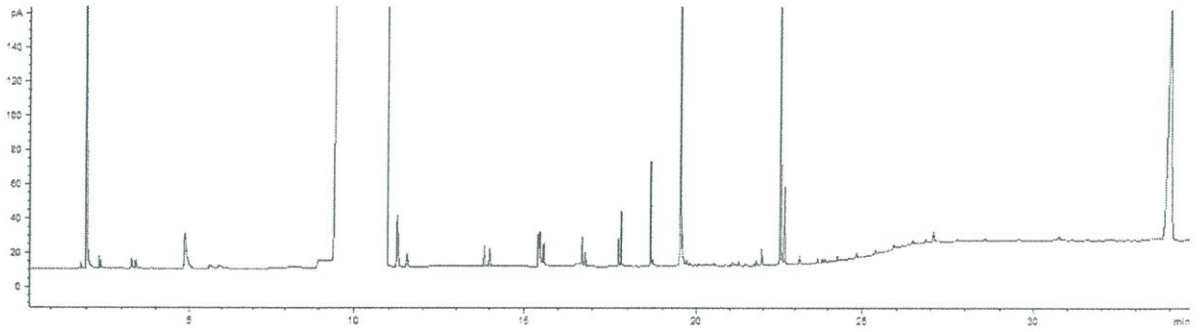

Figure C1 The GC chromatogram of ketonization of palmitic acid.

APPENDIX D

Reaction Data

D1: Study of contact time

Table D1: The yield of palmitic deoxygenation at contact time = 900 g.hr/mol

Time on stream (h)	Conversion (%)	Yield(%)				
		C-31 ketone	C-17 ketone	Heavy ketone	C-14 hydrocarbons	Smaller hydrocarbons
90	95.8	63.7	5.8	6.8	10.1	9.4
135	75.7	50.7	3.4	4.7	10	6.9
180	74.7	49.6	5.7	5.5	8	5.6
225	66.9	41.5	5.8	4.8	8.9	6
270	69.4	37.1	1.7	4.7	7.8	7
315	70.1	47.8	2.2	5.5	10	8
360	62.2	40.6	1.8	4.5	8.4	7

Reaction conditions : 375°C, 15 ml/min of N_2, 5%wt palmitic acid in p-xylene, contact time900 g.hr/mol.

Table D2: The yield of palmitic acid for deoxygenation at contact time = 1500 g.hr/mol.

Time on stream (h)	Conversion (%)	Yield (%)				
		C-31 ketone	C-17 ketone	Heavy ketone	C-14 hydrocarbons	Smaller hydrocarbons
90	93.77	68.8	4.4	2.5	11.9	4.7
135	84.72	54.2	4,4	3.3	12.6	7.1
180	78.29	52.7	3.7	3.1	10.9	5.7
225	70.18	42	3.4	2.6	11.9	7.3
270	70.14	42.2	3.3	2.3	12	7.5
315	73.87	49.1	2.5	2.2	12	6.4
360	69.74	53	2	1.8	12.2	6.7

Reaction conditions : 375°C, 15 ml/min of N_2, 5%wt palmitic acid in p-xylene, contact time1500g.hr/mol.

D2: Study of temperature.

Table D3: The yield of palmitic acid for deoxygenation over KLi at 375 °C.

Time on stream (h)	Conversion (%)	Yield (%)				
		C-31 ketone	C-17 ketone	Heavy ketone	C-14 hydrocarbons	Smaller hydrocarbons
90	100	45.3	15.3	2.4	20.9	45.3
135	96.23	35.2	22.2	2.7	21.1	35.2
180	97.46	37.4	23.9	3.5	19.9	37.4
225	97	32.5	26.7	3.8	20.4	32.5
270	97.31	31.7	27.8	5.5	19.8	31.7
315	96.55	40.7	22.3	5.2	16.9	40.7
360	95.72	33.5	23.6	5.5	20.8	33.5

Reaction conditions : 375°C, 15 ml/min of N_2, 5%wt palmitic acid in p-xylene, contact time1500g.hr/mol.

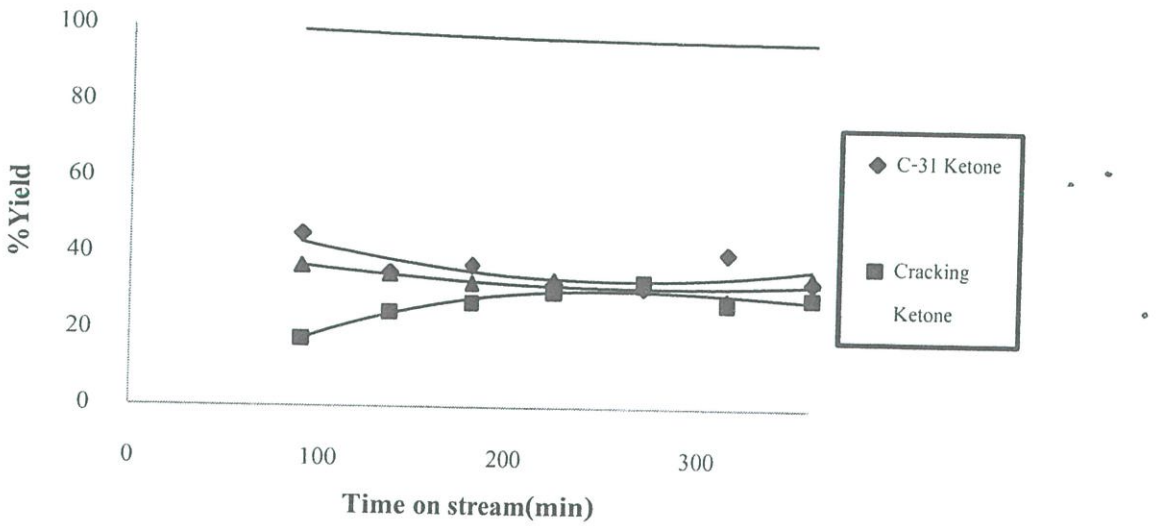

Figure D1 The palmitic acid conversion over KLi catalyst as a function of time on stream at 375°C.

Reaction conditions : 375°C, 15 ml/min of N_2, 5%wt palmitic acid in p-xylene, contact time1500g.hr/mol.

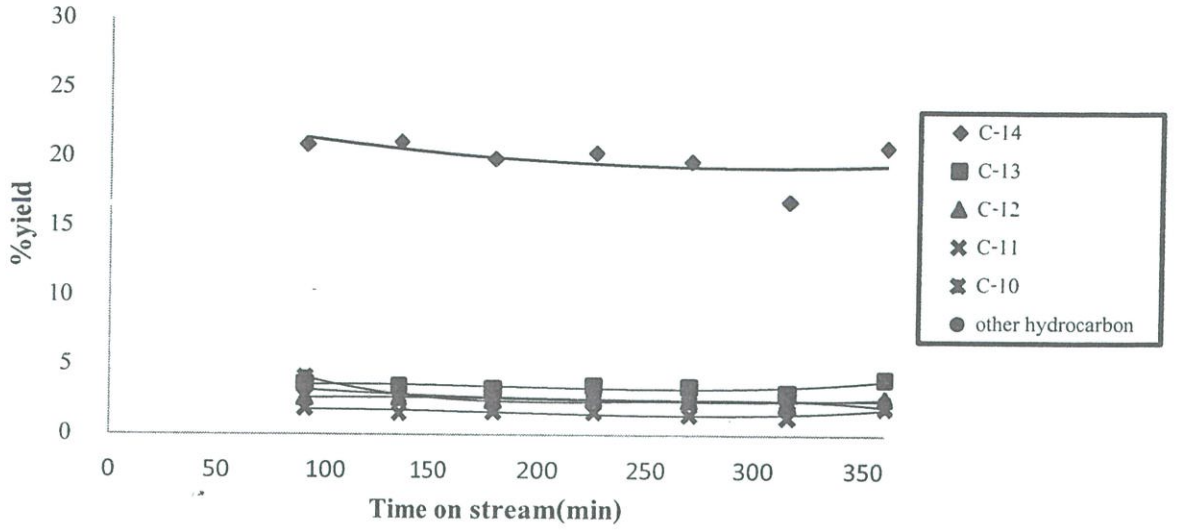

Figure D2 Yield of hydrocarbon product from the reaction of palmitic acid over KLi as function of time on stream (min) at 375 °C.

Reaction conditions : 375°C, 15 ml/min of N_2, 5%wt palmitic acid in p-xylene, contact time1500g.hr/mol.

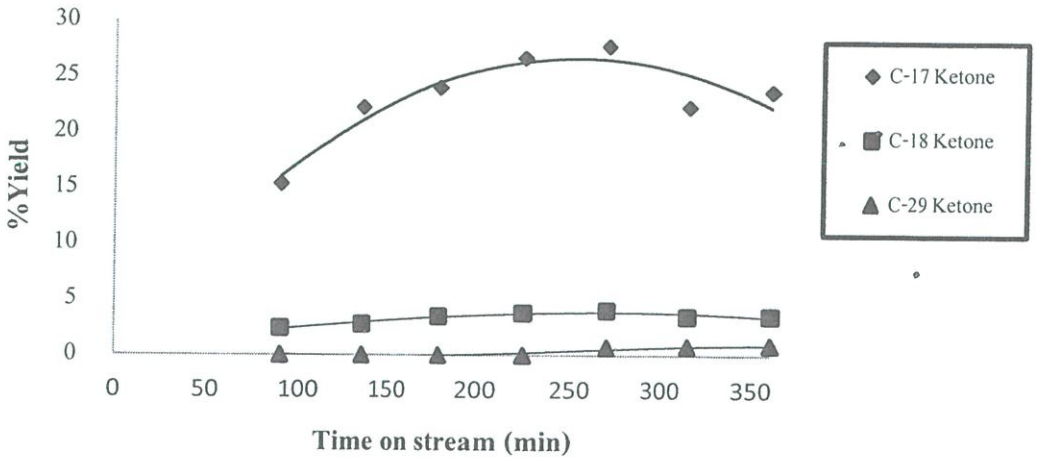

Figure D3 Yield of ketone product from the reaction of palmitic acid over KLi as a function of time on stream (min) at 375 °C.

Reaction conditions : 375°C, 15 ml/min of N_2, 5%wt palmitic acid in p-xylene, contactime1500g.hr/mol.

Table D4: The yield of palmitic acid for deoxygenation over KLi at 400 °C.

Time on stream (h)	Conversion (%)	Yield (%)				
		C-31 ketone	C-17 ketone	Heavy ketone	C-14 hydrocarbons	Smaller hydrocarbons
90	100	37	16.8	1.4	20.9	45.3
135	100	27.7	23.9	2.6	21.1	35.2
180	100	29.3	24.5	3.7	19.9	37.4
225	100	25.8	23.2	3.6	20.4	32.5
270	100	29.1	19.5	2.9	19.8	31.7
315	100	24.1	20.4	2.9	16.9	40.7
360	100	31.6	18.6	4.1	20.8	33.5

Reaction conditions : 400°C, 15 ml/min of N_2, 5%wt Palmitic acid in p-xylene, contact time1500g.hr/mol.

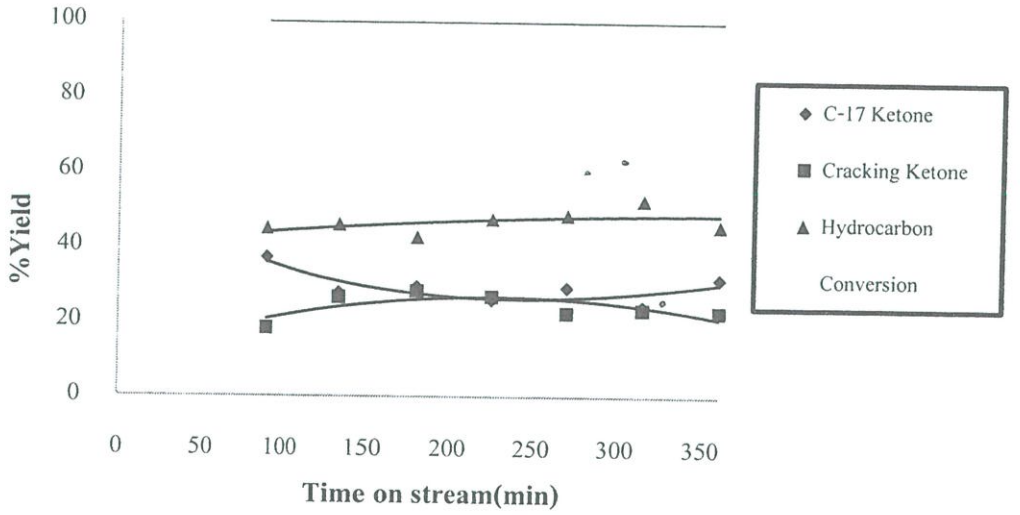

Figure D4 The palmitic acid conversion over KLi catalyst as a function of time on stream at 400°C.

Reaction conditions : 400°C, 15 ml/min of N_2, 5%wt palmitic acid in p-xylene, contact time1500g.hr/mol.

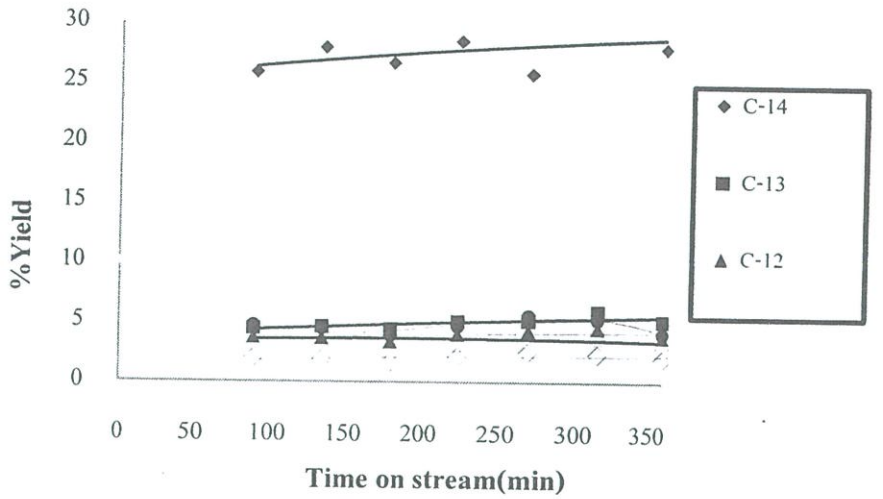

Figure D5 Yield of hydrocarbon product from the reaction of palmitic acid over KLi as a function of time on stream (min) at 400 °C.

Reaction conditions : 400°C, 15 ml/min of N_2. 5%wt palmitic acid in p-xylene, contact time1500g.hr/mol.

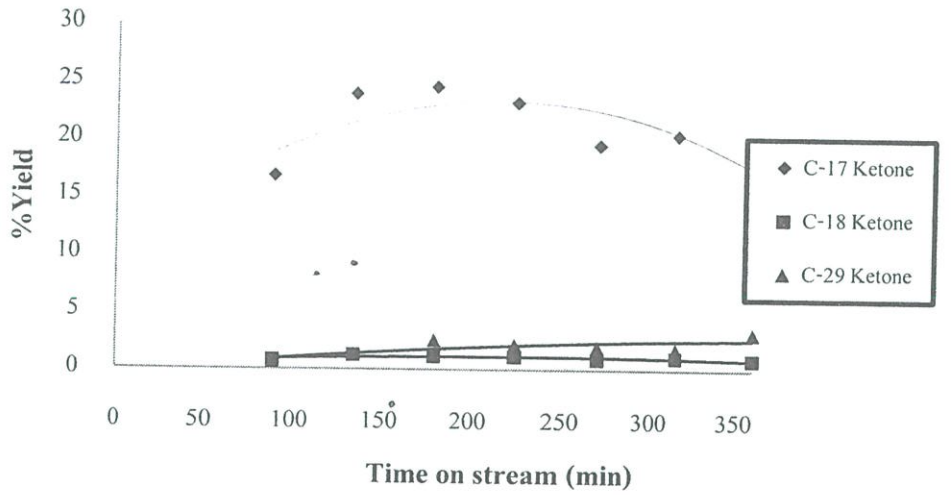

Figure D6 Yield of ketone product from the reaction of palmitic acid over KLi as a function of time on stream (min) at 400 °C.

Reaction conditions : 400°C, 15 ml/min of N_2, 5%wt palmitic acid in p-xylene, contact time1500g.hr/mol.

D3: Study of catalyst.

Table D5: The yield of palmitic acid for deoxygenation over KMg.

Time on stream (h)	Conversion (%)	Yield (%)				
		C-31 ketone	C-17 ketone	Heavy ketone	C-14 hydrocarbons	Smaller hydrocarbons
90	100	18	9.9	5.7	35.3	9.9
135	100	39.5	19.1	11.6	18.8	19.1
180	95.67	41.7	17.7	9.8	15.5	17.7
225	93.89	43.1	17.4	8.8	15.2	17.4
270	89.43	44	13.5	6.2	12.9	13.5
315	85.45	42.7	12.1	5.3	14.5	12.1
360	86.92	47.1	9.5	4.2	15.9	9.5

Reaction conditions : 375°C, 15 ml/min of N_2, 5%wt palmitic acid in p-xylene, contact time1500g.hr/mol.

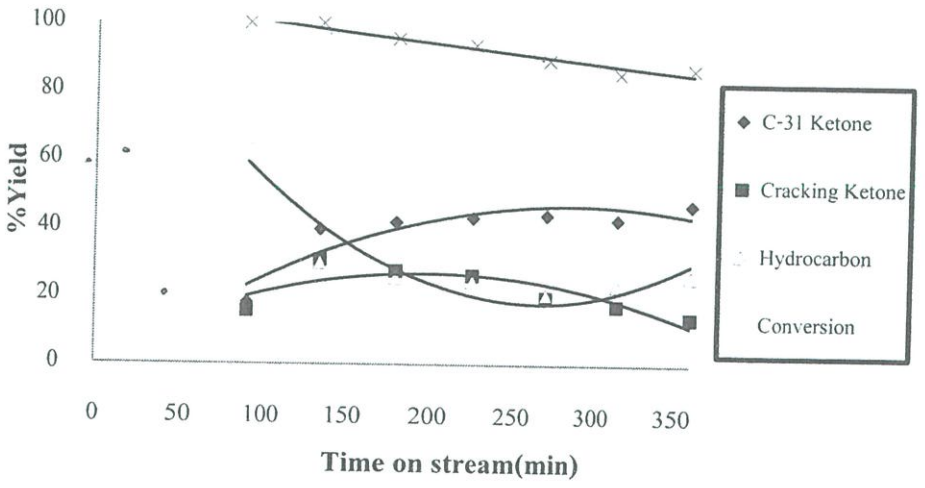

Figure D7 The palmitic acid conversion over KMg catalyst as a function of time on stream.

Reaction conditions : 375°C, 15 ml/min of N_2, 5%wt Palmitic acid in p-xylene, contact time1500g.hr/mol.

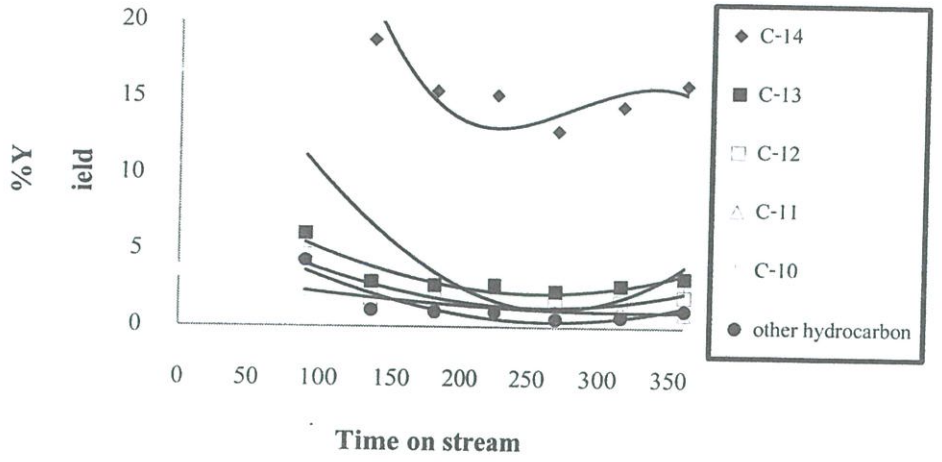

Figure D8 Yield of hydrocarbon product from the reaction of palmitic acid over KMg as a function of time on stream (min).

Reaction conditions : 375°C, 15 ml/min of N_2, 5%wt palmitic acid in p-xylene, contact time1500g.hr/mol.

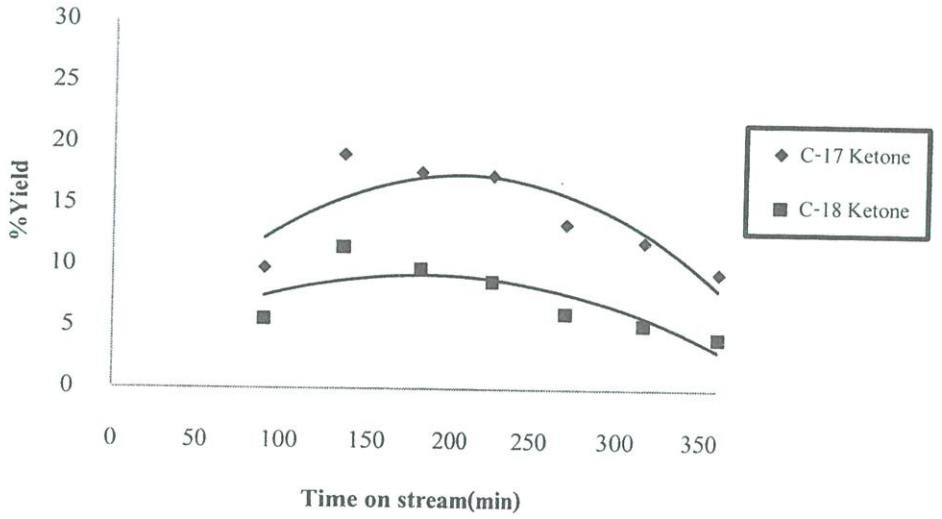

Figure D9 Yield of ketone product from the reaction of palmitic acid over KMg as a function of time on stream (min).

Reaction conditions : 375°C, 15 ml/min of N_2, 5%wt palmitic acid in p-xylene, contact time1500g.hr/mol.

Table D6 The yield of palmitic acid for deoxygenation over re-assembled KZn (TBA).

Time on stream (h)	Conversion (%)	Yield (%)				
		C-31 ketone	C-17 ketone	Heavy ketone	C-14 hydrocarbons	Smaller hydrocarbons
90	97	73.3	8.1	2.5	4.7	6.6
135	96.27	62.9	17.9	3.5	4.6	5.9
180	94.73	64	14.8	3.1	5.1	6.3
225	96.87	71.1	11.5	3.2	4.4	5.3
270	95.47	74.3	9.8	3.2	3.9	4.8
315	93.21	70.8	8.6	2.7	3.8	4.7
360	94.24	75.8	8.4	1.8	3.9	4.1

Reaction conditions : 375°C, 15 ml/min of N_2, 5%wt palmitic acid in p-xylene, contact time1500g.hr/mol.

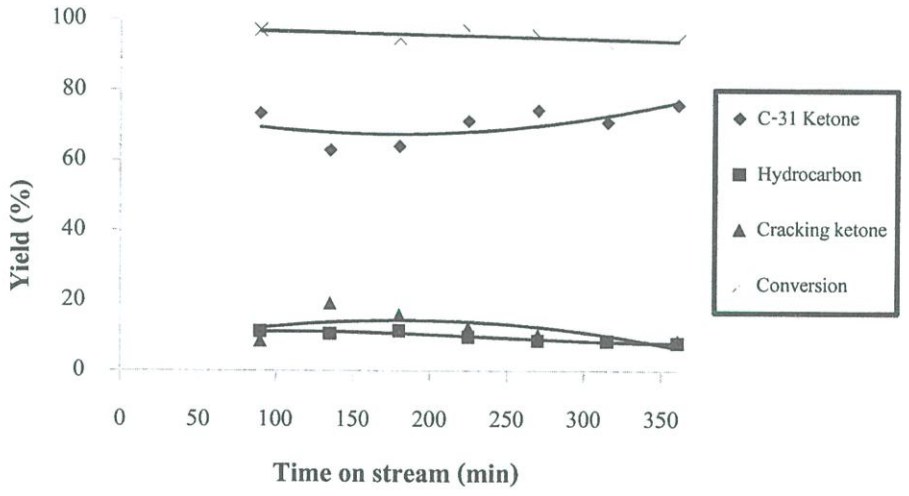

Figure D10 The palmitic acid conversion over re-assembled KZn (TBA) catalyst as a function of time on stream(min).

Reaction conditions : 375°C, 15 ml/min of N_2, 5%wt palmitic acid in p-xylene, contact time1500g.hr/mol.

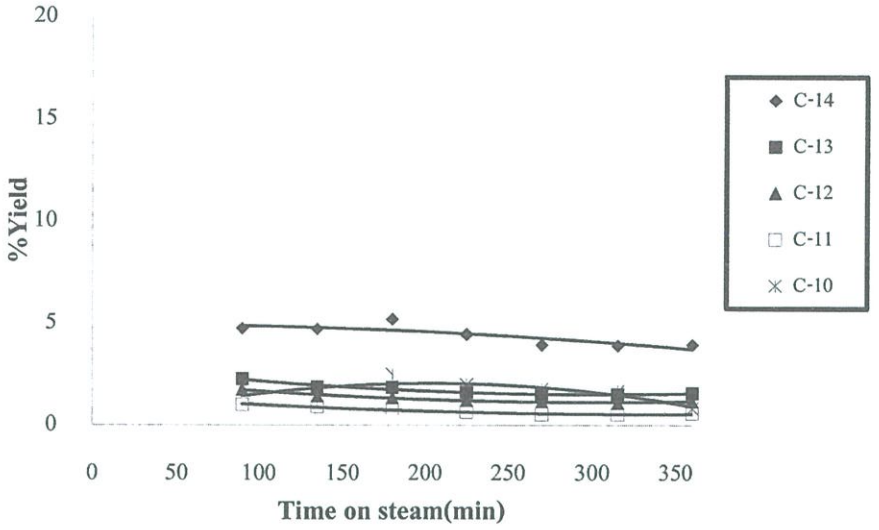

Figure D11 Yield of hydrocarbon product from the reaction of palmitic acid over re-assembled KZn (TBA) as a function of time on stream (min).

Reaction conditions : 375°C, 15 ml/min of N_2, 5%wt palmitic acid in p-xylene, contact time1500g.hr/mol.

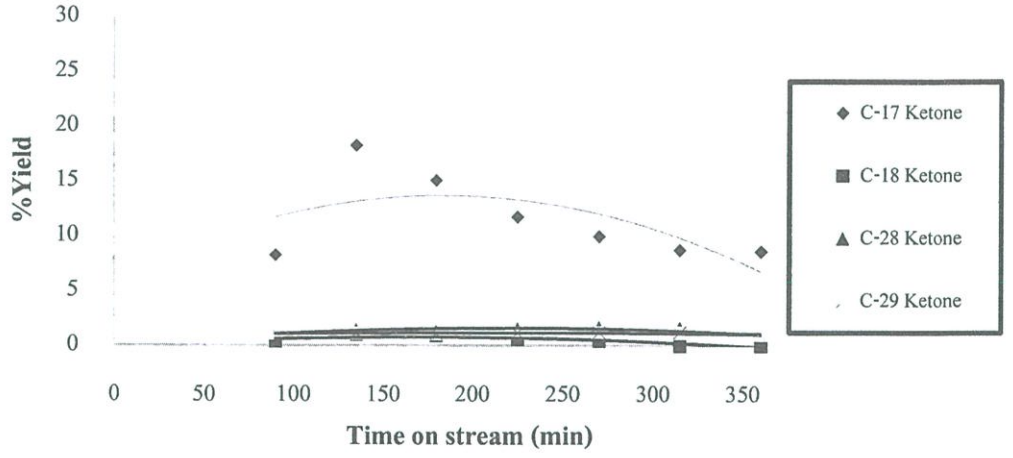

Figure D12 Yield of ketone product from the reaction of palmitic acid over re-assembled KZn (TBA) as a function of time on stream (min).

Reaction conditions : 375°C, 15 ml/min of N_2, 5%wt palmitic acid in p-xylene, contact time1500g.hr/mol.

Table D7: The yield of palmitic acid for deoxygenation over re-assembled KZn (TMA).

Time on stream (h)	Conversion (%)	Yield (%)				
		C-31 ketone	C-17 ketone	Heavy ketone	C-14 hydrocarbons	Smaller hydrocarbons
90	96.86	62.2	13.8	4.1	6.7	7.5
135	97.93	55.4	16.2	5.9	9.1	6.5
180	94.92	57.1	15.2	5.1	9.3	6.8
225	96.32	62.1	12.7	5.6	8.5	6.3
270	97.16	63.4	12.9	5.9	6.9	6.5
315	95.84	68.1	10.6	6.4	5.5	3.7
360	96.33	72.2	9.4	5.5	4.5	3.1

Reaction conditions : 375°C, 15 ml/min of N_2, 5%wt palmitic acid in p-xylene, contact time1500g.hr/mol.

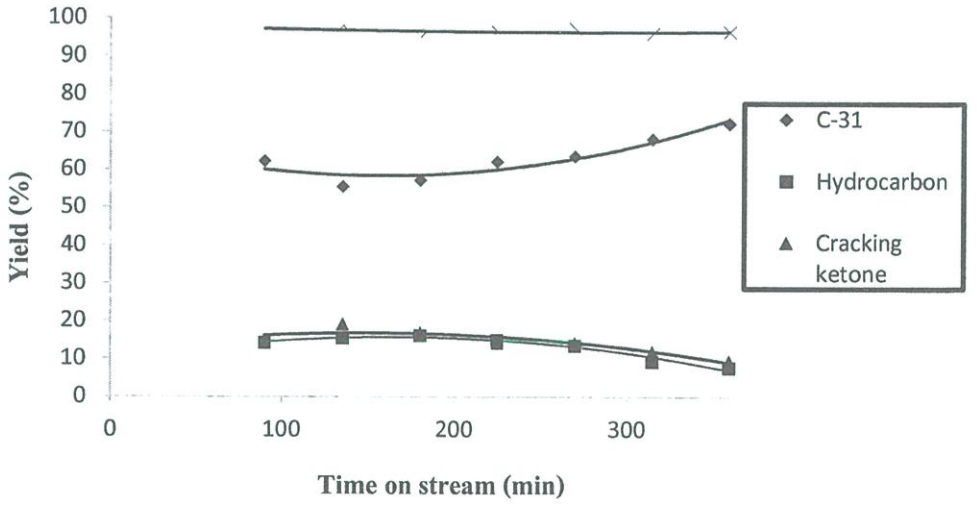

Figure D13 Yield palmitic acid conversion over re-assembled KZn(TMA) catalyst as a function of time on stream.

Reaction conditions : 375°C, 15 ml/min of N_2, 5%wt palmitic acid in p-xylene, contact time1500g.hr/mol.

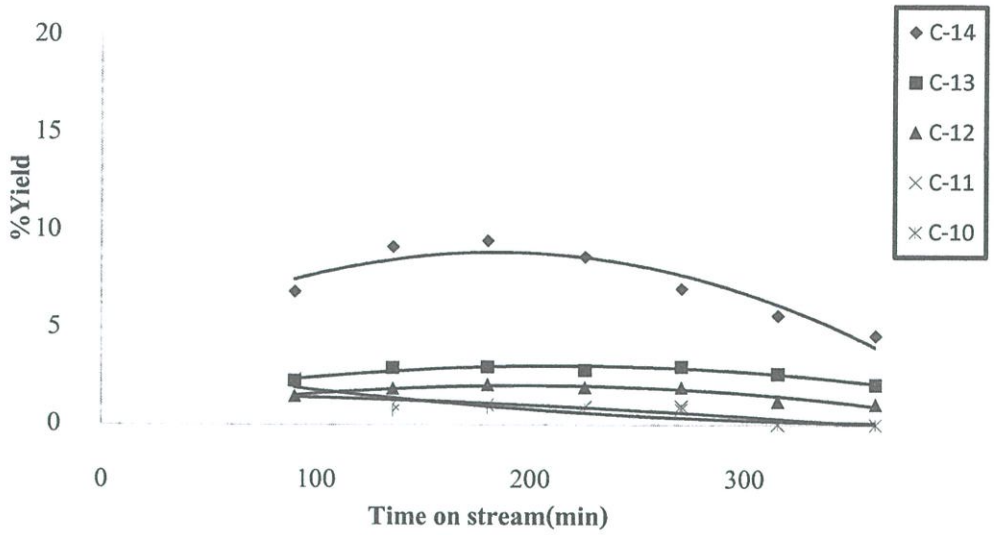

Figure D14 Yield of hydrocarbon product from the reaction of palmitic acid over re-assembled KZn (TMA) as a function of time on stream (min).

Reaction conditions : 375°C, 15 ml/min of N_2, 5%wt palmitic acid in p-xylene, contact time1500g.hr/mol.

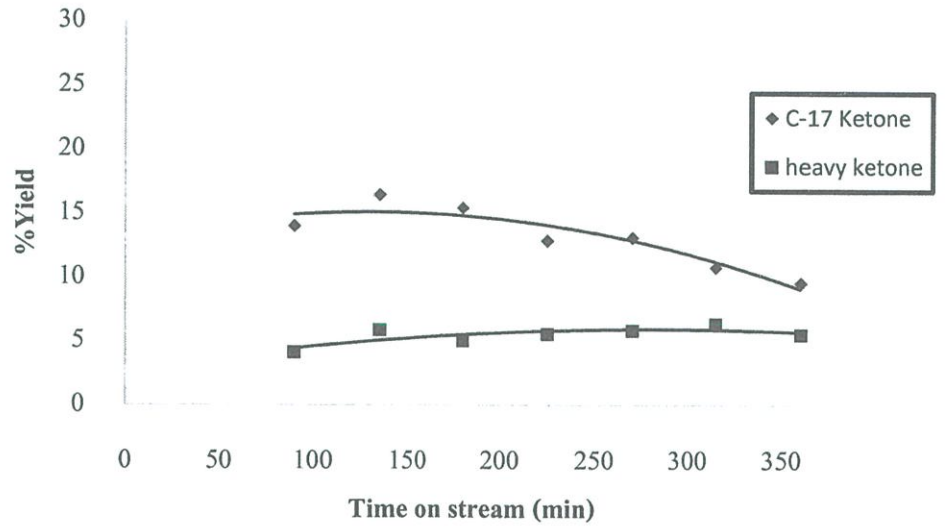

Figure D15 Yield of ketone product from the reaction of palmitic acid over re-assembled KZn (TMA) as a function of time on stream (min)

Reaction conditions : 375°C, 15 ml/min of N_2, 5%wt palmitic acid in p-xylene, contact time1500g.hr/mol.

Table D8: The yield of palmitic acid for deoxygenation over re-assembled KZn (TMA).

Time on stream (h)	Conversion (%)	Yield (%)				
		C-31 ketone	C-17 ketone	Heavy ketone	C-14 hydrocarbons	Smaller hydrocarbons
90	100	36	19.1	17.9	2.6	22.7
135	97.65	36.6	22.7	16.4	2.2	17.4
180	96.64	34.1	20.8	14.3	2.4	20.7
225	95.64	42.8	21.6	13.1	1.8	13.6
270	94.54	48.5	18.1	11.8	1.7	14.3
315	94.39	53.7	17.1	10.6	1.6	11.2
360	92.4	46.6	16.9	10.7	2.1	16.8

Reaction conditions : 375°C, 15 ml/min of N_2, 5%wt palmitic acid in p-xylene, contact time1500g.hr/mol.

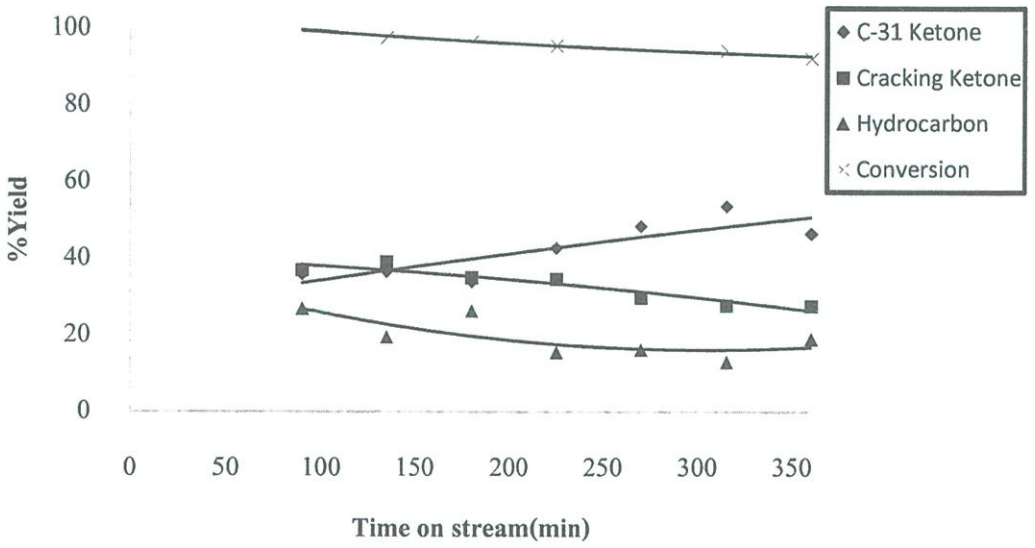

Figure D16 Yield palmitic acid conversion over hydrotalcite 2.5 catalyst as a function of time on stream.

Reaction conditions : 375°C, 15 ml/min of N_2, 5%wt palmitic acid in p-xylene, contact time1500g.hr/mol.

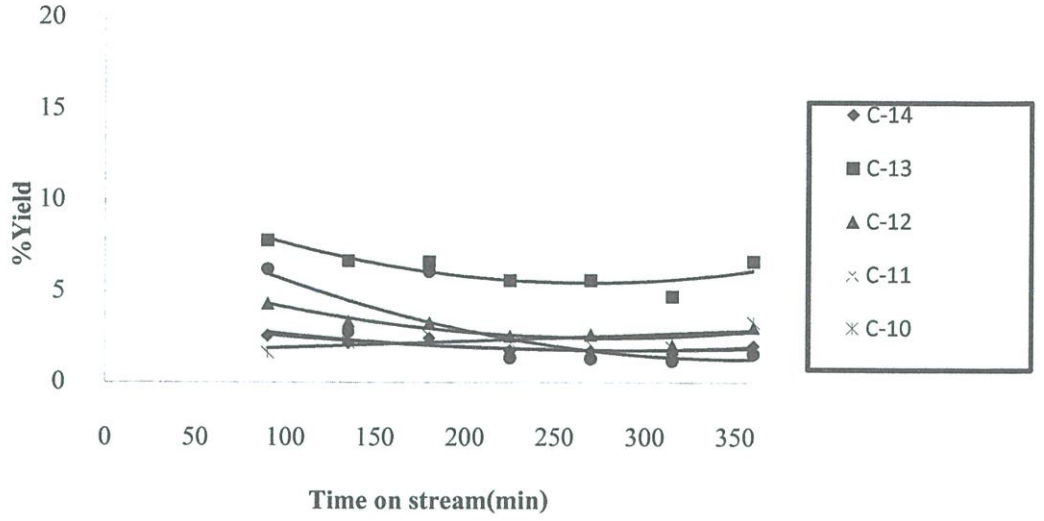

Figure D17 Yield of hydrocarbon product from the reaction of palmitic acid over hydrotalcite ratio 2.5 as a function of time on stream (min).

Reaction conditions : 375°C, 15 ml/min of N_2, 5%wt palmitic acid in p-xylene, contact time1500g.hr/mol.

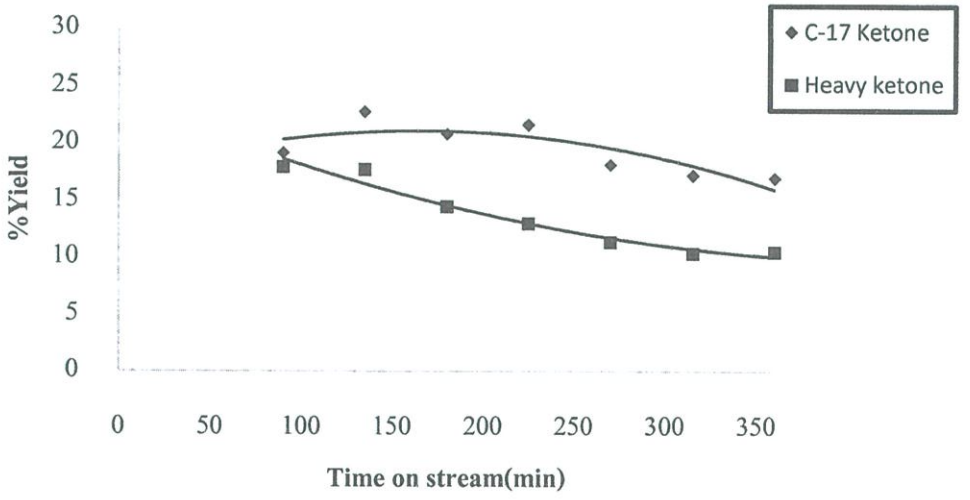

Figure D17 Yield of ketone product from the reaction of palmitic acid over hydrotalcite ratio 2.5 as a function of time on stream (min).

Reaction conditions : 375°C, 15 ml/min of N_2, 5%wt palmitic acid in p-xylene, contact time1500g.hr/mol.